HYDRODYNAMIC MODELING AND FEASIBILITY STUDY OF HARNESSING TIDAL POWER AT THE BAY OF FUNDY

by

Jen Chang

A Dissertation Presented to the
FACULTY OF THE GRADUATE SCHOOL
UNIVERSITY OF SOUTHERN CALIFORNIA
In partial Fulfillment of the
Requirements for the Degree
DOCTOR OF PHILOSOPHY
(CIVIL ENGINEERING)

May 2008

Acknowledgements

The writer would like to express his deepest gratitude to his academic advisor, Dr. J.J. Lee, for his patient guidance, understanding and full support. The writer is also grateful for the instruction form Drs. G. V. Chilingar, J. E. Moore, L. C. Wellford, and H. L. Wong of the guidance committee.

Thanks are also due to Dr. C. P. Lai for his counsel on developing numerical model, and to Professor M. Eskijian for the help on offshore structure cost estimation.

Table of Contents

List of Tables

List of Figures

Abstract

Due to rising fuel costs and environmental concerns, energy generation from alternative power source has become one of the most important issues in energy policy. Tidal power is one of the alternative energy sources. The tidal range at the Bay of Fundy is the largest in the world (approximately 16 meters). It represents a prime location for harnessing tidal power using the daily rising and ebbing tide.

In this study, a two dimensional finite element model has been developed and applied to simulate the tidal responses, including water level and flow velocity, in the Bay of Fundy region. The simulation results are used to choose the suitable location for energy development and to predict possible energy generated from different types of generation methods.

Fluid motion is assumed to be governed by the shallow water equation since the wave length associated with tide is much longer than the water depth in the Bay of Fundy. By using a real time series of water elevation at the entrance of the bay, the computer model finds tidal response for each node in the study area, which is then verified by the observation record from several tidal gauge stations inside the bay.

This study shows that the at-site cost of the energy for barrage type tidal power plants is around \$0.065 to \$0.097 per kWh at the recommended Shepody Bay, Cumberland Basin, and Cobequid Bay. The cost of energy for the current turbine type tidal power plants is \$0.13 /kWh to \$0.24/kWh at the area with highest current velocity. Compared with the recent bill of the local power company, the at-site unit cost of energy from the barrage type of tidal power plant is feasible, but the

environmental concerns of channel blocking by barrage present a formidable constraint. For the current turbine type of tidal power plant, even the most suitable sites are not financially feasible under current technology, but this type of power generation may become feasible as oil prices continue to increase and more efficient turbines become available.

Chapter 1: Introduction

Energy is one of the major factors influencing the development of modern society. The world underwent an industrial revolution when James Watts built the world's first steam engine in 1765, and with the help of this powerful machine, people were able to grow more food and produce more goods than ever before. Thanks to this continuous progress in technology we were even able to conquer the sky and eventually space. Until now, human life has depended on one type of machine or another, but these machines will be useless without fuel or energy to supply them. Thus, modern society is critically dependent on the existence of an energy supply and the technology to use it efficiently.

The natural resources we rely on, however, will one day be exhausted. The dominant source of energy, crude oil, is estimated to run out within the near future. Compared the amount of proved reserves with annual consumption rate of recent years, crude oil will be exhausted within 40 to 50 years, and the natural gas will last for about 60 years. In order to maintain our modern standard of living and continued societal development, human beings must find other sustainable energy sources to meet the energy demands of the future.

Not only are alternative energy sources critical to the continued societal growth, but our current energy practices have negatively affected the environment, as well. Although the "greenhouse effect" is a natural phenomenon that helps keep the temperatures on Earth at tolerable levels, due to the general use of fossil fuels, the amount of greenhouse gases have increased and enhanced the greenhouse effect. Some believe that this enhancement has caused the average temperature of the Earth to increase, and has altered regional climates. The use of fossil fuels has also more directly impacted society through increased levels of urban air and water pollution.

Renewable energy sources offer an opportunity to save the quickly depleting fossil fuel resources, restore better air quality and ease global climate change. This study is devoted to exploring the use of tidal energy and compares several renewable energy technologies available. It will estimate the physical feasibility of tidal power using a two dimensional numerical model applied to the highest tidal range in the world, the Bay of Fundy, in Nova Scotia, Canada. The financial feasibility will also be presented along with suggested technologies that make this renewable energy more economically efficient. By synthesizing the information available on the physics and economics related to tidal energy and the recent maturity of the related technologies, the developmental prospects will be offered for a renewable tidal energy supply.

Chapter 2: Issues Related to Energy Development

A comprehensive approach of energy development has to consider the social, economic and environmental impacts. One part can no longer be compromised by another. In recent decades, issues about sustainable development and environmental protection have been emphasized in developed and developing countries. With the current trend of rising oil prices, more and more renewable energy techniques are being explored and utilized.

2.1 Sustainable Development

The concept of sustainable development is to meet the needs of the present without compromising the ability of future generations to meet their own needs. Sustainable development guarantees the existence of human society. For decades, the environment has suffered due to some false pretense that the environmental sustainability can only be achieved at an economic expense. From the loss of rainforests to over-fishing, the negative effects on the environment are being felt. This way of development is a burden on the planet and cannot be sustained. When the population of the world continues to increase, the available resources and environmental systems such as water, land and air cannot go on forever.

Other than that, human society still has problems to solve to supply basic living needs. According to Department of Economic and Social Development of the

United Nations, at least one billion people live under the poverty level, without safe drinking water or sanitation. About two billion people have no access to modern energy services. If no action is taken, more species will become extinct and land will turn to desert. Further, exhaustion of our resources, environmental damage due to population growth, and social unbalance will all impact society more as time goes on. We need to face the problems and take action immediately.

Even though the entire of human society has a common future, the request for sustainable development is different from nation to nation even district to district. Conflicts in values usually occur in countries under rapid industrial development where conditions are in transition. The particular conditions relate to the country's history, geography, culture, economy, society and legal system, and the people must work towards not only their own regional goals but common goals as well.

Countries may work on their own democracy and economy by making suitable laws and using advance technology while still pursuing the global goal. In 1992, the Rio Earth Summit articulated this goal as "Think Globally, Act Locally" to initiate local action (Norway's Special Report to Earth Summit+5, United Nations). This report is the follow-up report to the UN General Assembly Special Session, five years after UNCED (the United Nations Conference on Environment and Development, also known as the Earth Summit) in Rio de Janeiro, Brazil. It indicated that local sustainability can be built under the globally accepted value of development, and the local development would be obtained while maintaining sustainable practices. Finally, by integrating all the effort from the local level, global sustainability can be achieved.

Among all the resources, Division for Sustainable Development, United Nations believes that energy is central to achieving sustainable development goals. In order to supply energy for sustainable development, we need to find ways to reconcile this necessity and demand with its impact on the natural resource base. One of the suggestions to achieve this goal from Division for Sustainable Development is to combine and develop advanced, cleaner, more efficient and cost-effective energy technologies.

2.2 Oil Price

Coal-fired energy systems were introduced in the nineteenth century and became popular in most large cities in North America and Europe. The expansion of this technology continued until World War II, when thermal power plants became the major energy source. After the War, the rapid development of the petroleum industry and cheap oil, gas and electricity in North America have played an important part in ordinary life.

The sudden rise of oil prices in the 1970s motivated the development of alternate energy systems. Many heating plants were modified to burn a variety of fuels such as oil, natural gas and garbage, as well as a variety of biomass fuels including woodchips, wood waste and straw. Rising oil prices also increased investments in producing power by other natural resources like wind, solar and tidal energy. However, when oil prices dropped from the peak in early 1980s, the techniques became less economically attractive compared with thermal power plants.

Figure 1 shows the spot price of several oil products (Energy Information Administration, Department of Energy, USA). It lists two types of crude oil and heating oil, compared with conventional gasoline and diesel prices. West Texas Intermediate, WTI, is a crude stream produced in Texas and southern Oklahoma. Europe Brent is produced in North Sea region. Both WTI's and Brent's prices serve as a reference or "marker" for pricing a number of other crude streams. The heating oil prices from New York Harbor or Gulf Coast indicates either spot or futures contracts for delivery in any port city in that category and also represents a reference price. Because of the cost of refinery process, spot prices for heating oil do not show a direct response to changing crude oil prices; they correlate in a long run. Figure 2 is modified by using the spot price of that year divided by the price in 1987. It proves that most of the crude oil refining products' prices can be represented by the crude oil prices.

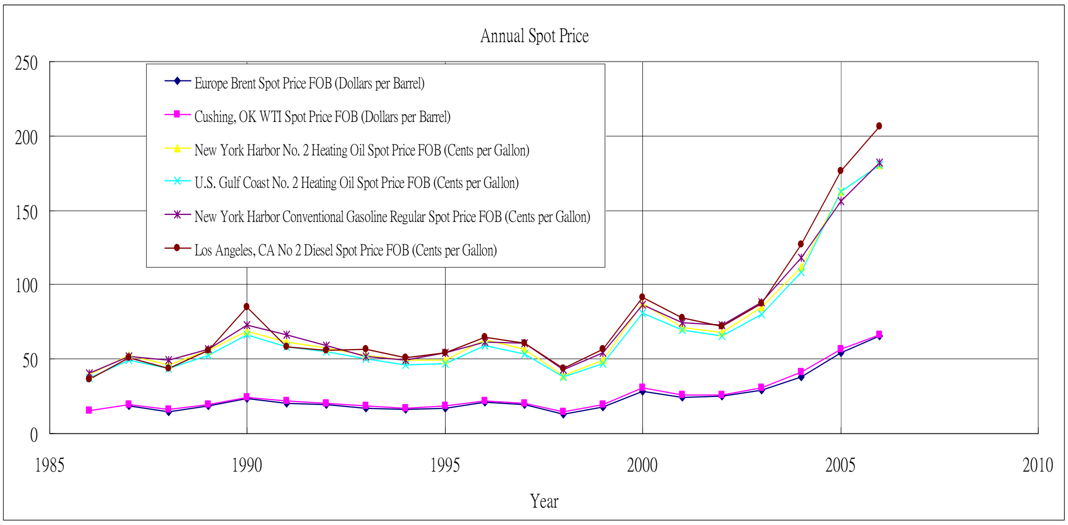

Figure 1: Annual spot price for crude oil products

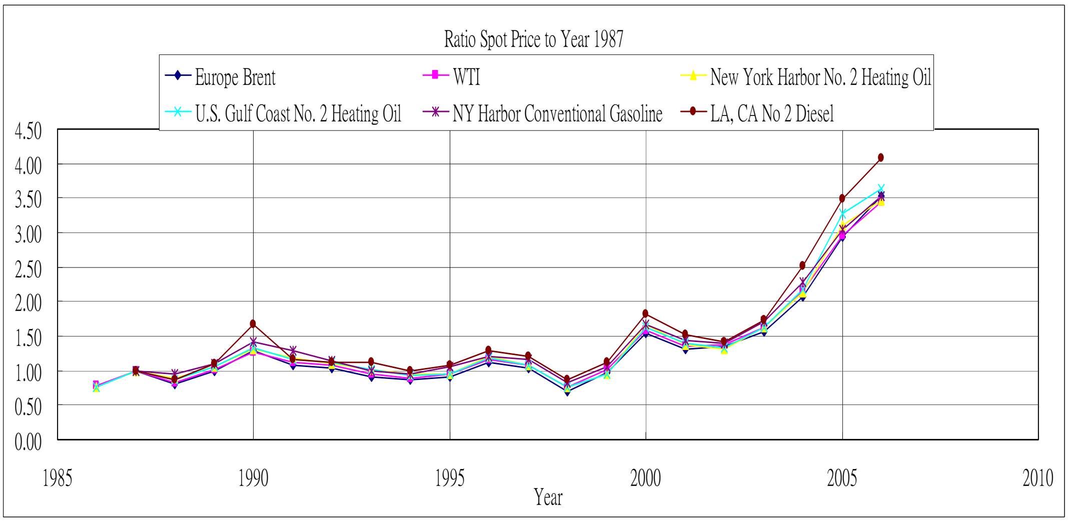

Figure 2: Ratio of spot price of crude oil products to the price at year 1987

In energy feasibility studies, the cost of energy should not only include the recent costs but also the future costs and that depends on future crude oil prices, since fossil fuels are the major energy source. Several studies attempt to estimate future crude oil prices since the 1970 oil crisis. Hubbert (1962) uses an empirical approach based on a bell-shaped curve to model crude oil production in the Unite States. This model predicted a peak of oil extraction in the US and then decline in production. After that, several researchers have used this ideal to predict the evolution of oil production and demand. MacAvoy (1982) and Horn (2004) use the relationship of supply, demand, and reserve amount in the world market as the basic factors to predict future crude oil prices. They use historical data to estimate the future discovery of oil reserves and oil consumption and find the elasticity of demand and supply by varying assumptions. Kaufmann (2005) defines the heating oil prices by crude oil price. They all predict that the energy demand will grow consistently, and the crude oil prices might be as high as $49/barrel by year 2020. Burdette (2005) presents a short term estimation by Energy Information Administration, US, for crude oil prices. He believed that prices would not go higher than $55/barrel by 2007. The predicted prices in these reports appear to be underestimates when we take a look at current crude oil prices, as indicated in Figure 3; however, this number does not account for the recent spike in oil prices and it might be much larger if these researchers' models incorporated recent data. It also indicates that the price prediction model does not fully work with important and vital commodities such as oil, for there are too many factors to be considered.

In Figures 3 and 4, data from year 1985 and earlier come from the New York State Energy Research and Development Authority, in the form of annual oil prices. Data after 1985 comes from the Energy Information Administration, Department of Energy, USA, in the format of weekly average prices. The red line indicates the average of the fifty two weekly average prices in that year, where the vertical bar shows the maximum and minimum of the weekly average prices in that year. For example, in 2006, the highest weekly price is almost 80 dollar and lowest weekly price is a little lower than 60 dollar from Figure 3. In Figure 4, we adjust the spot prices for each data to the constant dollar in 1973 by using inflation factors (Bureau of Labor Statistics, U.S. Department of Labor), and then we can evaluate the price for each year. In Figure 3 and 4, we can see the recent trend is going higher and more expensive since year 2002. We can also find the recent highest oil price is actually more expensive than the highest point in the past (year 1981). That tells us the crude oil price will maintain at this high level or get even higher.

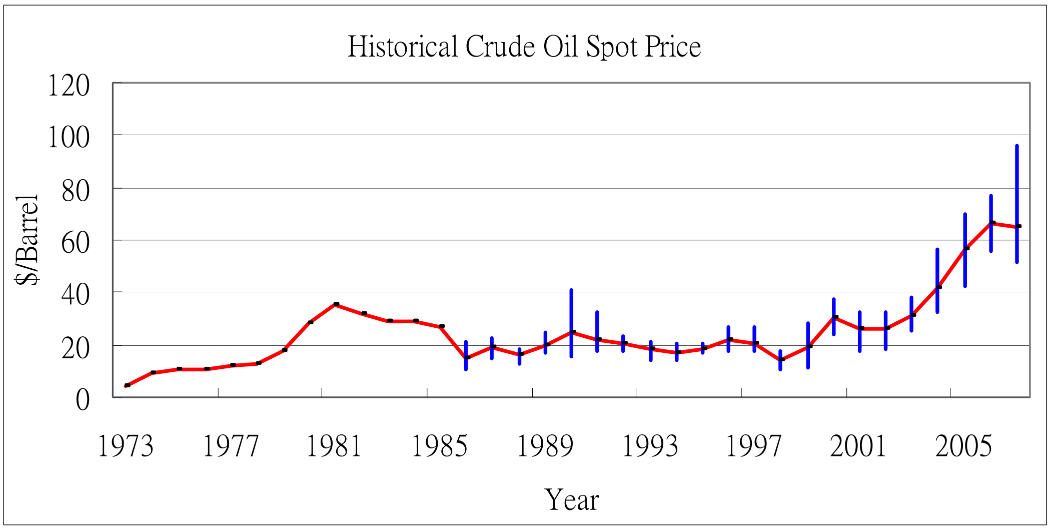

Figure 3: Crude oil spot price
Source: New York State Energy Research and Development Authority
Energy Information Administration, Department of Energy, USA

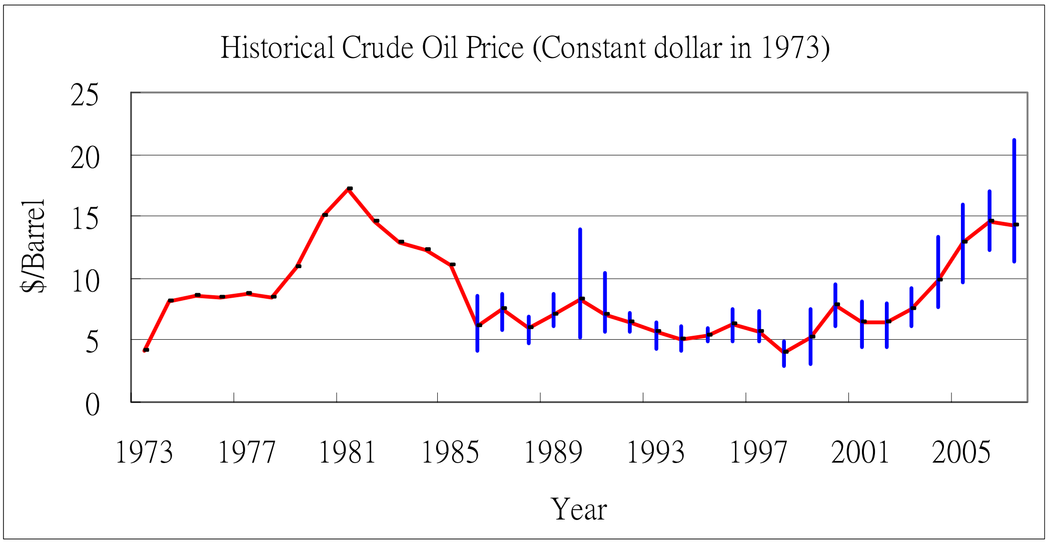

Figure 4: Historical crude oil price as measure by constant dollar in 1973

In order to make a more realistic prediction, the EIA predicts future oil prices in a maximum/average-reference/minimum way in a recent report (International Energy Outlook 2007). Their prediction prices come from one model with three different sets of factors, one set for an average economic situation, one for a very high oil price case and one for a very low oil price case. In this way, its prediction model shows a range of predicted prices. Its result is shown in Figure 5, and the oil price for each barrel is based on the 2005 constant dollar. We can see that the reference case maintains a stable oil price or gets an even lower price in the report's estimation. However, when we compare the recent variation of oil prices with EIA predictions, the high price case will more accurately present the future oil price. If this high oil price assumption becomes real, the price of crude oil will reach 90 dollar per barrel in 2021 and 100 dollar in 2030.

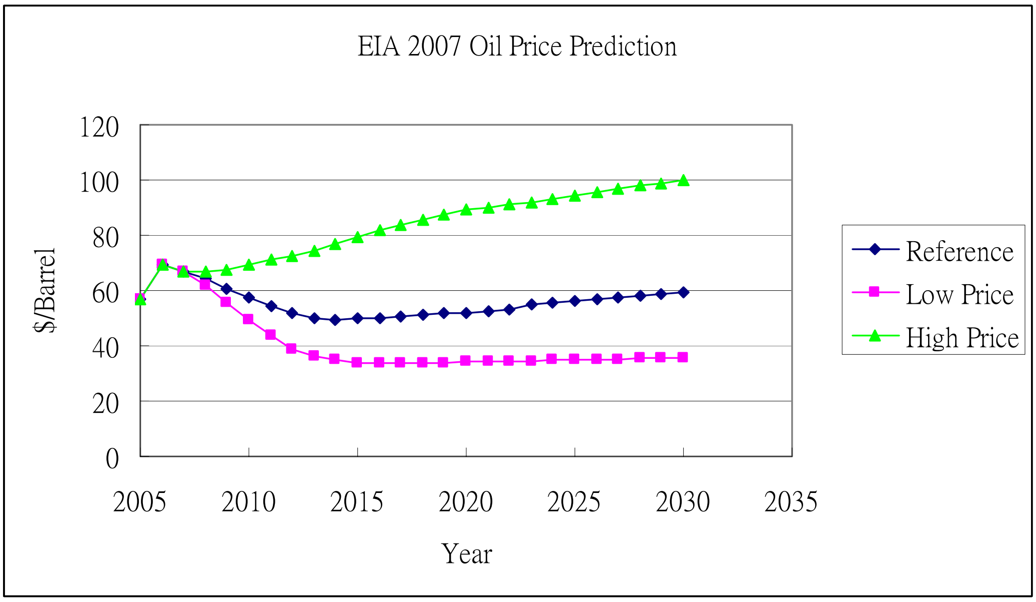

Figure 5: Predict oil price (EIA 2007)

2.3 Crude Oil and Natural Gas Demand and Discovery

Some researchers--Noreng and Tauris (2002), and Abosedra and Baghestani (2004)--doubt the accuracy of the oil price prediction models using past and recent reservation/consumption relationships. They believed that other human behavioral factors, such as OPEC's production constraint and other political issues, influence the resulting demand and production of crude oil and consequently its price. Furthermore, Bentley's (2002) and Laherrere's (2003) studies show that produced crude oil has reached almost half of the earth's reserves (due to recent mining techniques and discoveries) as shown in Figure 6. In this figure, world oil demand since 1970 and the other data after the year 2000 come from the Energy Information

Administration, Department of Energy, USA. The predicted oil demand (both constrained and unconstrained) and new discovery, and natural gas demand and new discovery before year 2000 come from Laherrere's (2003). The unit for crude oil and natural gas is in billion oil-equivalent barrels. The constrained and unconstrained models for oil are simulation results which assume the crude oil demand/consumption for a constrained or unconstrained market, when a constrained market is for some reason under intentional controls by governments or organizations.

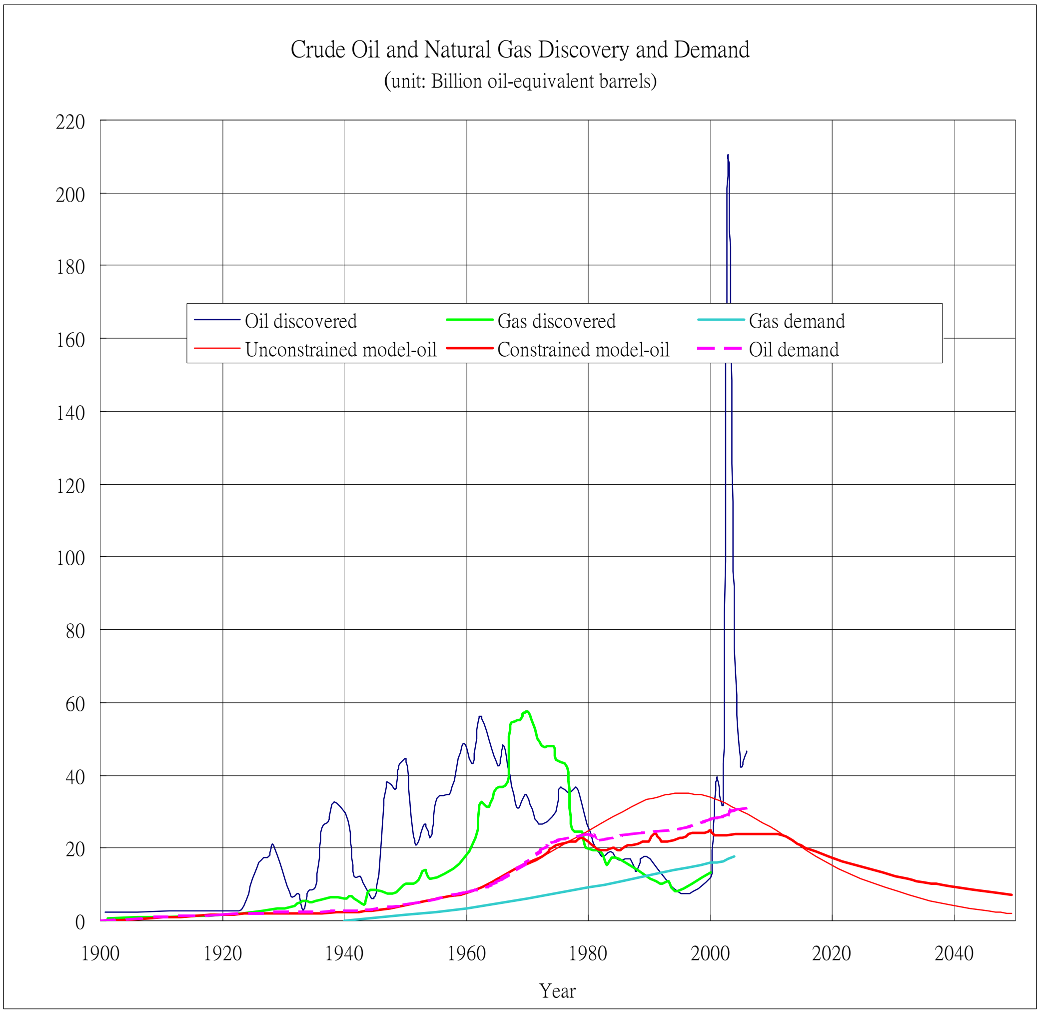

Figure 6: Crude oil discovery and demand

Source: Laherrere (2003) and EIA, DOE

An unconstrained model, like those represented in section 2.2, uses the Hubbert curve and the equation in which the production of oil is a function of the rate of new oil well discovery; a "Hubbert peak" in the oil extraction rate will thus be followed by a gradual decline of oil production. In reality, Laherrere (2000) says that when the economy changes from good to bad, the poorer conditions will reduce oil demand, and crude production will display neither a smooth peak nor an angular high peak, but a bumpy plateau. He believes that an unconstrained model using the simple Hubbert curve can be applied only when there is a large population of fields (such that the sum of a large number of asymmetrical distributions becomes symmetrical), and when exploration follows a natural pattern unimpeded by political events or significant economic factors (for example: OPEC artificially cuts production). Laherrere (2003), in his comments on the article by P. Holberg & R. Hirsch, states that Hubbert assumes that oil needs to be found before being produced and that the production pattern of a country is similar to the discovery pattern. However, discoveries usually occur in cycles, and production is often constrained by demand in most countries. Such examples can be shown in 1979 when world oil production peaked because of the prediction of future high oil prices. In his experience, the results from a constrained model are more realistic in predicting the world production.

Even though Karbuz (2004) claims that it is very hard to work on oil statistics because of the difficulty in defining correct conversion factors, we can see that the recent trend of the rise in oil prices is going to continue. In order to secure the energy supply, governments have to look for alternate energy sources. Bardi (2005) presents on a model in the shape of an oil production curve. In his simulation, the production curve of a non-renewable resource like crude oil will be affected by factors such as a search strategy or improvement of technology. He concludes that the after-peak downward slope might turn out to be steeper than the upward slope for the worldwide crude oil production. That is, the reserved crude oil might run out faster than previously estimated. Such situation would have a significant negative impact on the economy.

How many years will the crude oil left if we keep the consumption rate of today? If we divide the reserved crude oil by the consumption of that year we will have the result shown in Figure 7. The same method gives us the result for natural gas shown in Figure 8. Data for both figures come from EIA. In Figure 7, “Years Left for Crude Oil” is jumping between 28 to 42 years since 1980; on the other hand, Figure 8 shows that we maintain the amount of natural gas for around sixty years usage since the year 1995, with a slow reducing trend. There is decreasing trend for crude oil before 1987 and between 1990 and 2002, but an increase from 30 to 41 years during 1987 to 1990, and 36 to 42 years during 2002 - 2003. It is possible that new discovery is motivated by the decreasing reservation/consumption rate or the increasing crude oil market price. This increased new discovery can be shown in Figure 6, where we can see an off-scale jump in new crude oil discovery at year 2003. Oil shale is one of the examples. It was always slightly more expensive than crude oil as an energy resource and it was overlooked until recent years. When the major energy source price rises to a certain level, people work on developing new methods or technology to harvest energy. When new technologies become feasible relative to the major source, the new energy source will become one of the supports to human society.

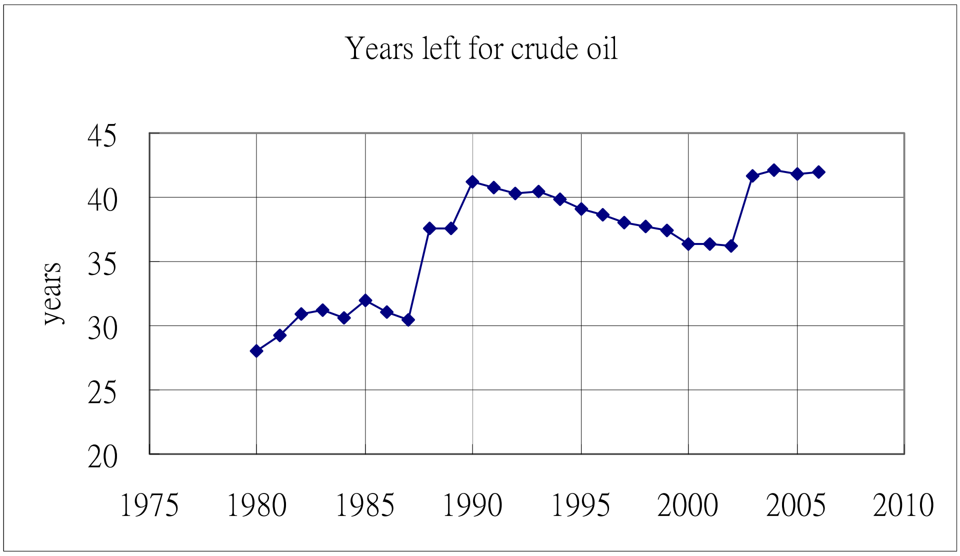

Figure 7: Years left for crude oil

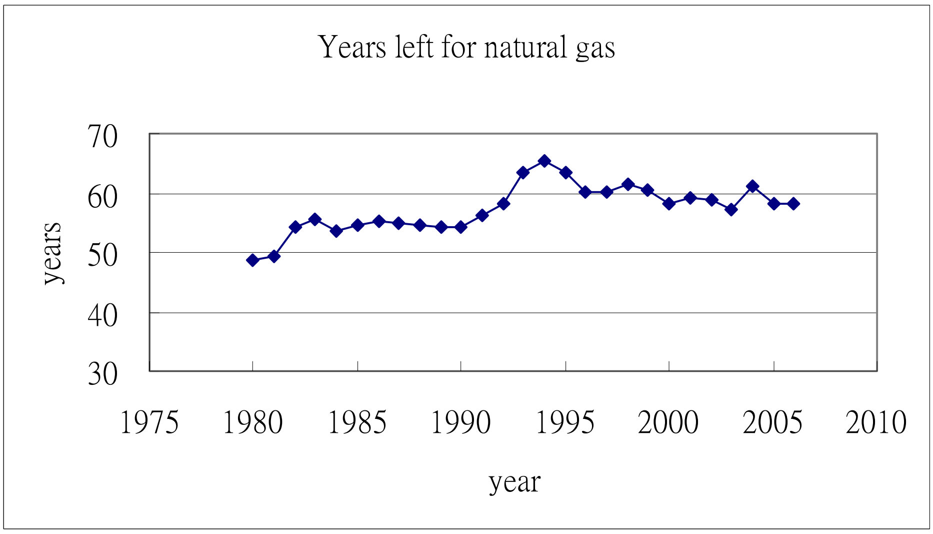

Figure 8: Years left for natural gas

It is noted that the data in Figure 6 are not correlated with the data in Figure 7 between years 1980 and 2000. The difference is due to different data sources: the data in Figure 6 come from Laherrer (April, 2003) and the data in Figures 7 and 8 come from the EIA. Laherrer (June, 2003) states that his research shows a decline in the new discovery of crude oil in smooth five year average curve since 1963 and the annual discovery becomes lower than the annual crude oil production since 1980. He says his result agrees with the results published by J.H. Longwell from Exxon-Mobil in 2002 and government agencies (EIA or other organizations) over-estimated the annual discovery and proved reserves. If what he says is more reliable than government agencies' result, the curve in Figure 7 will be below 30 (years) and go into a decline trend after 1980.

2.4 Environmental Considerations

The extensive use of fossil fuels has caused many problems. The burning of this fuel produces smoke (aerosols) and odor, and increases the well-known greenhouse gases. It is important to note that the greenhouse effect is a natural phenomenon. According to Khilyuk and Chilingar (2004), Earth's climate was determined by the energy radiated from the Sun. This energy heats the surface of the Earth and approximately 30 percent of solar radiation is reflected off at longer wavelengths. The remaining energy is absorbed by the Earth's surface and by the molecules of "greenhouse gases" in the atmosphere which warm the planet. As a result, greenhouse gases help regulate the temperature of the Earth's surface and the lower atmosphere to a level warm enough for natural life. If the concentration of the greenhouse gases increases, more energy will be absorbed to heat the Earth, and finally the climate may change. The process is called the "greenhouse effect." Since we have adopted the use of fossil fuels, the atmosphere has accumulated more carbon dioxide and other anthropogenic gases. Many people believe that the presence of these additional gases has increased the rate of heat absorption of the atmosphere, and thus increased the temperature of the Earth's surface. Khilyuk and Chilingar do not agree that the temperature increase is solely caused by the human-induced carbon dioxide. However, human activities do produce air pollution and certain anthropogenic gases have even damaged the ozone layer at higher latitudes and increased the intrusion of the radiation from the Sun. For example, according to EIA, DOE, carbon dioxide emissions from the consumption and flaring of natural gas are from 3.1 to 5.6 billion metric tons, and emissions from petroleum oil are from 8.8 to 10.8 billion metric tons around the world every year (from 1980 to 2004). The pollution caused by the consumption of oil or natural gas is a cost associated with energy production.

	Energy Source	Environmental Cost	Basic Cost	Total Cost
		cent/kWh	cent/kWh	cent/kWh
Traditional	Coal (1.2% sulfur)	5.7	3.1	8.8
	Coal (1.1% sulfur,AFBC)	2.8	3.1	5.9
	Oil(2.2% sulfur)	6.7	3.9	10.6
	Oil(1% sulfur)	3.8	3.9	7.7
	Natural Gas	1.0	6.1	7.1
	Nuclear	2.9	2.8	5.7
Renewable	Waste Energy	4.0	3.6-7.2	7.6~11.2
	Solar	0.4	6~8	6~8
	Wind	0.1	5~7	5~7.1
	Biomass	0.7	4.6-7	4.6-7.7
	Hydro	0.2	3.6-7.2	3.6-7.4
	Geothermal			5.7~7.5

AFBC = Atmospheric Fluidized Bed Combustion
Source: Bureau of Energy, MOEA, Taiwan(May, 1999)

Table 1: Environmental cost for energy sources

Table 1 shows an estimation of environmental cost per unit energy from different sources. In this table, basic cost is the production cost without the concern of environmental impact during the development of energy, including the cost for civic work, mechanical and electrical equipment and installation, indirect expenses and contingency, and maintenance. We can see that for traditional types of energy development, environmental cost plays a significant part in the total cost, even though it was usually not considered in a feasibility study ten years ago. On the other hand, renewable energy--except waste energy--consumes minor environmental costs. Although the generation of energy from waste causes some environmental concern, it actually helps to process waste and benefits to the environment. In a sense, renewable energy is competitive with traditional resources if environmental impact is considered.

After the passing of the Kyoto Protocol, the countries which have ratified the Protocol have agreed to reduce the world's carbon dioxide emissions below 1990 levels by the year 2012. The Protocol is an indication of the international effort to minimize human influence on the environment. In fact, it is critical for public health, and in helping to protect the natural environment while achieving sustainability. Regardless of whether they signed the protocol or not, many countries make an effort to follow the spirit of the treaty and declare sincere intention internationally, and to promote green energy and the concept of sustainable development for their people, and in turn to increase their competitiveness globally.

In addition to the Kyoto Protocol, countries are imposing restrictions on imported products if the products damage the environment by their materials or by their manufacturing processes. For example, European countries inspect the source of their imported electronic products. Thus, even products excellently designed may be barred from importation into Europe if they do not meet the required standards in the European Union by 2010.

The international trend is toward promoting "zero waste." Instead of spending money to process waste, some countries invest in reusing or recycling the waste, and produce more job opportunities. For example, New Zealand and the EU have both proposed the target of zero waste by 2020, so has the American State of Georgia. Meanwhile, Australia's capital city, Canberra, intends to achieve that goal by 2010 (Zero Waste New Zealand Trust.) By contrast, Taiwan's goal is to achieve a waste level of that is 60 percent of their 1988 level by the year 2010, and to reduce it to 70 percent of the level by 2020, according to Yu Shu-wei, director of the Center for Environmental, Safety and Health Technology Development of the Industrial Technology Research Institute of Taiwan. This goal can be achieved by modifying the waste handling and recycling methods as well as the initial product design standard. The Taiwanese government plans to use three environmental technology parks and a budget of US$149 million for industries targeted at energy recycling and environmental protection-related products. (Industrial Technology Research Institute of Taiwan)

The World Commission on Environment and Development points it out that the crises with the environment, economic development and energy are related. It argues that "they are not separate crises: an environmental crisis, a development crisis, an energy crisis. They are all one" (April, 1987). According to this statement, we can solve the energy crises while working the environmental and developmental problems, as well.

In order to save energy, to enhance air quality, and to ease global warming and climate change, we should look towards using renewable or 'green' energy.

Governments set up plans to promote green industries by encouraging them to adjust their structures and develop environmentally friendly, innovative, value-added enterprises. Governments define new regulations, help the exchange and flow of information, technological research and development. They also offer a sound financial system for raising capital and recruiting talent to nurture start-up green businesses. These efforts call for close cooperation between business and governments, and with this joint effort, the development of green energy can be more reliable in the near future.

2.5 Renewable Energy

The recent upward trend in the price of oil and natural gas has caused many countries to reflect on the finite nature of fossil fuels and to take another look at renewable sources. They are discovering that renewable energy technologies are much better developed and reliable than those in the early 1970's.

Several natural resources have been studied for hundreds of years. Other than producing energy by burning fossil fuel or nuclear reaction, energy generated from technologies and renewable resources such as the Sun, wind, hydropower, the Earth's natural heat and biomass. Because they provide energy that is renewable, and produce less pollution, they are also called green energy.

Scientists have been developing techniques to harvest energy from natural sources. For example, people build dams to accumulate water and transform the hydropower to electric power, and the watermill has been used for centuries, to irrigate farmland or grind barley. People also build windmills using wind energy, and in the twentieth century, have adapted the design to incorporate electric power generators. To make use of solar radiation, buildings are designed so that the passive solar energy is used for lighting and heating. Some design features include large south-facing windows, materials that absorb and slowly release the Sun's heat, and solar heaters to heat either water or a heat-transfer fluid in collectors. Photovoltaic solar cells, which were developed along with the space program and are made of semi-conducting materials, directly convert sunlight into electricity. Similar to the simplest cells used to power watches and calculators, the more complex systems can light houses and even provide power to the electric grid.

Biomass technologies use renewable biomass resources to produce energy-related products. The term "biomass" represents any organic matter available on a renewable basis. For example, trees, agricultural food and feed crops, agricultural crop wastes and residues, municipal wastes, and other waste materials can be used to provide heat, chemicals or other energy products, including electricity, liquid, solid, and gaseous fuels. Biomass technologies provide a way to use renewable energy in a solid or liquid form for transportation purpose. The two most common bio-fuels are ethanol and bio-diesel. Ethanol, an alcohol, is made by fermenting high-carbohydrate biomass, like corn, and is mostly used as a fuel additive to cut down on a vehicle's carbon monoxide and other smog-causing emissions. Bio-diesel is made from vegetable oils, animal fats, algae, or even recycled cooking greases, and works either as diesel additive to reduce vehicle emissions, or to fuel a vehicle by itself.

Biomass energy can be converted to electric power by direct-combustion technology. According to U.S. Department of Energy, with ten giga-watts of installed capacity and three percent of the primary energy production, bioenergy is just second to hydropower in renewable U.S. primary energy production in the United States.

Geothermal energy is the heat extracted from the Earth. It comes both from the shallow ground, such as hot water or hot rock found within a few miles beneath the Earth's surface, and from even deeper levels, the extremely high temperatures of the molten rock called magma. Geothermal energy technologies use the heat of the Earth for direct-use applications, geothermal heat pumps, and electrical power production. For example, given a heat exchanger, a family can attach a heat pump and transfer heat to the indoor air delivery system in the winter, and reverse the process in the summer. Additionally, large underground reservoirs of hot water or steam, which are heated by the magma underneath, can be captured for electrical power production.

Zarnikau (2003) introduces several studies and also conducts a survey himself about the consumer responses concerning the willingness to pay for electric utilities generated by green resources. For an increase of \$3 to \$12 per month, many residential energy consumers in the United States are willing to pay for minimal environmental impact. More than 50% of consumers agree to pay at least $1 extra toward their monthly electric bill for green energy. He also suggests that intensive exposure to energy resource issues lead to an increased interest in paying modest premiums to support utility investments in renewable energy and/or energy efficiency.

In order to reduce greenhouse gas production and create a wider spectrum of available energy resources, more government energy agencies must offer policies suitable to promote renewable energy systems (Hass, 2004). Those policies may come in the form of tax credits, guaranty selling tariffs, or reduced loan interest rates on a variety of renewable energy systems. These policies will reduce the cost and risk to whomever invests in the new energy system, as well as promote more project possibility and encourage public acceptance and involvement.

This study will focus on the technology to harvest the energy from tides.

Chapter 3: Tide and Tidal Energy in Bay of Fundy

3.1 Tide

The Moon has been rotating around the Earth and the Earth has been rotating around the Sun. As the Moon and the Earth rotate around the Sun, these celestial bodies experience mutual attraction forces thus causing the Earth's water to rise and fall in a periodic manner. The tide is the composed of longest ocean waves and usually rises and falls every half day or a day. The flooding period is when the tide rises and water flows into the coastal basin, the reverse is the falling tide, it is also called the ebb tide. Tidal flow is usually considered a coastal phenomenon because it is noticeable by an observer in reference to the coast or other landmark. Thus, an observer will describe a tide "flow in" during flood tide and "flow out" during ebb tide. The change of water level due to tidal current occurs everywhere in the sea. However, the change is most significant in the coastal zone due to the shallower water depth in the coastal region.

The relationship between the cycles of the Moon and the tide has been known since ancient times. High tides are highest and low tides are lowest when the Moon is full or new, respectively. Additionally, the time of high tide and low tide is usually related to the location of the Moon relative to the Earth. The Sun also has an effect on the tide, even though it is not as dominant as the influence of the Moon. After the publication of Issac Newton's "Principia" people knew more about the relationship of tides and the Earth-Moon-Sun system. According to his theory, tides on Earth are produced by the force of gravity from a massive astronomical body, like the Sun or Moon, on large bodies of water. Depending on the location at the Earth's surface, the force moves the water to form a flood or ebb tide.

Brown, et al (1999) explains the concept of tide-producing force. The tide-producing force at any point is a combination of gravitational force and centrifugal force. Although the Sun's mass is much larger than the Moon's, the Moon is much closer to the Earth, and the variation in the Moon's force across the Earth's diameter is about two times larger than the variation in the Sun's force. Thus, the influence of the Moon is considerably larger than that of the Sun. However, the pair of forces aligns and combines to produce "spring" tides when the Moon is new or full, and became unaligned to produce "neap" tides when the Moon is at first or third quarter. To describe the strength of the tide, the difference in water elevation between high tide and low tide is called the tidal range. Another factor having a substantial influence on tidal ranges is the elliptical shape of the Moon's orbit. Although the Moon is only 9 to 14% closer at its close point to Earth (perigee) than at its far point (apogee), the gravitational force is inversely proportional to the square of the distance. Adding up the centrifugal force in this Earth-Moon system, we can show that the tide-producing force at one point on Earth is proportional to D^{-3}, where D is the distance between the position at the Earth's surface and the Moon, and the Moon's tidal influence is 30 to 48% greater at perigee than at apogee. In some locations, where there is a large tidal range, we can observe that the perigee-apogee influence of the Moon is greater than the spring-neap influence. Although the variation of the Moon's distance is not readily apparent to observers viewing the Moon directly, at certain locations, the large increase in the vertical tidal range makes it obvious when the Moon is near perigee.

The position of the astronomical bodies relative to the Earth is periodic, as is the influence of these bodies. In most locations, the tide rises and falls twice per day, and called the semi-diurnal tide. Dronkers (1964) indicates that in part of the Gulf of Mexico, the Gulf of St. Lawrence, the Indonesian Archipel, and the Chinese Sea, the tides are irregular and diurnal during part of each month. In order to predict a tide at a specific location, a harmonic method is developed. The harmonic method is the most common method of predicting tidal high, and gets acceptable results. It is based on the concept that the tide is the summation of the partial tides, and each partial tide has its own period which corresponds to the period, or some component, of certain astronomical movements, like Sun to Earth, Moon to Earth, or all three together. For a specific point along either the coast line or the middle of sea, each partial tide has a particular amplitude and phase. The phase represents the fraction of the partial tidal cycle that has been passed at a reference point in time. Depending on the period of component tide producing the force, strength and lag of the cycle at the certain location, we are able to define the period, amplitude and phase for the specific partial tide. By adding a great number of partial tides, the user gets a wave form which is closer to the observed tide at a particular location. The accuracy of the wave form is increased when more partial tides can be included in the sum, if the record is sufficiently long to analyze the factors of these partial tides.

In order to get better results on tide predictions for important locations, including the harbors, the amplitude and phase must be determined for as many as possible partial tides. This usually requires a long history of observed tidal records covering about 400 harmonic constituents which have been identified. Such a long record is difficult to obtain and analyze to retrieve all the harmonic constituents. Since some of the astronomical motions have a larger effect on tidal flows, a relatively good approximation can be achieved by adding only a few major tide components. The following table shows the most important partial tide for most locations, including four semi-diurnal, three diurnal and two longer-period components.

Tidal Component		Symbol	Period (hours)
Semi-diurnal:	Principal lunar	M2	12.42
	Principal solar	S2	12.00
	Larger lunar elliptic	N2	12.66
	Luni-solar	K2	11.97
Diurnal:	Luni-solar	K1	23.93
	Principal lunar	O1	25.82
	Principal solar	P1	24.07
Longer Period	Lunar fortnightly	Mf	327.86(13.66 days)
	Lunar monthly	Mm	661.30(27.5 days)

Table 2: Major tidal components

Water elevation (η) can be represented as the following equation, assumed it is a sum of all the partial tides:

$$\eta = \sum a_i \cdot \cos(\frac{2\pi}{T_i} t + \arg - \phi_i) \qquad (3.1)$$

where arg: tide argument

ϕ_i : phase angle

T_i : period of each tide component

a_i : amplitude of each tide component

Among all the tidal components, M2, S2 of semi-diurnal partial tides and K1 of diurnal tides are the most significant, since the amplitudes of these three tide components are usually greatest and dominate the observed tides. However, there are other factors which affect the propagation of tidal waves, and any one of the tidal components may be dominant.

In addition to astronomical factors, the tides on Earth are strongly influenced by the sizes, boundaries, and bathymetry of the costal basins and inlets. Typical tidal ranges are about one or two meters, though there are regions in the oceans where various influences cooperate to produce virtually no tides at all, and other regions where the tides are greatly amplified. There are several locations where large tidal ranges are observed: the Sea of Okhotsk and Korea's west coast on northwest of Pacific Ocean, the northern coast of Australia, the Bristol Channel on the west coast of England, the Ungava Bay in northern Quebec, Canada, and the Bay of Fundy between New Brunswick and Nova Scotia. The tidal ranges in these regions are of the order of ten meters.

The highest tides on Earth occur in the Minas Basin, located at the eastern extremity of the Bay of Fundy, where the average tidal range is 12 meters and can reach 16 meters when various high tide-promoting factors occur concurrently.

3.2 The Bay of Fundy

Figure 9: The Bay of Fundy

Source: http://www.all-science-fair-projects.com/science_fair_projects_encyclopedia/Bay_of_Fundy

The Bay of Fundy is located northeast of the state of Maine, between New Brunswick and Nova Scotia, Canada, and is made up of two sections in the upper zone: Chignecto Bay and Cobequid Bay (see Figure 9). It covers 620 square kilometers (239 square miles), including 168 square kilometers (65 square miles) in Minas Basin, Nova Scotia and 50 square kilometers (19.5 square miles) in Shepody Bay, New Brunswick. The region is mostly intertidal mudflat and salt marsh around the head of the Bay of Fundy, where tides rise and fall over 12-15 meters (36-45 feet) twice daily. Sediments range from coarse sand to fine silt and clay (Museum of Natural History, Nova Scotia). Most of the salt marshes have been drained for agriculture.

Minas Basin, the northeast arm of the Bay of Fundy, is famous for being the highest tidal range in the world. Bishop introduces a view of the surrounding area. Wolfville, located on the southern shore of Minas Basin, offers the most dramatic views of the tidal rise and fall, including vast areas of sea bottom uncovered by the falling tide. These extensive intertidal mudflats provide a rich source of food for many shorebirds in these areas. However, since the seventeenth century, Acadian settlers have moved in and built dykes to convert tidal flats into rich farmland and many of the original flats now lie behind man-made dykes. A tidal bore forms as the incoming tide flows upstream against the freshwater of the river, and tumbles upstream in some of the rivers which flow into Minas Basin (e.g. the Meander River near Windsor, east of Wolfville, and the Shubenacadie River and Salmon River near Truro).

The most significant tides or current activities are found around Cape Split. It is located on the southern side of the entrance to Minas Basin, and, at its maximum flow, experiences turbulence of the waters surging over the submarine ridges below for a considerable distance. This maximum tidal current exceed eight knots (4m/s), and the flow rate thru the deep, five kilometer-wide channel on the north side of Cape Split is about four cubic kilometers per hour. This kind of current repeats itself about three hours later in the opposite direction. In total, almost 14 billion tons (14 cubic kilometers) of muddy sea water flows into and out of Minas Basin every six hours.

The primary cause of the immense tides at the Bay of Fundy is a resonance of the Bay of Fundy-Gulf of Maine system at the tidal period. The area is bounded to the north by the edge of the continental shelf and gradually increases in depth. Researchers believe that the system has a natural period of approximately 13 hours, which is close to the 12.42 hour period of the dominant lunar tide (M2) of the Atlantic Ocean.

3.3 Tidal Power Development in Bay of Fundy

Given the significant tidal range, the Bay of Fundy is considered one of the premier locations for the development of tidal power. Other than the 16-meter tidal range, the surrounding environment and the social economic development of the region are also encouraging the use of this green energy:

- *Favorable topography*

  By the curving coast line and narrow channels, a tidal power plant can be built with a relatively shorter barrage, minimizing the cost of construction.
- *Predicted energy shortages*

  The surrounding area is not heavily populated, but it is estimated that the population will grow significantly in the near future and increase the energy demand further and in turn require new energy supply resources.
- *Most hydroelectric potential has been developed*

  There are several rivers in the surrounding area with steep channels, which have been suitable in yielding cheap energy through hydroelectric power plants. Most of the hydro resources, however, have been developed and can not supply the extra energy needed in the future.
- *Rising fuel cost*

  In order to supply extra energy for the expected growth, The Bay of Fundy and the surrounding area would need more fire power plants and heating oil if a new energy source were not developed.

The government of Canada and the provincial governments of New Brunswick and Nova Scotia began a comprehensive investigation in August, 1966 to analyse the feasibility of developing a large scale tidal power plant in the area of the Bay of

Fundy. The investigations were reported by the Atlantic Tidal Power Programming Board (ATPPB), and concluded that, although technically feasible, the proposed tidal power plants could not exploit energy at a competitive cost to energy from traditional sources. But the Programming Board also suggested that further studies should be required when one or more of the following situations occurred, making a tidal power plant economically feasible:

(i) the interest rate of construction loan drops sufficiently;

(ii) there is a major breakthrough in construction costs or in the cost of generating the necessary equipment;

(iii) pollution abatement requirements magnify the cost of using alternative sources of power;

(iv) alternative sources or more economic power supply become exhausted.

In February, 1972, when the cost of energy supply increased, the governments of Canada, New Brunswick and Nova Scotia established the Bay of Fundy Tidal Power Review Board (FTPRB) to make a critical review of the findings of the ATPPB. FTPRB also recommended procedures for an appropriate reassessment of economic feasibility.

The Review Board completed its preliminary study in September, 1974 and indicated that tidal power had become significantly more economically competitive since the 1969 report (FTPRB 1974). The Board's major concerns were based on the significant changes in the international price of fuel oil and the trends in power system development. Other than the requirements for a financial feasibility, they also noticed additional merits that might attract tidal power development, such as reduced air/water pollution and better energy management by reduce fossil-fire energy production. Reductions in fossil-fired energy production would reduce atmospheric and water pollution and increased oil and gas reserves which could be diverted to more critical uses. However, the report also mentioned that the transmission facilities were needed to support a tidal power project and more interchange of power within and between power systems of eastern Canada.

Upon the recommendations of the Review Board, the governments of Canada along with New Brunswick and Nova Scotia agreed in December, 1975 that it was in the public interest for further investigation on the tidal power energy resource in the Atlantic region and authorized a series studies. These studies were divided into two phases. Phase I consisted of a series of technical and economic assessments aimed at determining the competitiveness of tidal power and Phase II would include more in-depth technical, environmental, economic and financial assessments of those projects selected from Phase I. However, Phase II was planned to proceed only if Phase I studies returned a positive project prospects. Both Phase I and II studies included assessments of environmental implications, resource availability and related socio-economic level of the surrounding area.

The Phase I studies required parallel consideration of five major interdependent tasks. The tasks included:

1. Tidal power plant design;
2. Tidal power generation;
3. Market and system analysis for supply and transmission;
4. Socio-economic aspect;
5. Environmental aspect.

Within Phase I, all five tasks went through parametric interact analysis. At first, tidal power plant and generation process was designed and compared to prospective tidal power sites and schemes. They then used preliminary aspects of system and market analysis to calculate the "at-site" and "at-market" costs of tidal energy and systems costs, compared with displaceable energy from alternative sources. By presenting the potential energy production and cost comparison, the studies provided a progressive screening of tidal sites, and limited the possible sites/design to a manageable number of representative projects for further analysis. Finally, the environmental impact and social-economic aspect were studied for the representative projects.

The Phase II studies, which were conducted given the economic competitiveness of tidal power, were suggested to provide further review, and to help optimize the most favorable project. The studies produced two economically viable sites--the Cumberland Basin and Cobequid Bay--with the potential of producing up to 6,000 megawatts of economic electricity, based on the assumptions made.

Eventually the process was held up in the “review” phase and no project was ever constructed. Because the proposed project was using the barrage type of design (to be discussed later) for the tidal plant, the large construction fee for the barrage and the large amount of capital investment required was the major reason for delaying the project. As it turns out, the development of barrages for the generation of tidal power is considered potentially hazardous to the surrounding ecosystem. At the landward edge of the barrage, water supplies, flooding, drainage and tidal estuary water quality could be affected. Additionally the new tidal regime, with a higher mean headpond level, could decrease the dyke stability. Reduced tidal mixing in estuaries behind the barrage may also accelerate water quality deterioration. Gordon and Dadswell (1984) presents a report on the tidal power developments study at the Cobequid Bay site, which is supported by the province of Nova Scotia. It indicated that the tidal power developments will drastically alter tidal oscillation patterns and, since then, no proposals have been under active consideration. Shepherd, et al. (1995) writes that the long-term changes in sediment quality and distribution, which were due to the construction of a causeway across the Petitcodiac River in Moncton, may have contributed to the change of invertebrate fauna in the intertidal mudflats in that area. As a result of studies similar to this, the Canadian Wildlife Service and the New Brunswick Department of Natural Resources & Energy prepared a Protection Plan for the New Brunswick and Nova Scotia sections of the Bay of Fundy Shorebird Hemispheric Reserve. These plans concentrate on protecting important shorebird roosting and feeding sites and surrounding lands. The environmental aspect and ecopolicy finally delayed the development of tidal power.

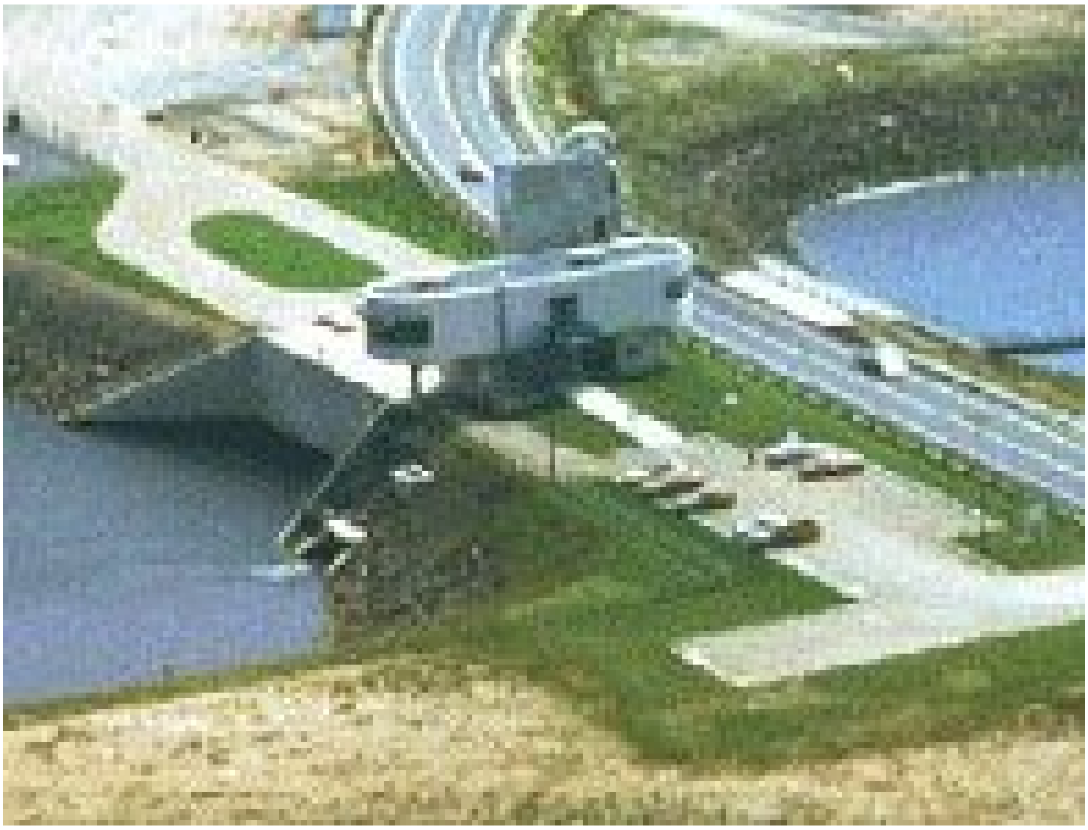

Figure 10: Annapolis Tidal Generating Station

(www.annapolisroyal.com)

Although the large-scale tidal power plant discussed above has not yet been successful, the Annapolis Tidal Generating Station located in the southeast region of the Bay, was completed in 1984 (see Figure 10). It is one of three tidal power plants in the world, and the first and only modern tidal plant in North America. It uses a twenty-megawatt straflo turbine, the largest in the world, to produce power for 4,000 homes, or roughly one percent of Nova Scotia's electrical power capacity. It was a pilot project sponsored by the provincial and federal governments designed to explore the potential of harnessing energy from the sea.

The reason of the Annapolis Tidal Generating Station was environmentally successful is because it made use of a pre-existing causeway to form a headpond, and uses the water stored in the headpond to generate power. Margaret Murphy, of Nova Scotia Power, reported the good, uninterrupted sustainable performance of this plant, but she also indicated that Nova Scotia would never build a tidal project like the one at Annapolis Royal because of the environmental concerns.

The concerns about tidal power development however, are all related to the barrage type of tidal power generation. The characteristic problems of barrage-type projects are the inevitable disconnected pathway and its environmental/ecosystem impact. Other concepts to develop tidal power are being studied, such as using the kinematical energy from tidal currents, as opposed to the potential energy used in barrage-type projects.

3.4 Types of Tidal Energy Development

There are two major types of tidal power plant design: the barrage type, using a dam to divide a basin to be a headpond in order to store water and harvest energy from the potential energy from the water; and the turbine type, deriving energy from kinematical force in a tidal current.

3.4.1 Barrage Type of Tidal Power Plant

The barrage type of tidal power plant, like the one at Annapolis, works like a river hydro power plant, with some differences in the activating forces. For example, in a river hydro power plant, the downward-acting terrestrial gravitation causes the water to flow on the Earth's surface, whereas with barrage tidal power plants, the upward-acting lunar gravitation causes oscillations in the estuaries. Additionally, there are differences in the hydraulics, machinery design and construction between these two types of development. The power and energy, however, can be developed at any tidal site or river dam depending upon the usable head which varies continuously, the area of the basin, the capacity of the sluiceways used to fill or empty the basin, the capacity of the generating units, and the method of operation.

3.4.1.1 Single Effect Operation

With a single basin or headpond, the sluices are closed until sea level reaches a certain head range above the basin. Flow is then permitted through the turbines, generating power. This is the simple operating principle of the old tidal mills and is known as "single-effect" operation since power is generated in only one direction (see Figure 11). To maximize energy production from a single-effect operation, energy is typically generated on the ebb-tide instead of flood tide, when water flows out of the headpond, because higher head range can be achieved in the upper level of the basin.

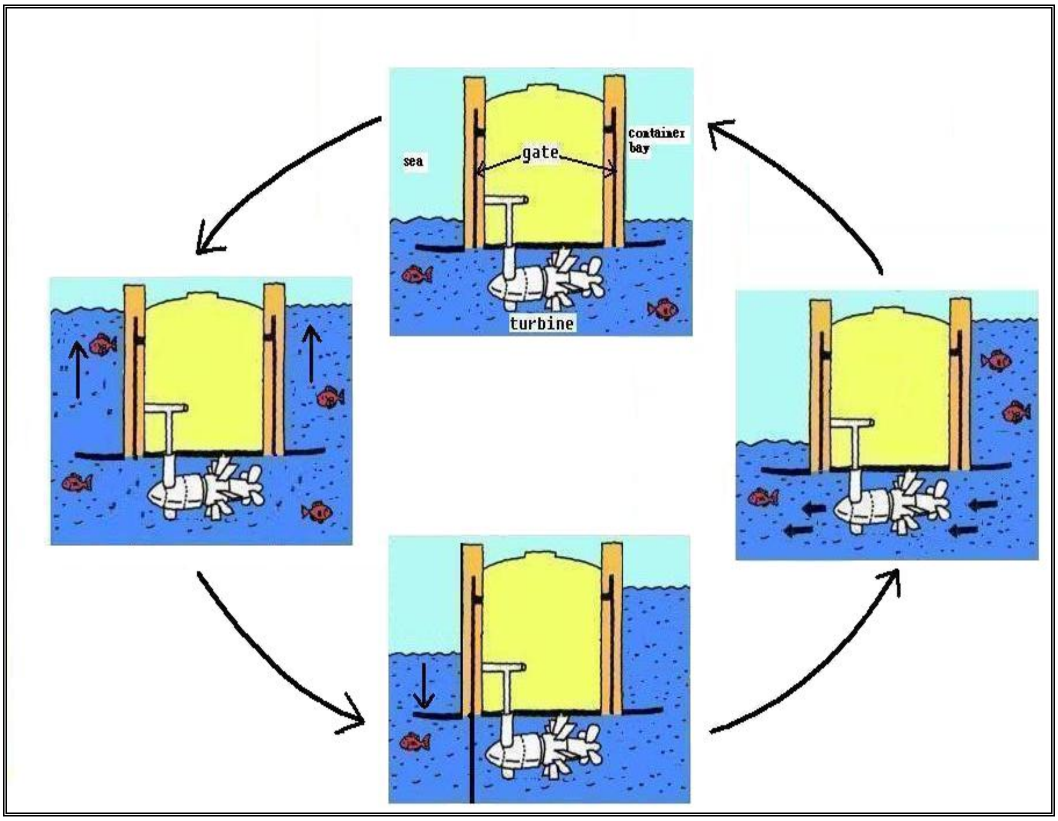

Figure 11: Single Effect Operation

The energy output of this simple scheme can also be improved by pumping water at appropriate times. For example, the water level of the basin can be raised by pumping so that the basin stores more water with higher head, and then the energy output can be increased. If the turbines are also designed to act as pumps, the pumping operation works at or near high tide, while the basin is being filled through the sluices, and for a short time after they have been closed. This way, little energy is needed to lift the water from sea level to headpond near high tide, but a larger amount of energy can be generated by the extra water with the larger head. Similar, the level of the basin can be lowered further by pumping water from basin to sea at or near ebb-tide. This would create additional filling capacity which would be advantageous if energy were being generated as the basin was being filled. It will be more profitable if such pumping is done during hours when relatively low-cost energy is available from the power system.

3.4.1.2 Double Effect Operation

Turbines can be designed to operate not only in the basin-to-sea direction, but also in the sea-to-basin direction, in addition to operating as pumps in either direction. Thus, energy can be produced from the flow in both directions: during the emptying and filling operations (Figure 10). The tidal power development installed in the La Rance, France, possesses these capabilities. This plant is a "single-basin" development with "double-effect" generation and "double-effect" pumping. Such an operation is illustrated in Figure 12 for comparison with the "single-effect" operation.

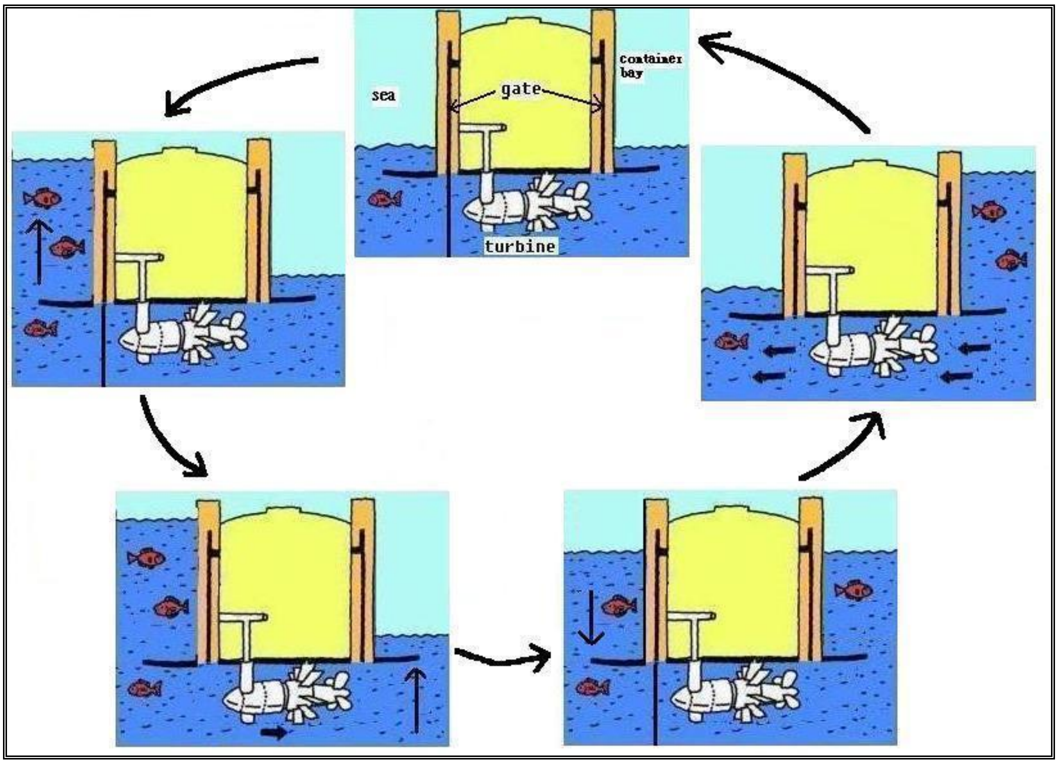

Figure 12: Double Effect Operation

3.4.1.3 Single Basin or Multi-basin

The barrage type of plant can use single basin or two basins. Civil works for the single-basin scheme are less complex and a shorter barrage can be constructed thus making the project less costly. However, the single-basin concept of development cannot produce firm capacity as the period of generation is limited by the times of the tides which vary from day to day. It is possible that such a system could be generating power at the time of low demand and low price.

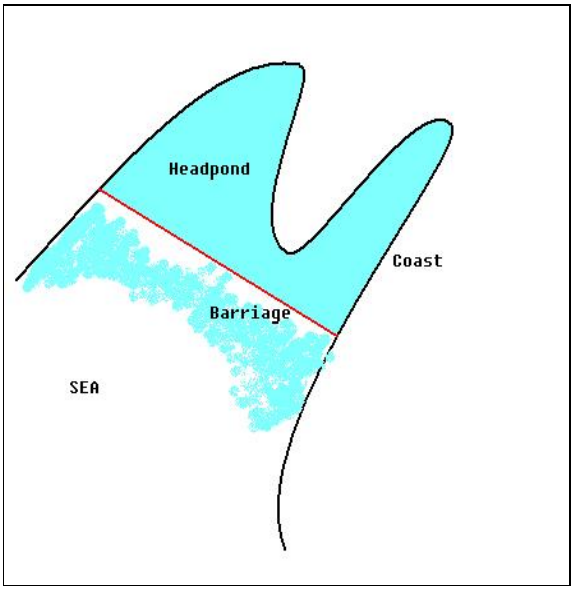

Figure 13: Single Basin

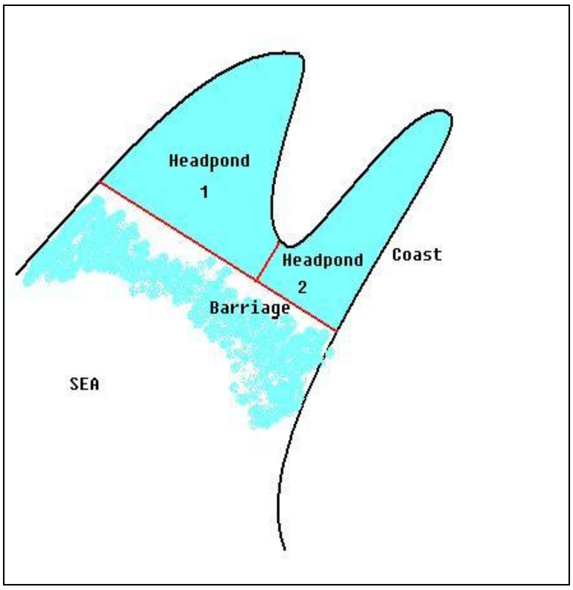

Figure 14: Double Basin

The problem of discontinuous energy output from a single-basin scheme (Figure 13) can be overcome by the two-basin design. This development concept (Figure 14) is possible when the coastal configuration is favorable to the creation of two basins. The water level in the larger basin is held high and that in the other, low, with generation always from the high to the low basin. The high basin is filled during high tide through one set of gates, and the low basin emptied during low tide through another set of gates. The major attraction of such a linked-basin arrangement is its ability to generate continuous energy. A major drawback, however, is that the energy production is less than that from a single-basin scheme using either of the basins separately. Moreover, since the linked-basin scheme requires an interconnecting waterway in which the power plant is located, as well as dyke and gate structures to control the levels of each basin, it tends to be high in capital cost.

However, due to the fact that a barrage must block a large area of sea, the huge environmental impact is inevitable. As with the Bay of Fundy project, this environmental impact presents a substantial obstacle to the tidal power development. When the idea of barrage type was put on hold, people started looking for another form of tidal energy, that is, the energy from tidal current.

3.4.2 Tidal Current Turbine

Instead of harvesting energy from the potential energy lifted by a tidal range, tidal turbines use the kinematical force of tidal current to rotate the turbine. Working like a windmill under sea, the tidal turbines are turned by water movement and go through a generator to make electricity. Compared to the air that acts on the windmill, the density of seawater passing through a current turbine is about 800 times denser than the air. That is, a current turbine produces 800 times more energy than a windmill with the same wind/current velocity, or, a current turbine requires lower current velocity to produce the same amount of energy. Another benefit of using tidal current, rather than wind, is the predictability factor, both in the time and the velocity of the current at a certain location. A proper design of tidal turbine can be made according to the data collected, and the performance can be more reliably predicted.

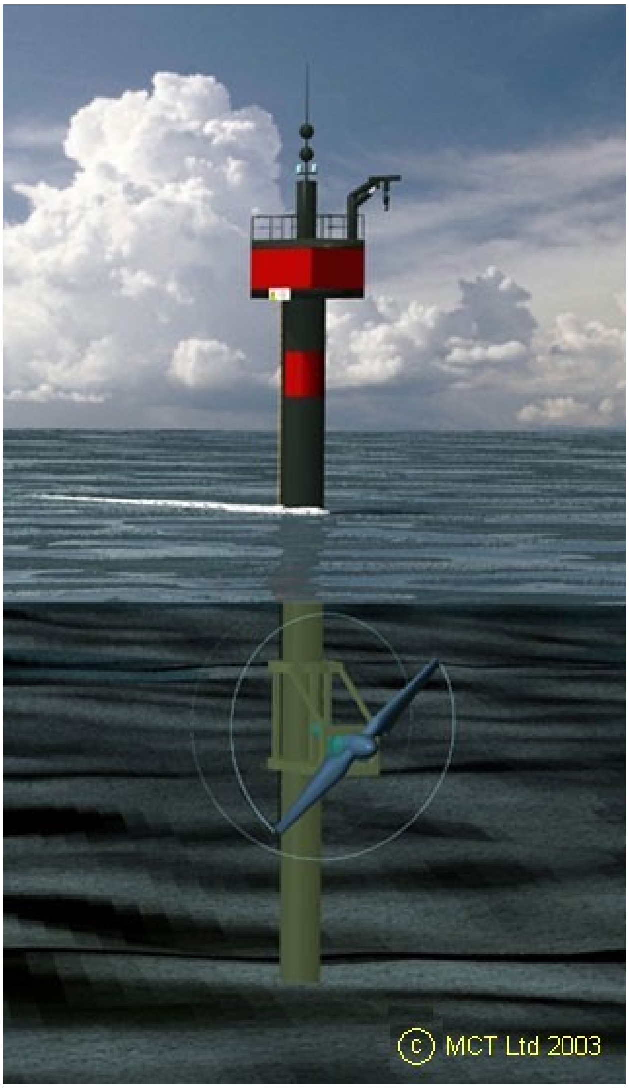

Figure 15: Tidal current turbine

Source: http://www.marineturbines.com

Contrary to the construction of a barrage, a tidal current turbine does not require the blocking of a waterway, and thus has less of an environmental impact and less capital investment. Tidal turbines are already being tested in pilot projects off England, Italy and on a small scale in the United States. One of the projects is supported by Marine Current Turbines Ltd., in Bristol, England. Its tidal current turbine (see Figure 15) occupies only a small section of seabed with an 11m diameter rotor system. The rotors turn at a maximum speed of 15 rpm, and marine biologists believe sea creatures can easily avoid the equipment. The company launched their pilot offshore tidal energy turbine off the English coast in 2003 at a cost of almost seven million US dollars, and the experimental turbine is capable of producing 300 kilowatts of electricity by the 2.7m/s (5.5 knot) current, enough to supply 200 households. According to its pilot project, the company suggests the requirements for cost-effective power generation from tidal streams using their technology are a mean spring peak velocity exceeding about 2.25 to 2.5m/s (4.5 to 5 knots) at a depth of 20 to 30m. Based on the success of this project, the company plans to install a one-megawatt commercial prototype in 2007 or 2008, which will start supplying power to households.

3.4.3 Energy Storage

The output from both the barrage type of tidal power plant and the tidal current turbine are constrained by the tide and may not produce power during the period of highest demand. Thus, it is necessary to preserve the tidal output using an energy storage device and meet the varying demand pattern. These energy storage devices do not necessarily need to match the total output of the tidal power development, as some of the energy can be used directly. Furthermore, when tidal power projects become integrated into the large interconnected power system, continuity of supply is assessed by the diversity of power sources feeding any given area. Once a tidal power project is viewed simply as another system source, an appreciable portion of the raw energy could be absorbed directly and displace thermal energy.

Chapter 4: Numerical Modeling

In order to find a better location with a larger tidal range or faster tidal current and achieve the highest economic potential, this study uses numerical model to simulate the response within the study area – Bay of Fundy.

4.1 Related Studies

Because of the significantly large tidal range in this region, several of numerical studies have been conducted. Rao (1968) finds that the natural wave period of the Bay of Fundy is close to the period of M2 tide. This explains the significant tidal range in this region. Greenberg (1969) works on a finite difference model to study the response of M2 tide in the Bay of Fundy. Lawton (1970) promotes the concept of generating power by tide. His study shows that the tidal power generation is feasible under some conditions. Greenberg, Shore and Shen (1997) develop a 3D finite element model for Passamaquoddy Bay. Sankaranarayanan, and McCay (2003) create a boundary-fitted coordinate hydrodynamic model for Saint John Harbour region. Both of the recent papers study smaller regions with a more detail scale. The studies show that the vertical circulation due to the tide is less significant than the horizontal movement in this region, and a two dimensional model is sufficient to be used here.

We can see that these studies were conducted base on wave with a single wavelength. Because the tide can be considered as a summation of series of single-wavelength tidal components, it is reasonable to study the tidal responses base on one tidal component such as M2, the dominant tidal component. However, in order to get a through study, a time series responses of this region is required.

4.2 Theoretical Framework

One of the major objections of the present study is to develop a mathematical model using finite element methods (FEM) for solving shallow water equations in order to simulate the current and water level in the Bay of Fundy. This study chooses to use the finite element method because it is able to represent the boundaries more efficiently than the conventional finite difference method. Finite element method also presents variable resolution capabilities. Oceanographers, especially in the tidal community use FE models to represent tidal interactions and resonance which occur at different scales, from ocean basin to coastal inlets (Connor and Wang, 1974, Lynch and Gray, 1979, Walters and Cheng, 1979).

The physical processes of water movement can be expressed by a set of equations derived from the conservation laws. The laws are the principles of conservation of mass and conservation of momentum. Assuming a constant water density, the set of equations governing the fluid flow in three dimensional space can be expressed as (Crowe, et al, 2001):

1. Equation of continuity (conservation of mass)

$$\frac{\partial u}{\partial x}+\frac{\partial v}{\partial y}+\frac{\partial w}{\partial z}=0 \tag{4.1}$$

2. Equation of motion (conservation of momentum)

$$\begin{aligned}
\rho(\frac{\partial u}{\partial t}+u\frac{\partial u}{\partial x}+v\frac{\partial u}{\partial y}+w\frac{\partial u}{\partial z}) &= -\frac{\partial p}{\partial x}+\frac{\partial \tau_{xx}}{\partial x}+\frac{\partial \tau_{yx}}{\partial y}+\frac{\partial \tau_{zx}}{\partial z}+F_{bx}\\
\rho(\frac{\partial v}{\partial t}+u\frac{\partial v}{\partial x}+v\frac{\partial v}{\partial y}+w\frac{\partial u}{\partial z}) &= -\frac{\partial p}{\partial y}+\frac{\partial \tau_{yy}}{\partial x}+\frac{\partial \tau_{xy}}{\partial y}+\frac{\partial \tau_{zy}}{\partial z}+F_{by}\\
\rho(\frac{\partial w}{\partial t}+u\frac{\partial w}{\partial x}+v\frac{\partial w}{\partial y}+w\frac{\partial w}{\partial z}) &= -\frac{\partial p}{\partial z}+\frac{\partial \tau_{zz}}{\partial x}+\frac{\partial \tau_{xz}}{\partial y}+\frac{\partial \tau_{yz}}{\partial z}+F_{bz}
\end{aligned} \tag{4.2}$$

The independent variables are the three components of the spatial coordinate system *(x, y, z)* and time *t*, and ρ is the water density. The dependent variables are:

u, v, w = velocity components in *x, y,* and *z* direction, and are function of *(x, y, z, t).*

P(x, y, z, t) = pressure, the normal stress on a water element.

F_b *(x, y, z, t)* = body force exerts on a water element, in *x, y,* and *z* direction.

Although the water depth may vary in a gulf or bay, the wavelength of tide is significantly larger than the water depth, thus allowing us to treat it as a shallow water system. The physical processes are dominated by horizontal movement and are relatively homogeneous in the vertical direction (z). Consequently, we can average the variable in vertical direction and simplify the three dimensional system to two dimensional.

This simplification also assumes the following condition:

1. The density of water is constant.
2. The pressure in the water is hydrostatic.
3. The shear stress by the vertical velocity is neglected.
4. Body force includes only gravity and Coriolis force.
5. The vertical distribution of velocity is constant.

In general, a property can be vertically averaged by the equation:

$$M(x, y, t) = \frac{1}{H}\int_0^H m(x, y, z, t)dz \tag{4.3}$$

where:

z = surface elevation in the vertical direction.

H = distance from bottom to the top.

m = dependent variable.

M = vertically-averaged dependent variable.

Applying this vertical average to our governing equations, the vertical dimension will be simplified and the system becomes two-dimensional. The equations become (Leendertse, 1970):

$$\frac{\partial H}{\partial t} + H(\frac{\partial u}{\partial x} + \frac{\partial v}{\partial y}) = 0 \qquad (4.4)$$

$$\begin{aligned} &\frac{\partial u}{\partial t} + u(\frac{\partial u}{\partial x} + \frac{\partial v}{\partial y}) + g\frac{\partial \zeta}{\partial x} - fv + \tau u - W_x = 0 \\ &\frac{\partial v}{\partial t} + v(\frac{\partial u}{\partial x} + \frac{\partial v}{\partial y}) + g\frac{\partial \zeta}{\partial y} + fu + \tau v - W_y = 0 \end{aligned} \qquad (4.5)$$

where all the dependent variables are vertically-averaged. f is the *Coriolis parameter,* where:

$$f = 2\omega \sin(\text{latitude}) \qquad (4.6)$$

and ω is the angular velocity vector for Earth's rotation.

τ is the bottom stress and W is the shear stress at the water surface due to wind. This set of equations is called "Shallow Water Equations" since they are working on flow movement in a shallow water basin.

4.3 Numerical Model Development

The finite element method provides estimation of the entire study domain by the sum of the response of each piece of the domain. If a functional requirement to the shape function is given, the convergence of the solution can be achieved as the subdomains are made infinitesimal. The size and the shape of the elements in a finite element model are easily chosen and modified to fit the property of study domain such as the water depth and complex domain boundary. In the Bay of Fundy, water depth is from few meters in the coastal region at the north end of the bay to several hundred meters at the mouth, and the coast line is very complex. A finite element model is a suited choice to study the response of tidal waves in the Bay of Fundy.

4.3.1 Related Studies

The shallow water equations are nonlinear, non-homogeneous, and hyperbolic, with the three independent variables (x, y, and t) and three dependent variables (water elevation, H, and velocity in x and y direction, u, v). Several studies have been conducted using finite element methods to solve this set of equations. For example, Grotkop (1973) uses Galerkin's method with six nodes triangular element to calculate the tidal oscillations in the North Sea. He used zero normal velocity at each node as the boundary conditions on the solid boundary (coastal line), and no specific velocity or elevation was assigned to the open boundary. Taylor and Davis (1975) also apply Galerkin's approach to formulate a finite element method model for tidal propagation and dispersion study.

Connor and Wang (1974) replace the velocity variables in the governing equations with unit transport variables and used an eddy viscosity coefficient for the energy dissipation, helping to reduce the error in their numerical simulation. They assumed the energy was reduced due to the internal friction force caused by turbulent eddy. In this study, three approaches where compared for time integration, and it was concluded that the Runge-Kutta method performed the best. Later on, they used a time-stepping scheme which integrated surface elevation and velocity at different time steps (Wang and Connor, 1975). They used triangular elements and Galerkin's approach. The tidal level or the normal flux across the boundary was used as boundary conditions. It is found that the time-split scheme is stable even without the eddy viscosity or Coriolis force. However, the size of the time step is limited by the Courant condition.

Norton and King published an operation manual for their horizontal flow model, RMA2 in 1978. This model used a vertically averaged continuity equation and the modified two-dimensional Navier-Stokes equation. The model analyzes the pressure by the hydraulic head, refers to as a datum, and presents shear stress induced by the wind stress on the water surface and frictional stress on the bottom. The velocity term is transformed into a flow transport rate per unit width. The program uses either quadratic triangular elements (6 nodes) or quadratic quadrilateral elements (8 nodes), and the water level is calculated by the average of the corner points. The dependent variables are expressed by a power series in time domain; they were used it to obtain the time derivatives. The eddy viscosity serves as the damping force to maintain the stability in the model and it is proportional to the size of the element.

In 1980, Walters and Cheng conducted several numerical experiments to test the accuracy and sensitivity of the RM2 model with a smooth-curve-sided element. They found that the boundary condition with a spatially constant water level across an open boundary performed less accurately. They suggested setting up the water level at only one point and assigning the direction of velocity on all other points along the open boundary.

4.3.2 Galerkin's Approach

Among the weighted residual methods, the Galerkin's approach is most commonly used. It generally offers better results and is easily implemented on a computer.

When using this method, it is assumed that the dependent variable can be calculated by a linear combination of shape functions:

Water surface elevation H :

$$H(x,y,t) \cong \sum_{j=1}^{N} H_j(t)\phi_j(x,y) \tag{4.7}$$

and velocity vector:

$$\begin{aligned} u(x,y,t) &\cong \sum_{j=1}^{N} u_j(t)\phi_j(x,y) \\ v(x,y,t) &\cong \sum_{j=1}^{N} v_j(t)\phi_j(x,y) \end{aligned} \tag{4.8}$$

Here ϕ_j is the shape function defined by space domain. The shape function for water elevation and velocity can be different from one another but in this study, the same shape function is used for simplicity. By using Galerkin's approach on equation (4.5) and (4.6), and making the equations orthogonal to the shape function ϕ_j, we get a set of nonlinear, ordinary differential equations in time domain:

$$\sum_{j=1}^{N} \frac{d}{dt} H_j < \phi_j, \phi_i > + < F_c(x,y,t), \phi_i >= 0 \qquad \text{i=1,2…N} \tag{4.9}$$

$$\begin{aligned} \sum_{j=1}^{N} \frac{d}{dt} u_j < \phi_j, \phi_i > + < F_{mx}(x,y,t), \phi_i >= 0 \\ \sum_{j=1}^{N} \frac{d}{dt} v_j < \phi_j, \phi_i > + < F_{mx}(x,y,t), \phi_i >= 0 \end{aligned} \qquad \text{i=1,2…N} \tag{4.10}$$

and

$$F_c(x,y,t) = H\left(\frac{\partial u}{\partial x} + \frac{\partial v}{\partial y}\right) \tag{4.11}$$

$$F_{mx}(x,y,t) = u(\frac{\partial u}{\partial x} + \frac{\partial v}{\partial y}) + g\frac{\partial \zeta}{\partial x} - fv + \tau u - W_x$$
$$F_{my}(x,y,t) = v(\frac{\partial u}{\partial x} + \frac{\partial v}{\partial y}) + g\frac{\partial \zeta}{\partial y} + fu + \tau v - W_y \quad (4.12)$$

Where <> represent integration over entire spatial domain. $F_c(x,y,t)$, $F_m(x,y,t)$ are force terms of the continuity equation and momentum equation.

4.3.3 Temporal approximation

From equations (4.9) and (4.10), we obtain a typical solution for a time dependent ordinary differential equation. In order to obtain an approximation in the time domain, finite Taylor series have been used. The finite Taylor series are Taylor series in which the higher order terms are neglected.

Using the concept of finite Taylor series, the water level can be approximated in the vertical averaged equations as follows:

$$H_{n+1} \approx H_n + \Delta t\frac{\partial H}{\partial t}|_n + \frac{\Delta t^2}{2}\frac{\partial^2 H}{\partial t^2}|_n + \frac{\Delta t^3}{6}\frac{\partial^3 H}{\partial t^3}|_n \quad (4.13)$$

$$H_{n-1} \approx H_n - \Delta t\frac{\partial H}{\partial t}|_n + \frac{\Delta t^2}{2}\frac{\partial^2 H}{\partial t^2}|_n - \frac{\Delta t^3}{6}\frac{\partial^3 H}{\partial t^3}|_n \quad (4.14)$$

where n represents time steps, and all other higher order terms are eliminated. Subtract equation (4.14) by (4.13), we obtain:

$$H_{n+1} \approx H_{n-1} + 2\Delta t \frac{\partial H}{\partial t}|_n + \frac{\Delta t^3}{3}\frac{\partial^3 H}{\partial t^3}|_n \tag{4.15}$$

If equation (4.15) is put into equation (4.7), we obtain:

$$< H_{n+1}, \phi_i > \approx < H_{n-1}, \phi_i > + 2\Delta t < \frac{\partial H}{\partial t}, \phi_i > + \frac{\Delta t^3}{3} < \frac{\partial^3 H}{\partial t^3}, \phi_i > \tag{4.16}$$

Using the same approach for the velocity vector, we find

$$\begin{aligned} &< u_{n+1}, \phi_i > \approx < u_{n-1}, \phi_i > + 2\Delta t < \frac{\partial u}{\partial t}, \phi_i > + \frac{\Delta t^3}{3} < \frac{\partial^3 u}{\partial t^3}, \phi_i > \\ &< v_{n+1}, \phi_i > \approx < v_{n-1}, \phi_i > + 2\Delta t < \frac{\partial v}{\partial t}, \phi_i > + \frac{\Delta t^3}{3} < \frac{\partial^3 v}{\partial t^3}, \phi_i > \end{aligned} \tag{4.17}$$

Equation (4.16) and (4.17) are the finite element forms of the continuity and momentum equations by using Galerkin's approach with centered-difference in time.

In equation (4.16) and (4.17), first order time derivative term $\frac{\partial H}{\partial t}, \frac{\partial u}{\partial t}, \frac{\partial v}{\partial t}$ can be obtained by equation (4.5), (4.6). Higher order terms can be obtained by taking the time derivative of them. The higher order terms of water level:

$$\begin{aligned} &\frac{\partial^2 H}{\partial t^2} \\ &= H[2(\frac{\partial u}{\partial x})^2 + 2(\frac{\partial v}{\partial y})^2 + 4(\frac{\partial u}{\partial x})(\frac{\partial v}{\partial y}) + u\frac{\partial^2 u}{\partial x^2} + v\frac{\partial^2 v}{\partial y^2} + u\frac{\partial^2 v}{\partial x \partial y} + v\frac{\partial^2 u}{\partial x \partial y}] \\ &+ gH(\frac{\partial^2 \zeta}{\partial x^2} + \frac{\partial^2 \zeta}{\partial y^2}) + fH(\frac{\partial u}{\partial y} - \frac{\partial v}{\partial x}) + \tau H(\frac{\partial u}{\partial x} + \frac{\partial v}{\partial y}) - H(\frac{\partial W_x}{\partial x} - \frac{\partial W_y}{\partial y}) \end{aligned}$$

(4.18)

and

$$\frac{\partial^3 H}{\partial t^3}=\frac{\partial H}{\partial t}(\frac{1}{H}\frac{\partial^2 H}{\partial t^2})+H\frac{\partial}{\partial t}(\frac{1}{H}\frac{\partial^2 H}{\partial t^2}) \tag{4.19}$$

where

$$\begin{aligned}
&\frac{\partial}{\partial t}(\frac{1}{H}\frac{\partial^2 H}{\partial t^2})\\
&=4(\frac{\partial u}{\partial x}+\frac{\partial v}{\partial y})(\frac{\partial}{\partial x}\frac{\partial u}{\partial t}+\frac{\partial}{\partial y}\frac{\partial v}{\partial t})\\
&+(\frac{\partial u}{\partial t}\frac{\partial^2 u}{\partial x^2}+u\frac{\partial^2}{\partial x^2}\frac{\partial u}{\partial t})+(\frac{\partial v}{\partial t}\frac{\partial^2 v}{\partial y^2}+v\frac{\partial^2}{\partial y^2}\frac{\partial v}{\partial t})\\
&+(\frac{\partial u}{\partial t}\frac{\partial^2 v}{\partial x\partial y}+u\frac{\partial^2}{\partial x\partial y}\frac{\partial v}{\partial t})+(\frac{\partial v}{\partial t}\frac{\partial^2 u}{\partial x\partial y}+v\frac{\partial^2}{\partial x\partial y}\frac{\partial u}{\partial t})+g(\frac{\partial^2}{\partial x^2}+\frac{\partial^2}{\partial y^2})\frac{\partial}{\partial t}\zeta\\
&+f(\frac{\partial}{\partial y}\frac{\partial u}{\partial t}-\frac{\partial}{\partial x}\frac{\partial v}{\partial t})+\tau(\frac{\partial}{\partial x}\frac{\partial u}{\partial t}+\frac{\partial}{\partial y}\frac{\partial v}{\partial t})-\frac{\partial}{\partial t}(\frac{\partial W_x}{\partial x}+\frac{\partial W_y}{\partial y})
\end{aligned} \tag{4.20}$$

Using the same method we can calculate the higher order terms for velocity in x-direction:

$$\frac{\partial^2 u}{\partial t^2}=-\frac{\partial u}{\partial t}(\frac{\partial u}{\partial x}+\frac{\partial v}{\partial y})-u(\frac{\partial}{\partial x}\frac{\partial u}{\partial t}+\frac{\partial}{\partial y}\frac{\partial v}{\partial t})-g\frac{\partial}{\partial x}\frac{\partial \zeta}{\partial t}+f\frac{\partial v}{\partial t}-\tau\frac{\partial u}{\partial t}+\frac{\partial W_x}{\partial t} \tag{4.21}$$

$$\frac{\partial^3 u}{\partial t^3}=-\frac{\partial^2 u}{\partial t^2}(\frac{\partial u}{\partial x}+\frac{\partial v}{\partial y})-2\frac{\partial u}{\partial t}(\frac{\partial}{\partial x}\frac{\partial u}{\partial t}+\frac{\partial}{\partial y}\frac{\partial v}{\partial t})-u(\frac{\partial}{\partial x}\frac{\partial^2 u}{\partial t^2}+\frac{\partial}{\partial y}\frac{\partial^2 v}{\partial t^2})$$

$$-g\frac{\partial}{\partial x}\frac{\partial^2\zeta}{\partial t^2}+f\frac{\partial^2 v}{\partial t^2}-\tau\frac{\partial^2 u}{\partial t^2}+\frac{\partial^2 W_x}{\partial t^2}$$

(4.22)

and in y- direction:

$$\frac{\partial^2 v}{\partial t^2}=-\frac{\partial v}{\partial t}(\frac{\partial u}{\partial x}+\frac{\partial v}{\partial y})-v(\frac{\partial}{\partial x}\frac{\partial u}{\partial t}+\frac{\partial}{\partial y}\frac{\partial v}{\partial t})-g\frac{\partial}{\partial y}\frac{\partial\zeta}{\partial t}-f\frac{\partial u}{\partial t}-\tau\frac{\partial v}{\partial t}+\frac{\partial W_y}{\partial t}$$

(4.23)

$$\frac{\partial^3 v}{\partial t^3}=-\frac{\partial^2 v}{\partial t^2}(\frac{\partial u}{\partial x}+\frac{\partial v}{\partial y})-2\frac{\partial v}{\partial t}(\frac{\partial}{\partial x}\frac{\partial u}{\partial t}+\frac{\partial}{\partial y}\frac{\partial v}{\partial t})-v(\frac{\partial}{\partial x}\frac{\partial^2 u}{\partial t^2}+\frac{\partial}{\partial y}\frac{\partial^2 v}{\partial t^2})$$

$$-g\frac{\partial}{\partial y}\frac{\partial^2\zeta}{\partial t^2}-f\frac{\partial^2 u}{\partial t^2}-\tau\frac{\partial^2 v}{\partial t^2}+\frac{\partial^2 W_y}{\partial t^2} \qquad (4.24)$$

where

$$\frac{\partial}{\partial x}\frac{\partial^2 u}{\partial t^2}+\frac{\partial}{\partial y}\frac{\partial^2 v}{\partial t^2}$$

$$=-\frac{\partial u}{\partial t}(\frac{\partial^2 u}{\partial x^2}+\frac{\partial^2 v}{\partial x\partial y})-\frac{\partial v}{\partial t}(\frac{\partial^2 v}{\partial y^2}+\frac{\partial^2 u}{\partial x\partial y})-2(\frac{\partial}{\partial x}\frac{\partial u}{\partial t}+\frac{\partial}{\partial y}\frac{\partial v}{\partial t})(\frac{\partial u}{\partial x}+\frac{\partial v}{\partial y})$$

$$-u(\frac{\partial^2}{\partial x^2}\frac{\partial u}{\partial t}+\frac{\partial^2}{\partial x\partial y}\frac{\partial v}{\partial t})-v(\frac{\partial^2}{\partial y^2}\frac{\partial v}{\partial t}+\frac{\partial^2}{\partial x\partial y}\frac{\partial u}{\partial t})$$

$$-g\frac{\partial}{\partial t}(\frac{\partial^2\zeta}{\partial x^2}+\frac{\partial^2\zeta}{\partial y^2})+f(\frac{\partial}{\partial x}\frac{\partial v}{\partial t}-\frac{\partial}{\partial y}\frac{\partial u}{\partial t})-\tau(\frac{\partial}{\partial x}\frac{\partial u}{\partial t}+\frac{\partial}{\partial y}\frac{\partial v}{\partial t})+\frac{\partial}{\partial t}(\frac{\partial W_x}{\partial x}+\frac{\partial W_y}{\partial y})$$

(4.25)

All the components in equation (4.18) to (4.25) can be obtained as follows:

$$\frac{\partial}{\partial x}\frac{\partial u}{\partial t}$$
$$=-\frac{\partial u}{\partial x}(\frac{\partial u}{\partial x}+\frac{\partial v}{\partial y})-u(\frac{\partial^2 u}{\partial x^2}+\frac{\partial^2 v}{\partial x\partial y})-g\frac{\partial^2 \zeta}{\partial x^2}+f\frac{\partial v}{\partial x}-\tau\frac{\partial u}{\partial x}+\frac{\partial W_x}{\partial x}$$

(4.26)

$$\frac{\partial^2}{\partial x^2}\frac{\partial u}{\partial t}$$
$$=-\frac{\partial^2 u}{\partial x^2}(\frac{\partial u}{\partial x}+\frac{\partial v}{\partial y})-2\frac{\partial u}{\partial x}(\frac{\partial^2 u}{\partial x^2}+\frac{\partial^2 v}{\partial x\partial y})-u(\frac{\partial^3 u}{\partial x^3}+\frac{\partial^3 v}{\partial x^2\partial y})$$
$$-g\frac{\partial^3 \zeta}{\partial x^3}+f\frac{\partial^2 v}{\partial x^2}-\tau\frac{\partial^2 u}{\partial x^2}+\frac{\partial^2 W_x}{\partial x^2}$$

(4.27)

$$\frac{\partial}{\partial y}\frac{\partial v}{\partial t}$$
$$=-\frac{\partial v}{\partial y}(\frac{\partial u}{\partial x}+\frac{\partial v}{\partial y})-v(\frac{\partial^2 v}{\partial y^2}+\frac{\partial^2 u}{\partial x\partial y})-g\frac{\partial^2 \zeta}{\partial y^2}-f\frac{\partial u}{\partial y}-\tau\frac{\partial v}{\partial y}+\frac{\partial W_y}{\partial y}$$

(4.28)

$$\frac{\partial^2}{\partial y^2}\frac{\partial v}{\partial t}$$
$$=-\frac{\partial^2 v}{\partial y^2}(\frac{\partial u}{\partial x}+\frac{\partial v}{\partial y})-2\frac{\partial v}{\partial y}(\frac{\partial^2 v}{\partial y^2}+\frac{\partial^2 u}{\partial x\partial y})-v(\frac{\partial^3 v}{\partial y^3}+\frac{\partial^3 u}{\partial x\partial y^2})$$
$$-g\frac{\partial^3 \zeta}{\partial y^3}-f\frac{\partial^2 u}{\partial y^2}-\tau\frac{\partial^2 v}{\partial y^2}+\frac{\partial^2 W_y}{\partial y^2}$$

(4.29)

$$
\begin{aligned}
&\frac{\partial^2}{\partial x\partial y}\frac{\partial u}{\partial t}\\
&=-\frac{\partial^2 u}{\partial x\partial y}(\frac{\partial u}{\partial x}+\frac{\partial v}{\partial y})-\frac{\partial u}{\partial x}(\frac{\partial^2 u}{\partial x\partial y}+\frac{\partial^2 v}{\partial y^2})-\frac{\partial u}{\partial y}(\frac{\partial^2 v}{\partial x\partial y}+\frac{\partial^2 u}{\partial x^2})-u(\frac{\partial^3 v}{\partial x\partial y^2}+\frac{\partial^3 u}{\partial x^2\partial y})\\
&-g\frac{\partial^3\zeta}{\partial x^2\partial y}+f\frac{\partial^2 v}{\partial x\partial y}-\tau\frac{\partial^2 u}{\partial x\partial y}+\frac{\partial^2 W_x}{\partial x\partial y}
\end{aligned}
\tag{4.30}
$$

$$
\begin{aligned}
&\frac{\partial^2}{\partial x\partial y}\frac{\partial v}{\partial t}\\
&=-\frac{\partial^2 v}{\partial x\partial y}(\frac{\partial u}{\partial x}+\frac{\partial v}{\partial y})-\frac{\partial v}{\partial x}(\frac{\partial^2 u}{\partial x\partial y}+\frac{\partial^2 v}{\partial y^2})-\frac{\partial v}{\partial y}(\frac{\partial^2 v}{\partial x\partial y}+\frac{\partial^2 u}{\partial x^2})-v(\frac{\partial^3 v}{\partial x\partial y^2}+\frac{\partial^3 u}{\partial x^2\partial y})\\
&-g\frac{\partial^3\zeta}{\partial x\partial y^2}-f\frac{\partial^2 u}{\partial x\partial y}-\tau\frac{\partial^2 v}{\partial x\partial y}+\frac{\partial^2 W_y}{\partial x\partial y}
\end{aligned}
\tag{4.31}
$$

For a forward difference approximation, we can generate the relationship of each time step by substituting the Taylor series expansion into equation (4.5) and (4.6):

$$
< H_{n+1},\phi_i > \approx < H_n,\phi_i > +\Delta t < \frac{\partial H}{\partial t},\phi_i > + \frac{\Delta t^2}{2} < \frac{\partial^2 H}{\partial t^2},\phi_i > \tag{4.32}
$$

$$
< V_{n+1},\phi_i > \approx < V_n,\phi_i > +\Delta t < \frac{\partial V}{\partial t},\phi_i > + \frac{\Delta t^2}{2} < \frac{\partial^2 V}{\partial t^2},\phi_i > \tag{4.33}
$$

Equation (4.32) and (4.33) show a one step, explicit scheme for two time step.

Using the weighted residual method to calculate dependent variables, such as H or V, in the time domain, we have:

$$\int W_i([m]\{H\}\{\dot{\psi}\}+[K]\{H\}\{\psi\}+\{F\}\{\psi\})dr=0 \qquad \text{i=1,2…N}$$

(4.34)

$$\int W_i([m]\{V\}\{\dot{\psi}\}+[K]\{V\}\{\psi\}+\{F\}\{\psi\})dr=0 \tag{4.35}$$

where

$$H(t)=\sum_{i=1}^{N} H_i\psi_i(t)$$

$$V(t)=\sum_{i=1}^{N} V_i\psi_i(t)$$

H_i and V_i = nodal value at time i.

ψ_i = shape function

W_i = weight function.

When using a linear time element between two nodal values at time step (n) and (n+1), the shape function for each element can be gotten in the local coordinate system:

$$\begin{matrix}\psi_n = 1-\xi \\ \psi_{n+1}=\xi\end{matrix} \quad \text{and} \quad \begin{matrix}\dot{\psi}_n = -1/\Delta t \\ \dot{\psi}_{n+1} = 1/\Delta t\end{matrix} \tag{4.36}$$

when $\xi = t/\Delta t$ and $0 \le \xi \le 1$

Put (4.26) into (4.24), we have:

$$([M]/\Delta t + [K]\theta)\{H\}_{n+1} = ([M]/\Delta t - [K](1-\theta))\{H\}_n - \{F\}_{n+1}\theta + \{F\}_n(1-\theta) \tag{4.37}$$

with $\theta = \int_0^1 w_i \xi d\xi / \int_0^1 w_i d\xi$

Similar calculations can be made for velocity vector (V).

If we use a forward scheme and collect value at time step (n), then $\theta = 0$. Equation (4.37) becomes:

$$[M]\{H\}_{n+1} = [M]\{H\}_n - ([K]\{H\}_n + \{F\}_n)\Delta t \tag{4.38}$$

and

$$\begin{aligned} [M]\{u\}_{n+1} &= [M]\{u\}_n - ([K]\{u\}_n + \{F\}_n)\Delta t \\ [M]\{v\}_{n+1} &= [M]\{v\}_n - ([K]\{v\}_n + \{F\}_n)\Delta t \end{aligned} \tag{4.39}$$

This is the temporal frame that is used in this study.

4.4 Hydrodynamic Simulation at Bay of Fundy

The hydrodynamic model was applied for the Bay of Fundy to compute the tidal response. The study area extends from the entrance of The Bay of Fundy to Chignecto Bay and Cobequid Bay/Minas Basin (see Figure 9). This region has been considered for possible basins for tidal power projects since 1930. The water depth is shallow relative to the tide, thus making the vertically averaged shallow water equations appropriate for the hydrodynamic model for this region. Furthermore, the very irregular coastline or the system boundary necessitates the use of finite element analysis.

4.4.1 Field Observation Data

The bathymetric data was collected from the navigation chart published by Canadian Hydrographic Service, Minister of Fisheries and Oceans Canada, 1990. The shore line and water depth were matched as closely as possible to prevent any possible distortion. Figure 16 is a contour map showing the water depth in the Bay of Fundy. The unit for X and Y coordinates is kilometers and the water depth is in meters. From this figure, the water depth of the Bay of Fundy is deeper in the mouth and center of the bay and gradually decreases when it approaches the north and the coastal line. The cross section area of the Bay also decreases and then divides into two major basins–Chignecto Bay in the northwest side and Minas Basin/Cobequid Bay on the northeast side.

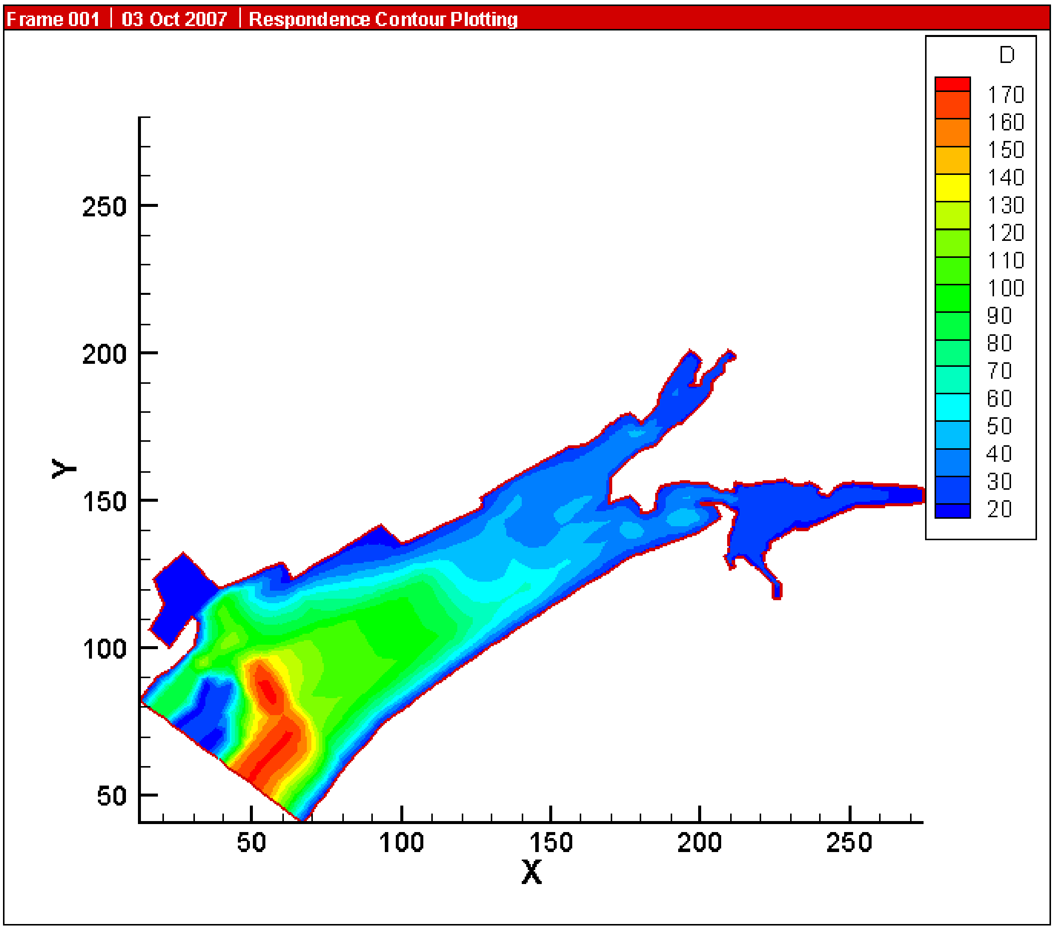

Figure 16: Water depth of Bay of Fundy

Tidal information was taken from The Bay of Fundy Tide Tables by Canadian Hydrographic Service, and from the home page of Canadian Hydrographic Service (CHS).

As Canada's national data center, the Marine Environmental Data Service (MEDS) acquires and processes tide and water level database for CHS. MEDS collects tidal data through several of tidal stations around the Gulf of St. Lawrence and the costal zone of the Atlantic Ocean. Table 3 shows the locations of tidal stations and data available during the past years. It shows that most tidal stations did not operate continuously and caused several gaps in the observation data. However, CHS's web site provides predicted times and heights of high and low waters, and the hourly water levels for over seven hundred stations in Canada. The predicted tidal data are processed based on the data collected by MEDS and by the method described in section 3.1. Thus, the predicted tidal data is influenced only by tides and without any impact from meteorological conditions such as atmospheric pressure changes, strong prolonged winds or variations of freshwater discharge. This is good for the present research because the variable meteorological conditions will not be sustained and would have to be removed to simulate a tidal response in the study region.

Station	Station Name	LAT.	LONG.	Duration of Data
10	NORTH HEAD	44.76	66.75	1964/09/10~1964/10/09, 2006/06/22~2006/08/15
102	MACDONALD POINT	45.72	66.05	1970/06/21~1970/07/31
103	CAMBRIDGE NARROWS	45.83	65.95	1970/06/21~1970/07/27
105	GAGETOWN	45.77	66.13	Several periods between 1913 and 1970
108	Upper Gagetown	45.85	66.23	Several periods between 1965 and 1969
114	MAUGERVILLE	45.87	66.47	Several periods between 1965 and 1970
120	FREDERICTON	45.97	66.65	Several periods between 1913 and 1969
122	NEWCASTLE CREEK	46.07	66.00	Several periods between 1965 and 1969
124	JEMSEG	45.83	66.12	Several periods between 1966 and 1970
140	HERRING COVE	45.57	64.97	1960/08/24~1960/09/22
170	HOPEWELL CAPE	45.85	64.58	Several periods between 1898 and 1965
172	BELLIVEAU VILLAGE	45.93	64.62	1968/07/14 to 30
173	DOVER	45.98	64.68	1968/07/14 to 29
174	DIEPPE (IRVING WHARF)	46.10	64.77	1968/07/14 to 30
175	MONCTON	46.08	64.77	1898/08/04~18, 1920/09/01~16
176	MONCTON (CAUSEWAY)	46.07	64.82	1968/07/13 to 30
215	TWO RIVERS COVE	45.68	64.47	1919/06/27~1919/07/28
240	CAPE D'OR	45.30	64.78	Several periods between 1965 and 1980
242	SPENCERS ISLAND	45.33	64.70	Several periods between 1980 and 1983
247	DILIGENT R.	45.40	64.45	1965/08/01~1965/10/08
260	FIVE ISLANDS	45.38	64.13	1965/06/03~1965/08/09, 1965/09/16~1965/10/25
270	BURNTCOAT HEAD	45.30	63.80	Several periods between 1916 and 1975
280	WINDSOR	44.98	64.15	1975/07/31~1975/09/03
282	HANTSPORT	45.07	64.17	1969/09/19~1969/10/31
289	BLOMIDON	45.27	64.35	1965/06/04~1965/07/03
30	LETITE HARBOUR	45.05	66.87	Several periods between 1957 and 1972
312	ILE HAUTE	45.25	65.00	1976/04/26~1976/07/30
315	MARGARETSVILLE	45.05	65.07	1961/07/28~1961/08/12, 1965/06/22~1965/08/26
320	PARKERS COVE	44.80	65.53	Several periods between 1970 and 1992
324	Digby Ferry Wharf	44.66	65.76	Several periods in 2003 and 2004
325	DIGBY	44.63	65.75	Several periods between 1898 and 2006
327	ANNAPOLIS ROYAL	44.75	65.52	1987/05/21 to 26

Table 3 Tidal stations of MEDS in the Gulf of St. Lawrence

Station	Station Name	LAT.	LONG.	Duration of Data
330	CULLODEN	44.67	65.83	1963/06/20~1963/07/20, 1964/08/19~1964/10/17
333	GRAND EDDY	44.40	66.20	1966/06/18~1966/07/13
334	TROUT COVE	44.55	66.03	1965/05/16~1965/09/09
335	SANDY COVE	44.50	66.10	1966/04/22~1966/07/13
336	EAST SANDY COVE	44.48	66.08	1966/05/10~1966/07/18
337	TIVERTON	44.38	66.22	1966/01/01~1966/11/17
338	TIVERTON (BOARS HEAD)	44.40	66.22	1966/01/01~9, 1966/05/01~1966/10/30
339	WEST NARROWS	44.40	66.22	1966/04/26~1966/07/19
340	WESTPORT	44.27	66.35	1966/05/22~1966/07/21
345	LIGHTHOUSE COVE	44.25	66.40	2006/06/01~2006/09/07
40139	CHIGNECTO	45.48	64.98	1976/08/18~1976/11/10
40160	GRINDSTONE (INSHORE 3)	45.72	64.60	1976/04/29~1976/07/29
40217	CUMBERLAND BASIN	45.67	64.52	1976/11/01 ~ 07
40258	MINAS BASIN (INSHORE 4)	45.32	64.20	1976/04/28~1976/07/26
40262	ECONOMY (INSHORE 5)	45.32	63.90	1976/04/28~1976/07/27
40264	COBEQUID BAY STN. 6	45.37	63.73	1976/04/28~1976/07/27
42	BLACKS HARBOUR	45.05	66.80	1986/09/12~1986/10/29
46	WEST DIPPER HARBOUR	45.10	66.43	Several periods between 1965 and 1988
52	FIVE FATHOM HOLE	45.18	66.27	2001/05/08~2001/07/03
53	MUSQUASH HARBOUR	45.15	66.25	1988/05/21~1988/06/09, 2001/05/01~2001/06/28
55	LORNEVILLE	45.18	66.15	1988/05/19~1988/06/07
65	SAINT JOHN	45.25	66.06	Several periods between 1896 and 2007
75	INDIANTOWN	45.27	66.08	Several periods between 1907 and 1970
85	KENNEBECASIS BAY	45.40	66.00	Several periods between 1912 and 1969
89	WESTFIELD BEACH	45.35	66.22	Several periods between 1965 and 1969
96	OAK POINT	45.52	66.08	Several periods between 1966 and 1970
97	HATFIELD POINT	45.62	65.92	Several periods between 1965 and 1970
98	EVANDALE	45.60	66.03	Several periods between 1965 and 1969
99	BELLE ISLE BAY	45.65	65.87	1970/05/27~1970/06/12

Table 3: Tidal stations of MEDS in the Gulf of St. Lawrence, continued

A Google Earth map of the region being simulated is shown in Figure 17. Several reference locations have been indicated as key locations referred in tide tables and CHS's website. There are five tidal stations at the mouth of the Bay of Fundy.

1. Wood Island is located at the west side of the mouth and close to Grand Manan Island. The tide station Outer Wood Island is an offshore tidal station located on the southeast side of Wood Island,

2. North Head is located north of Wood Island, and it is at the northeast coast of Grand Manan Island,

3. Lighthouse Cove is on the east side of the mouth of the Bay,

4. Tiverton is also on the east side of the mouth of the Bay, north of Lighthouse Cove,

5. Yarmouth is on the southwest coast of Nova Scotia which is located at west of the line connecting Lighthouse Cove and Wood Island.

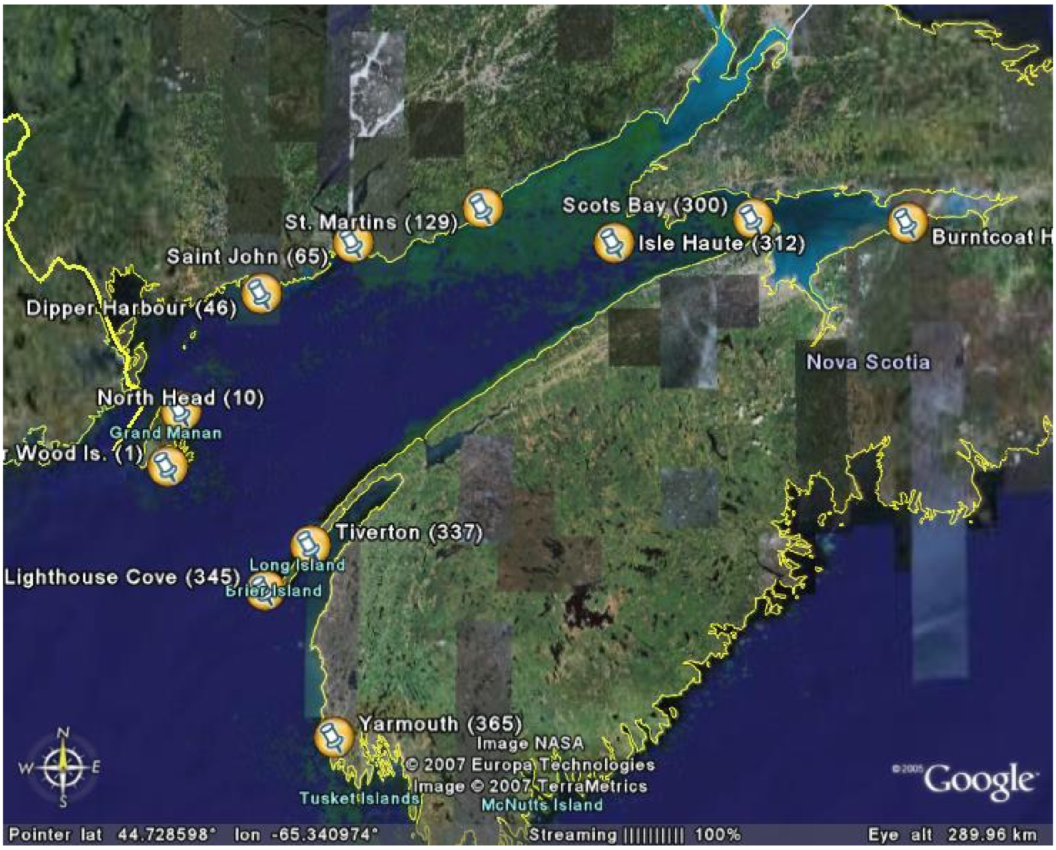

Figure 17: Reference points in the Bay of Fundy

Source: Google Earth

Figure 18 shows the tidal records between December 14 and December 20, 2006 at the mouth of the Bay of Fundy for five indicated stations. By comparing of the data from five stations, we see that Lighthouse Cove and Tiverton have similar tidal responses as the Outer Wood Island station. The present numerical model assumes that the tidal elevations are the same for the locations between Wood Island and

Lighthouse Cove (the mouth of the bay), and uses the tidal elevation in this strip zone to represent the incident tide.

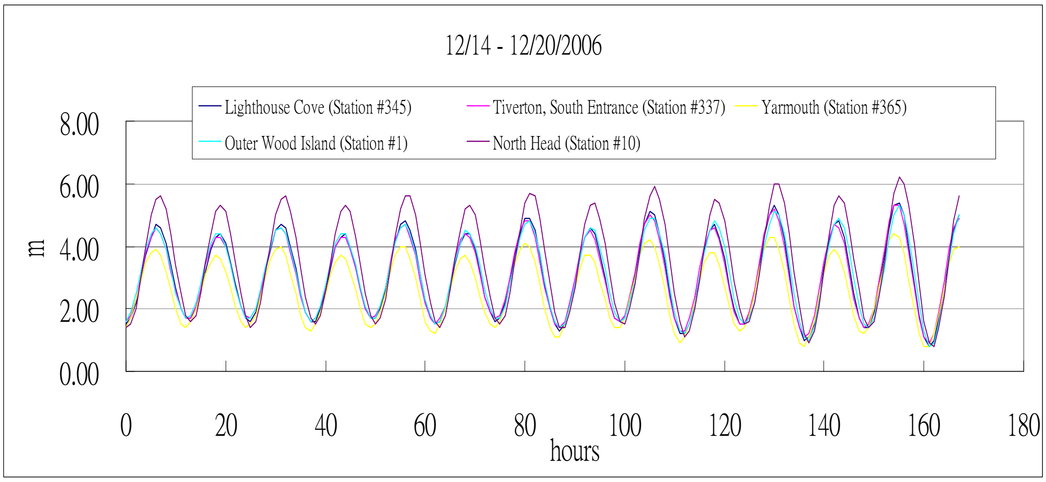

Figure 18: Tidal records at the mouth of the Bay of Fundy between 12/14 and 12/20/2006

Six reference tidal stations have been chosen for the calibration and verification of the numerical model. Dipper Harbour and Saint John are the major cities and harbor on the north/west bank of the bay. St. Martins is also located on the north/west bank and before the entrance of Chignecto Bay. Scots Bay is located at outside of Minas Channel and the entrance of Cobequid Bay/ Minas Basin, where Isle Haute is in the middle of the Bay of Fundy. They measure the tide before it transfers into the smaller bays. In the middle of the Cobequid bay, on the south bank, Burntcoat Head monitors the tide at the end of the bay. This region is one of the proposed tidal plant sites in 60' and 70'.

Two sets of tidal elevation record are presented in Figure 19 and 20 to show the change of tidal range at the reference points in the Bay of Fundy. These data have also been used to calibrate and verify the numerical simulation model.   Days with a relatively uniform tide are chosen, from December 14 to December 20, 2006 (Figure 19). The second set of tidal records taken from February 23 and March 1, 2006 is shown in Figure 20. It is seen from Figure 20 that the tidal ranges start small and grow bigger with time.

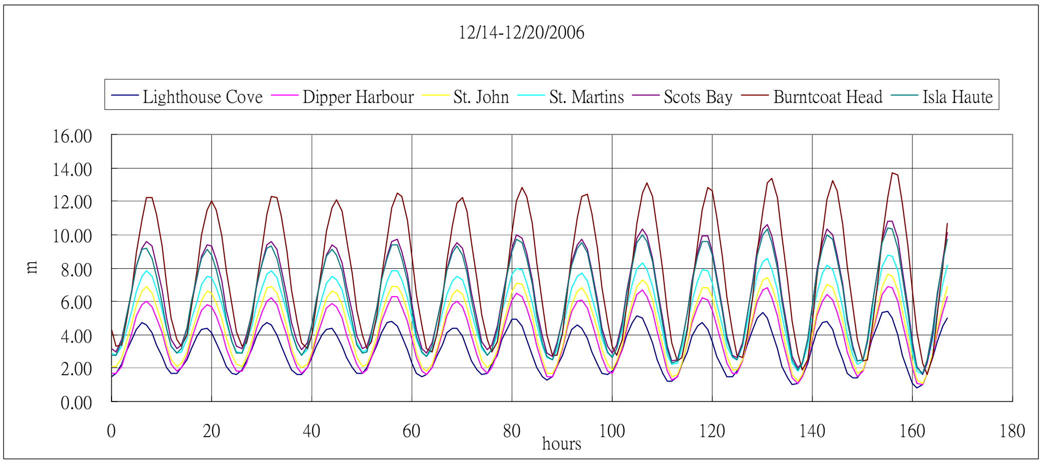

Figure 19: Tidal records between 12/14 and 12/20/2006

From these records it is seen that the tidal range in Lighthouse Cove is about three to four meters at the beginning of data and it gradually increases to eight to 11 meters at Burntcoat Head during December 14 to December 20, 2006. From Figure 20, it is seen that the tidal range in Lighthouse Cove is about three to six meters and gradually increases to ten to 16 meters at Burntcoat Head during February 23 and March 1, 2006.

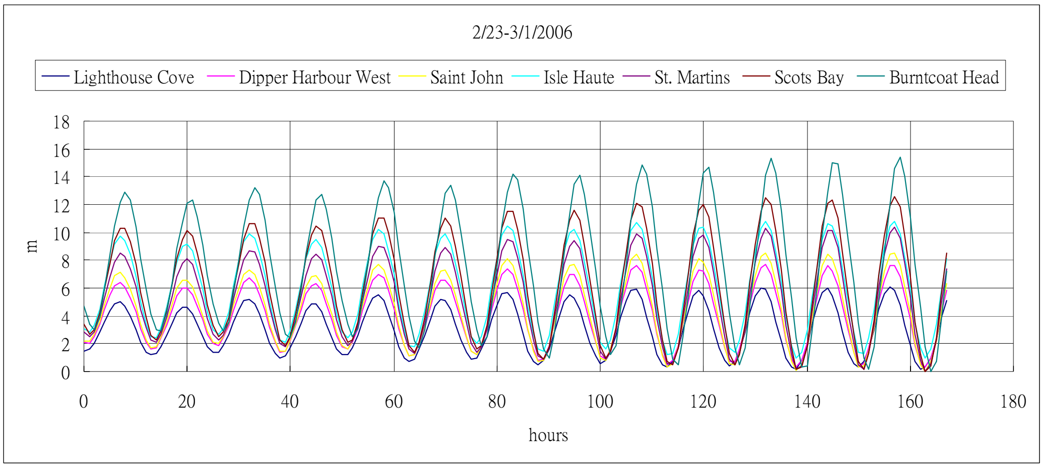

Figure 20: Tidal records between 2/23 and 3/1/2006

4.4.2 Numerical Simulation

For the present study, linear triangular elements are used; this provides increased geometrical flexibility. The sketch in Figure 21 shows the property zones. The study region is divided into several property zones. The properties such as the Manning coefficient or grid size for nodal points or elements in each zone are specified using the available topographical information. A grid system with a total of 8008 elements with 4363 nodal points is used to model the entire study area, this is presented in Figure 22. The element size and time step are chosen to be small enough to adequately describe any possible shorter period (higher frequency) oscillation. Each triangle in the grid is also made as equilateral as possible for a better approximation.

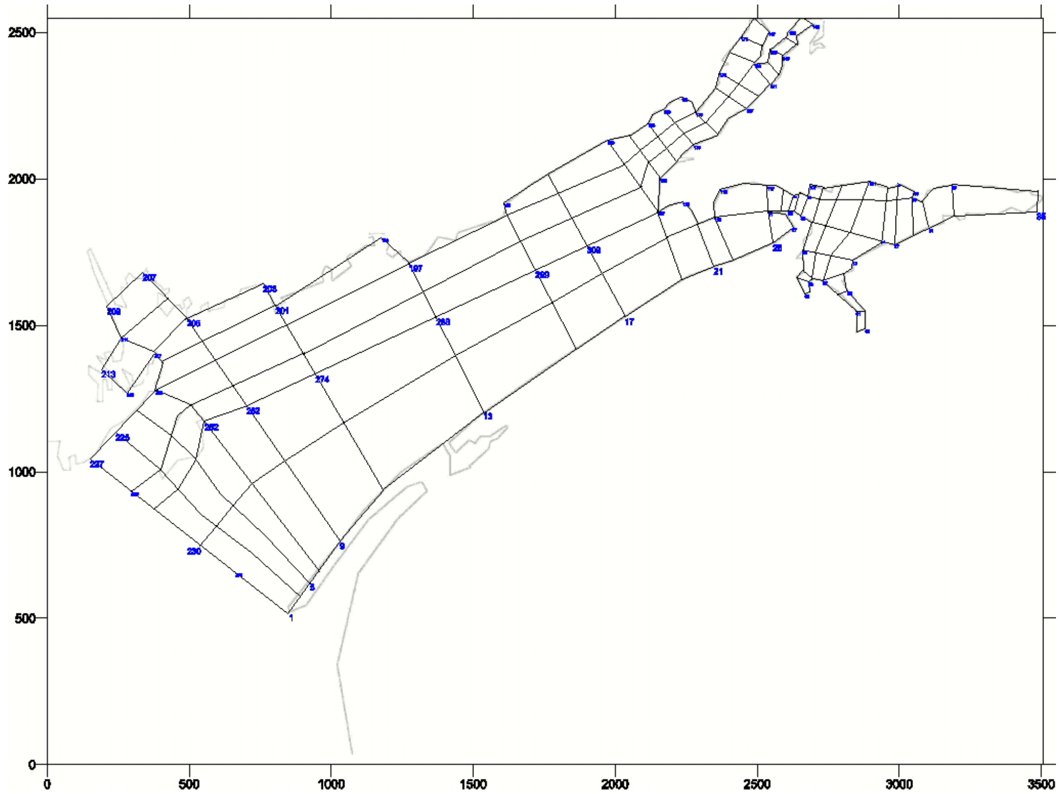

Figure 21: Property zones

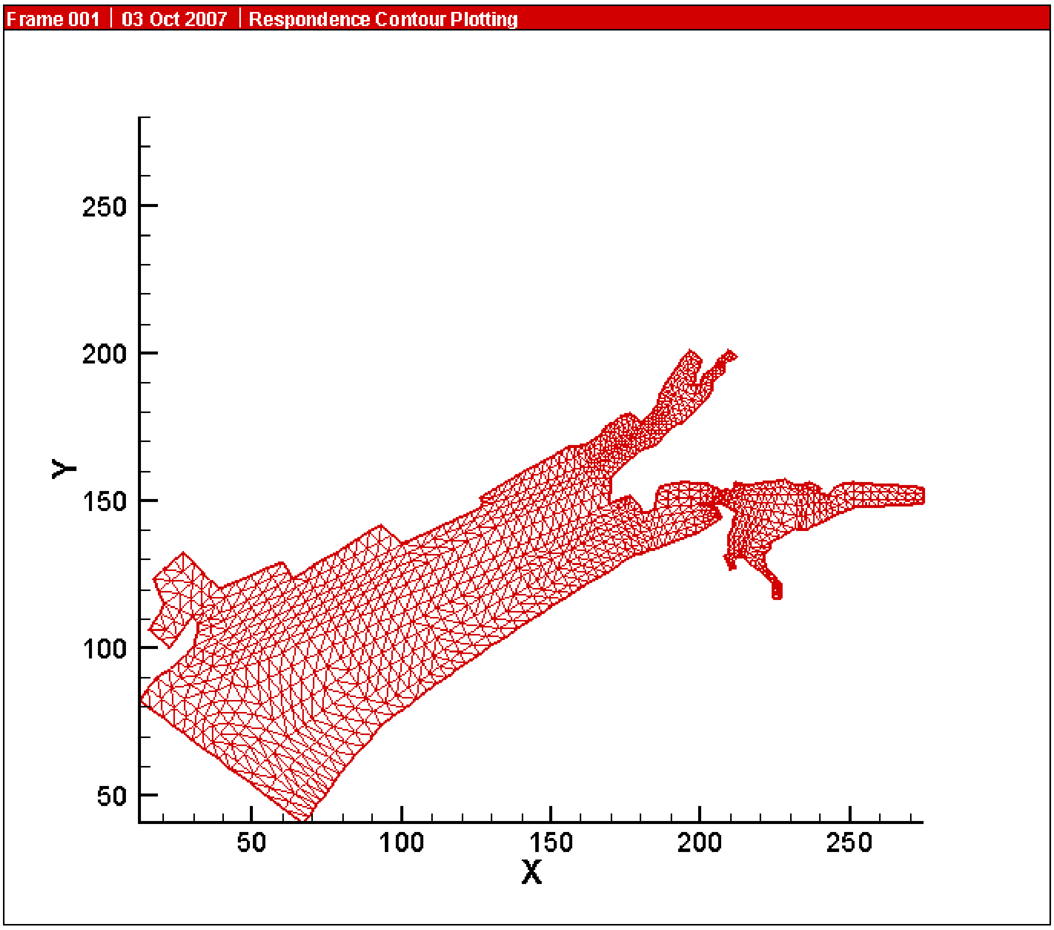

Figure 22: Grid layouts for numerical simulation

The bottom stress term can be expressed as a function of bottom roughness, velocity components, water depth and the Manning's roughness (n) as follows (see Lee et al, 1985):

$$\tau = gn^2 H^{-1/3} \sqrt{u^2 + v^2} \tag{4.40}$$

where n is the Manning's coefficient. The value for Manning's coefficient has been given in textbooks with a range of 0.025 and 0.05 ($\sec m^{1/3}$) depending on the bed form and material describing the sea bottom (Brater et al, 1996). In order to get a better result, Manning coefficient was assigned for each of the nodes. For model calibration, simulated runs are conducted by varying the value of n. The simulation result is compared with the tidal data at some key tidal stations (reference points) until the simulation result agree well as the measure data. In this study, several n values have been tested with the largest value of n=0.055 at some regions to maintain the stability of the program.

Along the mouth of the Bay, the water level is assigned for each node along the open boundary line. The water level information is given every 10 or 15 minutes and then interpolated using cubit spine distribution at each time step. In this way, the water level information can be given as real water level and the program simulates a real-time response.

A fixed boundary is set up along the coastline and a zero normal flow condition is applied at the coastal line.

4.4.3 Simulation Result

Results from the simulation are shown in Figures 23 and 24. The water level was recorded at selected nodes, which refer to the reference stations where the tidal data is provided. Since the reference level (water level = 0) of the tidal data from tidal gauge stations refers to lower low water level, the simulation result from the numerical model is shifted to compare with the record from the tidal gauge stations. The unit used for the water level is in meters; the tidal ranges selected here can be easily converted to an amplification factor for each tidal gauge station relative to the tidal height at the entrance wave of the Bay.

4.4.3.1 Simulation Result between 12/14 and 12/20/2006 (for calibration)

The numerical simulation result was used to calibrate the model by comparing with the tide data for the period December 14 and December 20, 2006 at the reference points. Through trial and error, the Manning's coefficient in each node has been modified and the final result is as shown. One node close to the entrance of the Bay is monitored and compared to tidal station at Lighthouse Cove to verify the accuracy of input data along the open boundary (the tidal elevation along the entrance of Bay of Fundy.)

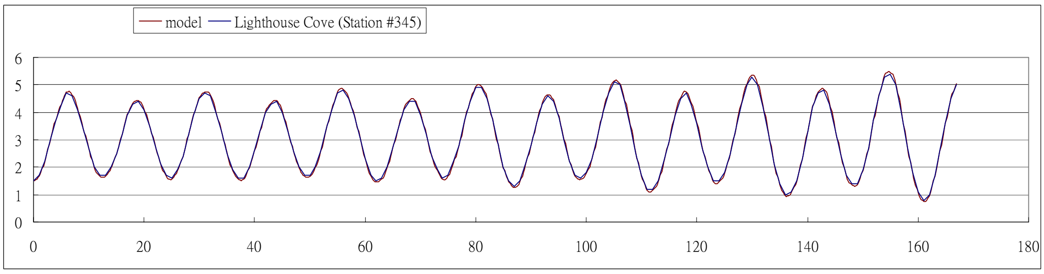

Figure 23- a: Simulation Result at the entrance of bay between 12/14 and 12/20/2006

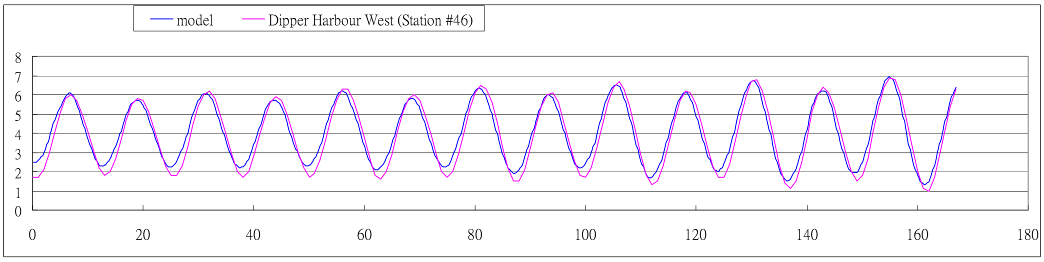

Figure 23- b: Simulation Result at the Dipper Harbour between 12/14 and 12/20/2006

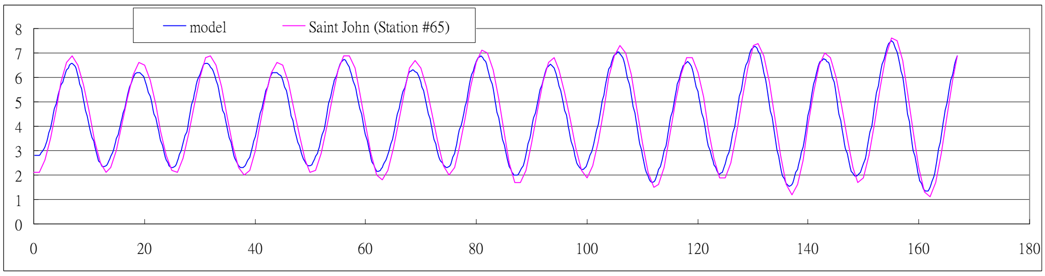

Figure 23- c: Simulation Result at St. John between 12/14 and 12/20/2006

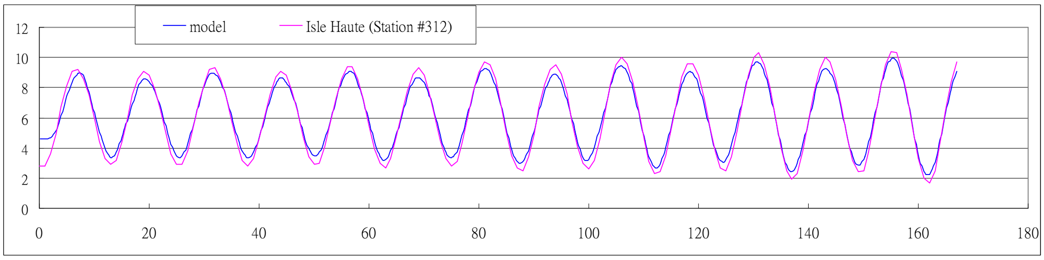

Figure 23- d: Simulation Result at Isle Haute between 12/14 and 12/20/2006

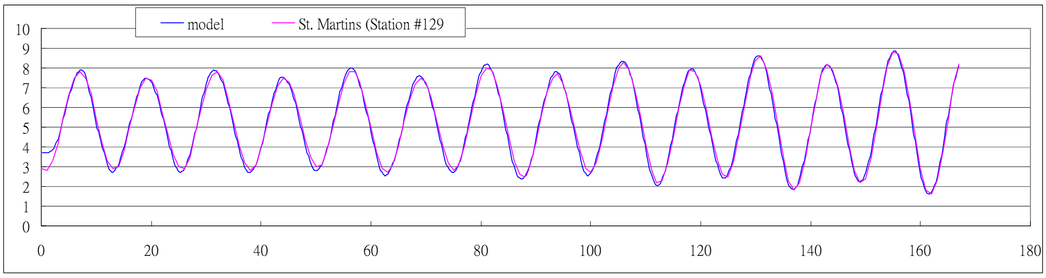

Figure 23- e Simulation Result at St. Martins between 12/14 and 12/20/2006

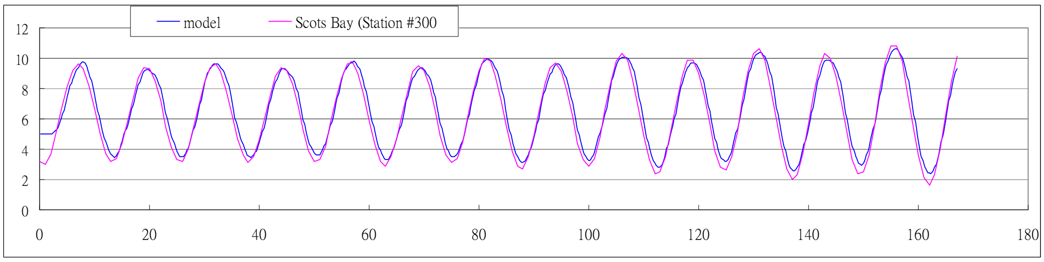

Figure 23- f: Simulation Result at Scots Bay between 12/14 and 12/20/2006

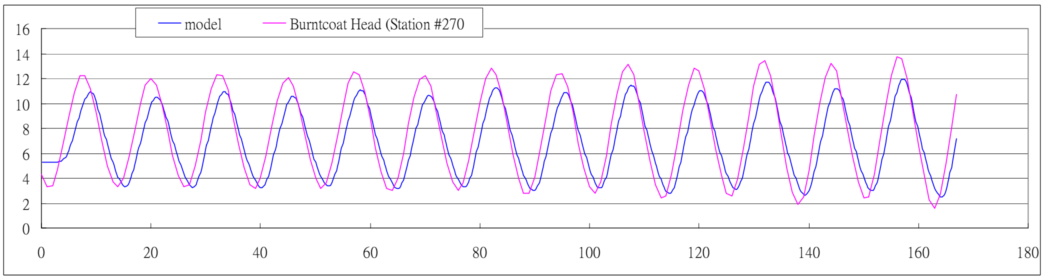

Figure 23- g: Simulation Result at Burntcoat Head between 12/14 and 12/20/2006

Comparing with the simulation results with the measured tide data it is seen that the computer simulation result is very close to the tidal station's record at most of the reference points. Most error occurs at Burntcoat Head. It should be noted that the error is due to Burntcoat Head's location deep inside the Cobequid Bay and is connected to The Bay of Fundy by a narrow entrance – Minas Channel. With such complicated coastline, narrowing and shallowing influences, it is expected that more deviation could occure between the simulation results and measured data. However, the error of the result at Burntcoat Head is less than fifteen percent, which is acceptable since the results at all other reference points are very close.

4.4.3.2 Simulation Result between 2/23 and 3/1/2006 (for verification)

After the model has been calibrated, another set of data is used to verify the numerical model to see if the model is capable of extending its simulation. The set of data which is chosen to verify the model possess a different pattern from the one which is chosen to calibrate the model. Since the data set used for calibration is pretty much uniform with similar tidal range in each cycle, tidal data between February 23 and March 1, 2006 has been chosen since it has more variances in the tidal range within the specified time period. The model results and the measured tide for the period of February 23 to March 1, 2006 are shown in Figures 24 for seven tidal stations.

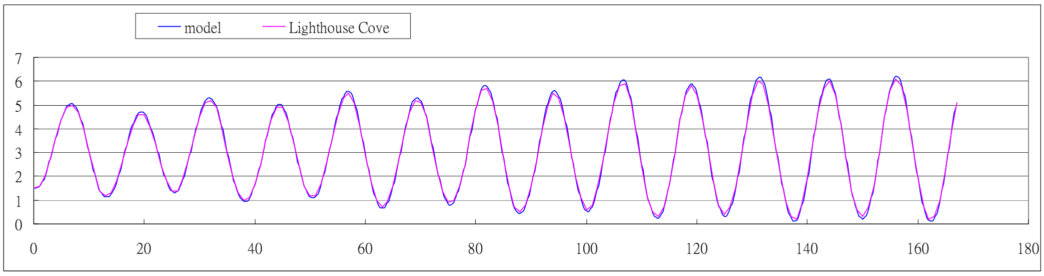

Figure 24- a Simulation Result at entrance of the bay between 2/23 and 3/1/2006

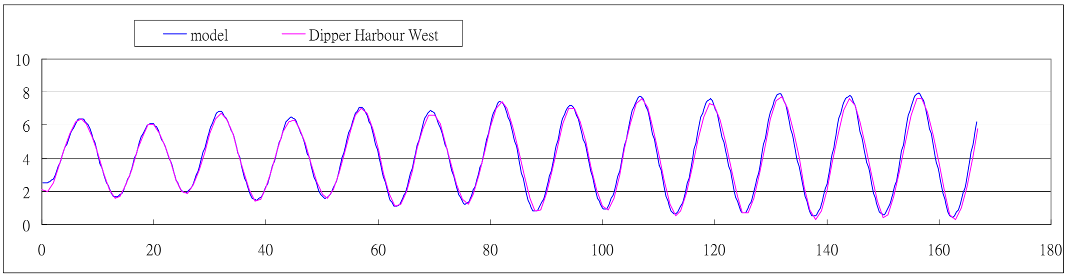

Figure 24- b Simulation Result at Dipper Harbour between 2/23 and 3/1/2006

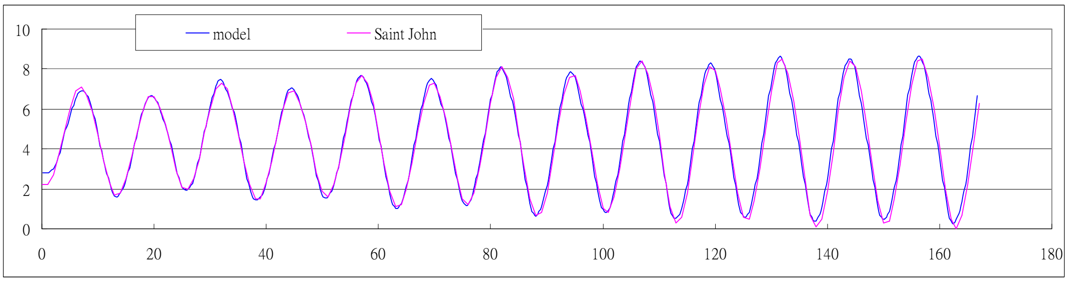

Figure 24- c Simulation Result at St. John between 2/23 and 3/1/2006

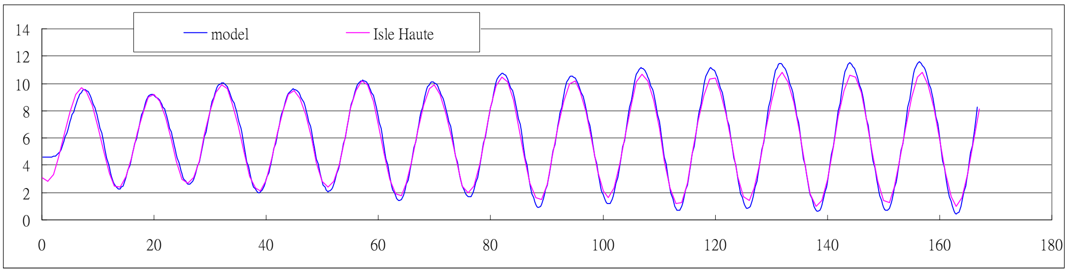

Figure 24- d Simulation Result at Isle Haute between 2/23 and 3/1/2006

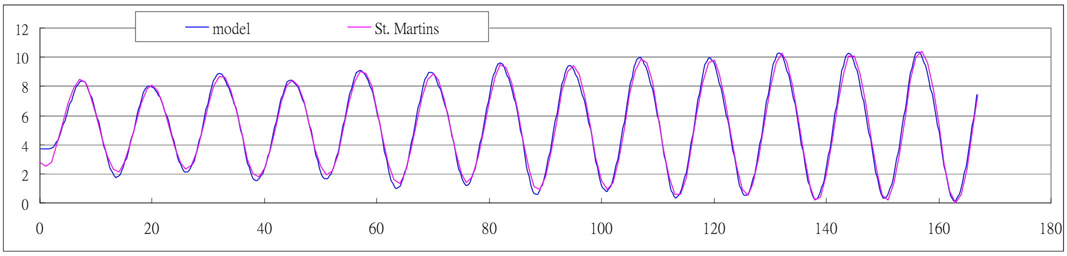

Figure 24- e Simulation Result at St. Martins between 2/23 and 3/1/2006

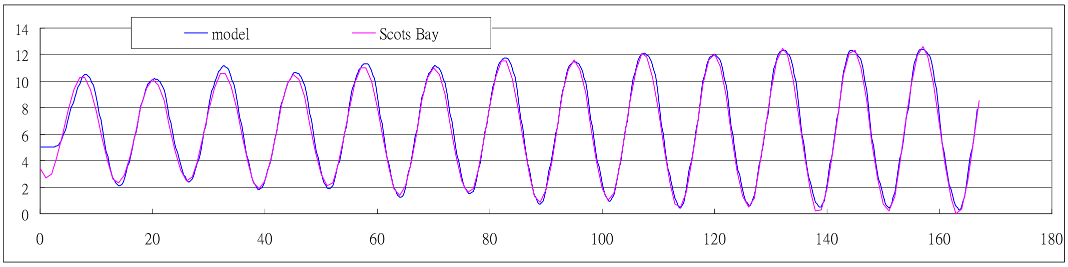

Figure 24- f Simulation Result at Scots Bay between 2/23 and 3/1/2006

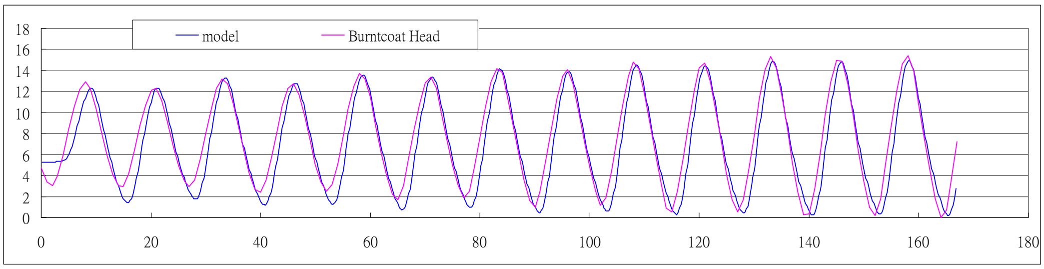

Figure 24- g Simulation Result at Burntcoat Head between 2/23 and 3/1/2006

The response of the tide at all reference points became stable within 10 hours after the simulation started. From Figures 24 the simulation response at each reference point from the hydrodynamic model compared very well with the data from tide gauge stations. The maximum deviations occurred at Burntcoat Head; however, the error was reduced after 60 hours. The result suggests that the current model is capable of handling different patterns of incident tides and it can be used to estimate the response to the incident tide during a long period of simulation. Therefore, it is reasonable to use the model result to predict the responses for other locations. The model results on the tidal range and current velocity pattern for the entire region are therefore used.

From the result of simulation between February 23 and March 1, 2006, we can calculate the tidal range amplification factor. This is shown in Table 4 for six key stations referred in Figure 17. The tidal range amplification factors are a ratio of the local tidal range to the tidal range at the entrance of the Bay.

Location	Tidal Range Amplification Factor	
	Observed	Computer Simulation
Dipper Harbour	1.08 – 1.29	1.08 – 1.29
Saint John	1.21 – 1.38	1.21 – 1.38
Isle Haute	1.71 – 1.76	1.71 – 1.80
St. Martins	1.53 – 1.79	1.53 – 1.79
Scots Bay	2.00 – 2.17	2.00 – 2.14
Burntcoat Head	2.47 – 2.66	2.50 – 2.76

Table 4: Tidal range amplification factor

From Figure 24 and Table 4, it is seen that the simulated result agrees well with the measured result and that the tidal range increases as the distance from the bay entrance is increased.

4.4.3.3 Simulation Result (tidal chart)

Figure 25 shows the tidal ranges at the Outer Wood Island station between January 1, 2006 and June 30, 2007. Because high tide and low tide happen more than once everyday, the tidal range which represented the difference of water elevation between high tide and low tide happens more than once everyday. From the statistics analysis, it shows the tidal range at the Outer Wood Island station is within the range of 2.3 and 5.5 meters, with an average of 3.95 meters and standard deviation equals to 0.71 meters. If we pick up the period of December 12, 2006 to

January 10, 2007, the tidal range in this period is also within the range of 2.3 and 5.5 meters, with an average of 3.94 meters and standard deviation equals to 0.55 meters. The agreement in statistics supports that the water elevation during the period of December 12, 2006 to January 10, 2007 is a common representative of the much longer period of January 1, 2006 and June 30, 2007, and it is suitable to use the result from the shorter period to represent the longer period.

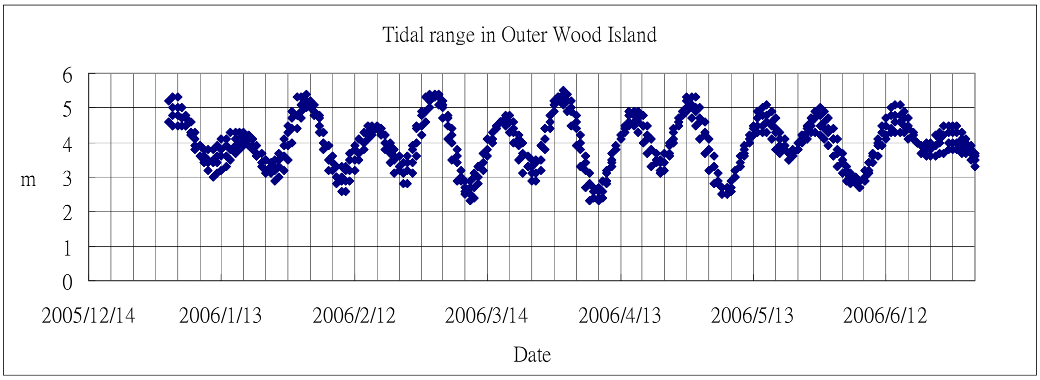

Figure 25- a Tidal range in Outer Wood Island between 1/1/2006 and 7/1/2006

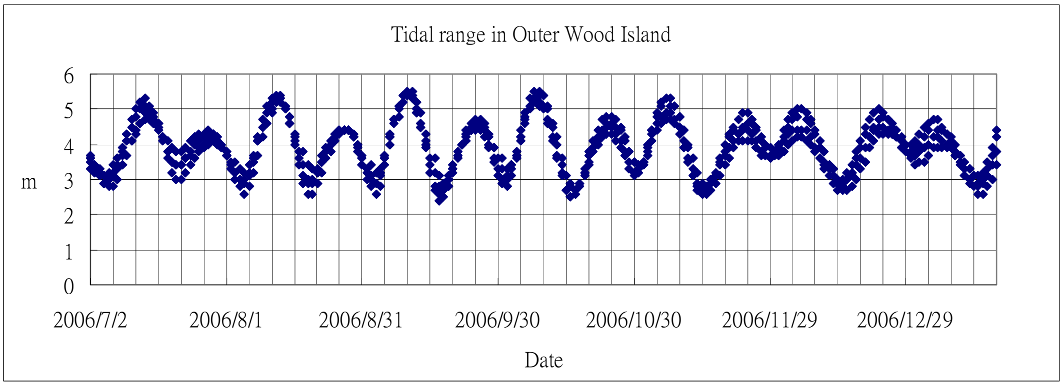

Figure 25- b Tidal range in Outer Wood Island between 7/2/2006 and 1/17/2007

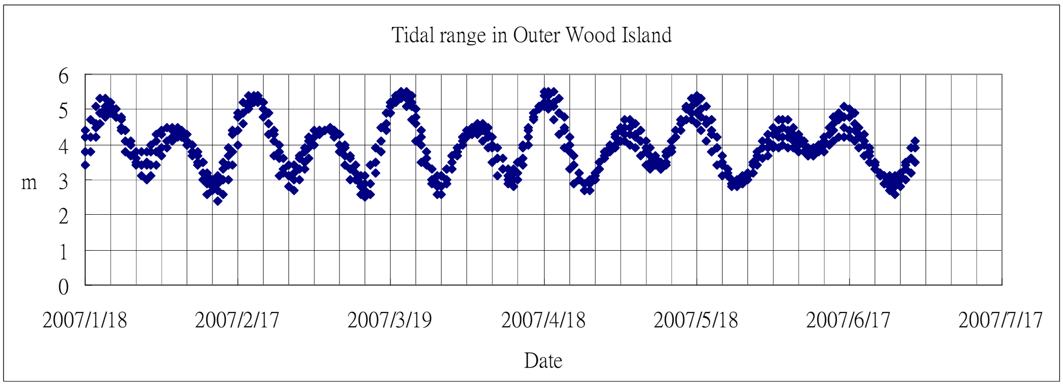

Figure 25- c Tidal range in Outer Wood Island between 1/18/2007 and 6/30/2007

The selected period of December 12, 2006 to January 10, 2007 is used to be the example to present the results of numerical simulation. Figure 26 shows the comparison of the simulation results and the tidal records from the reference stations. Since the comparison for the period of December 12, to December 18, 2006 has been shown in previous section, Figure 26 shows the rest of the time. The data in Figure 26-a are used as the input data for incident wave at the entrance of the Bay of Fundy. As mentioned in the previous section, the simulation results are shifted to lower low water level as the reference level as tidal records do. We can see that the simulation results agree well with the tide record for each tidal station. This provides confidence in using the simulated results for the entire study region.

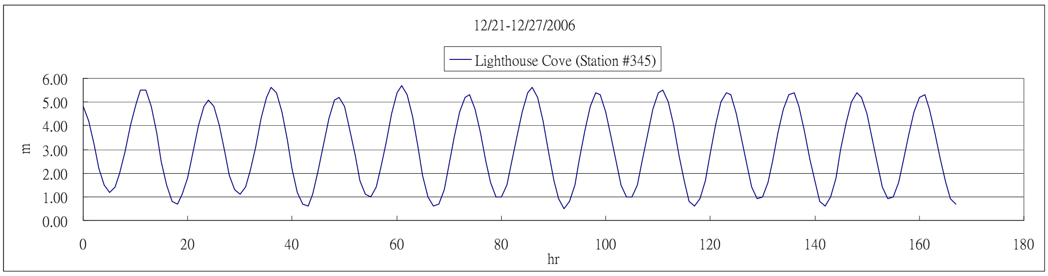

Figure 26- a1:Tidal record at the entrance of bay between 12/21 and 12/27/2006

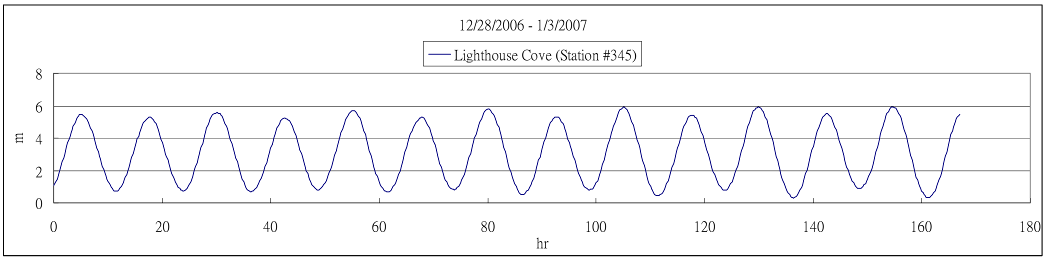

Figure 26- a2: Tidal record at the entrance of bay between 12/28/2006 and 1/3/2007

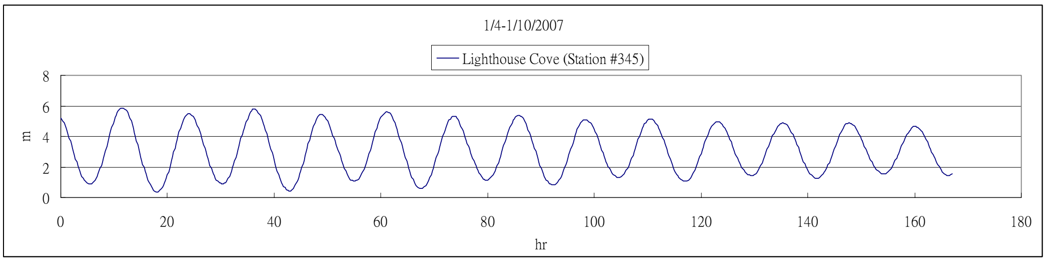

Figure 26- a3: Tidal record at the entrance of bay between 1/4 and 1/10/2007

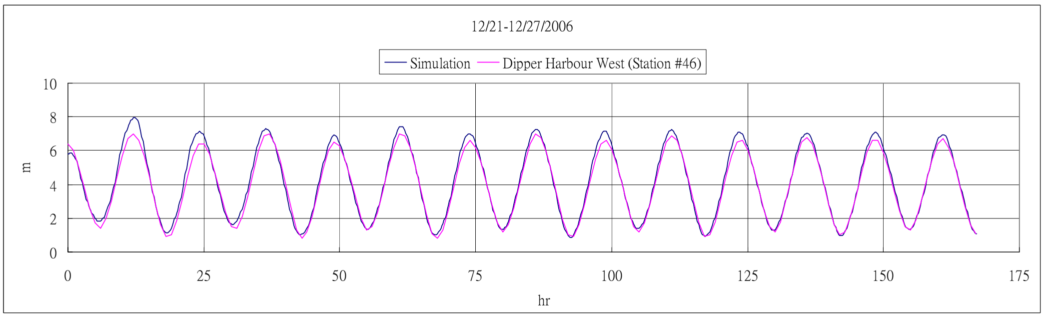

Figure 26- b1: Simulation Result at the Dipper Harbour between 12/21 and 12/27/2006

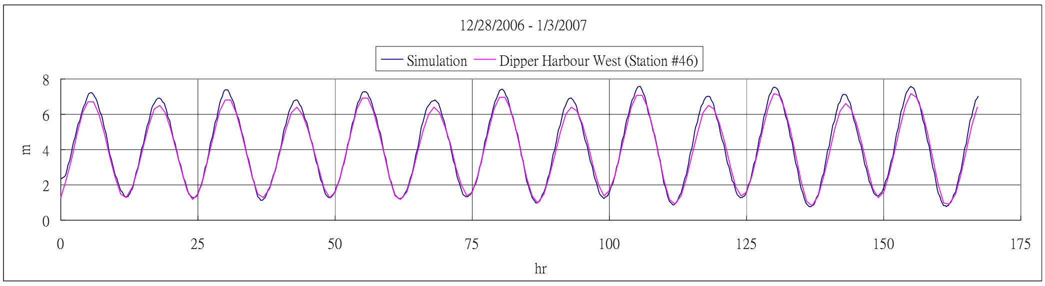

Figure 26- b2: Simulation Result at the Dipper Harbour between 12/28/2006 and 1/3/2007

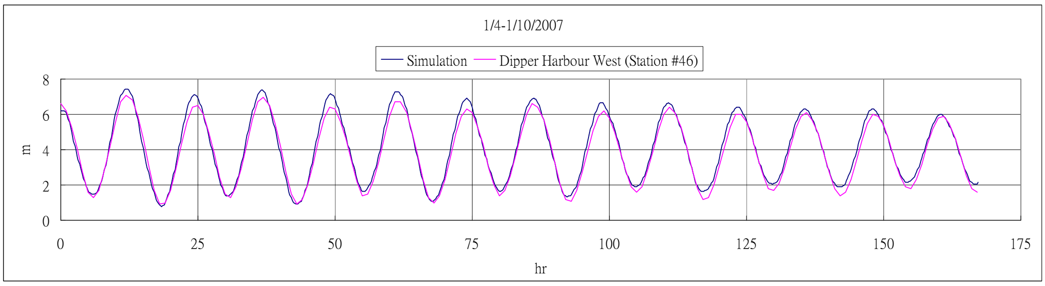

Figure 26- b3: Simulation Result at the Dipper Harbour between 1/4 and 1/10/2007

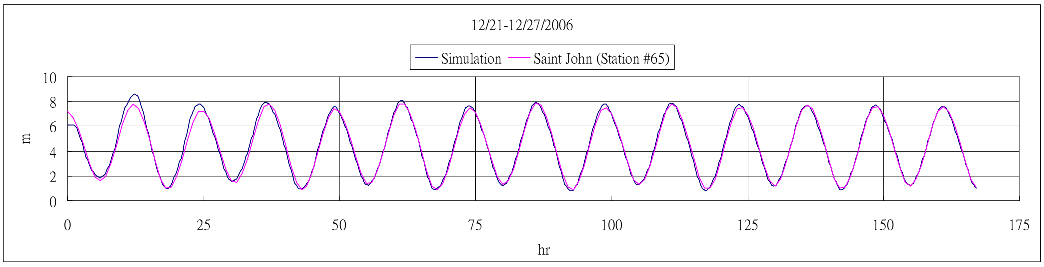

Figure 26- c1: Simulation Result at St. John between 12/21 and 12/27/2006

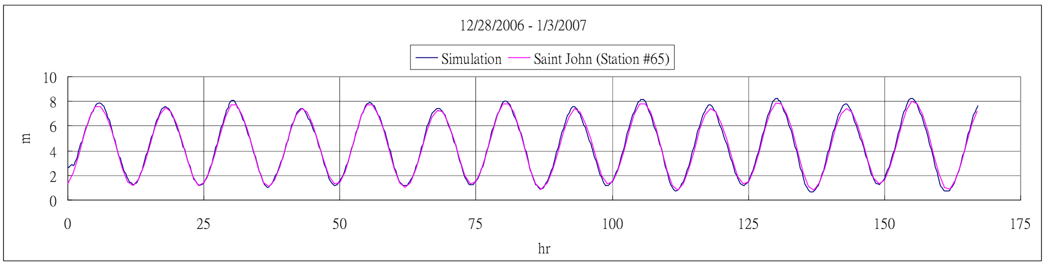

Figure 26- c2: Simulation Result at St. John between 12/28/2006 and 1/3/2007

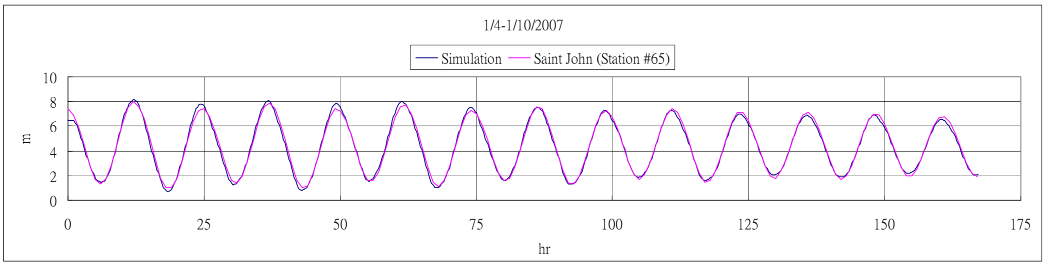

Figure 26- c3: Simulation Result at St. John between 1/4 and 1/10/2007

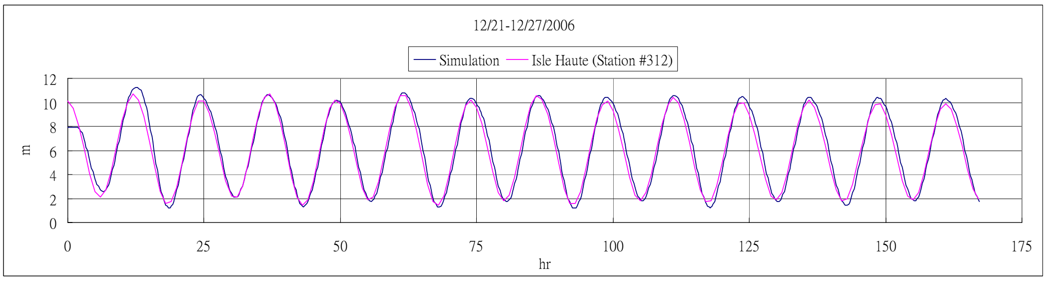

Figure 26- d1: Simulation Result at Isle Haute between 12/21 and 12/27/2006

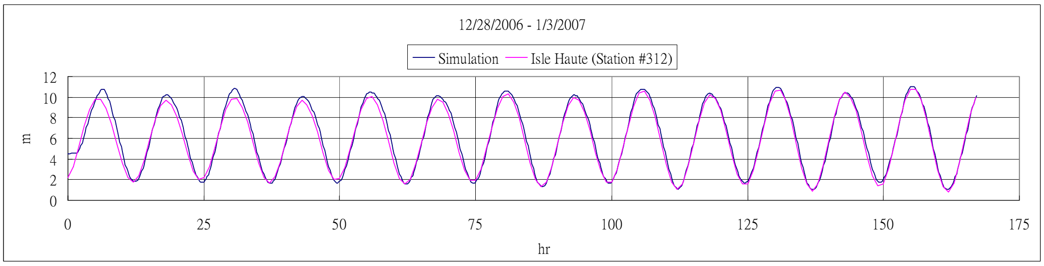

Figure 26- d2: Simulation Result at Isle Haute between 12/28/2006 and 1/3/2007

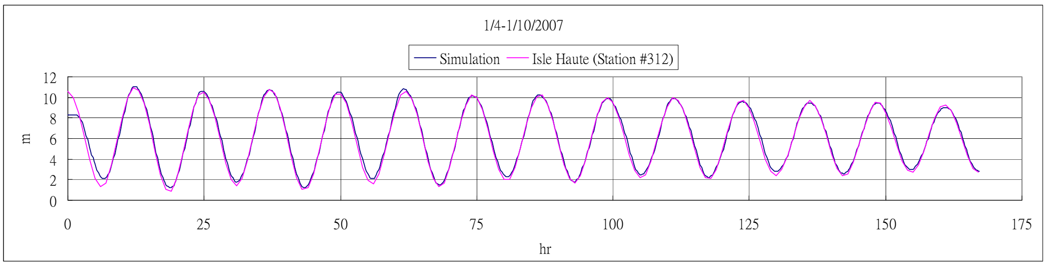

Figure 26- d3: Simulation Result at Isle Haute between 1/4 and 1/10/2007

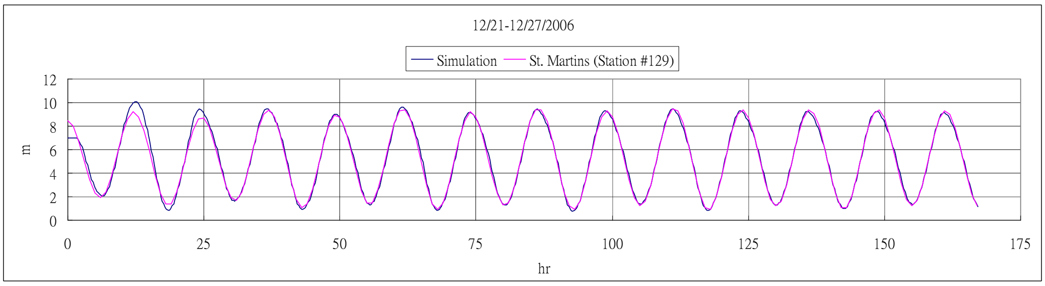

Figure 26- e1: Simulation Result at St. Martins between 12/21 and 12/27/2006

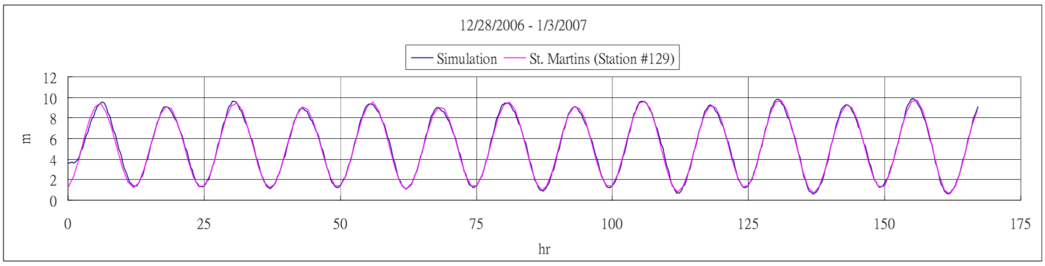

Figure 26- e2: Simulation Result at St. Martins between 12/28/2006 and 1/3/2007

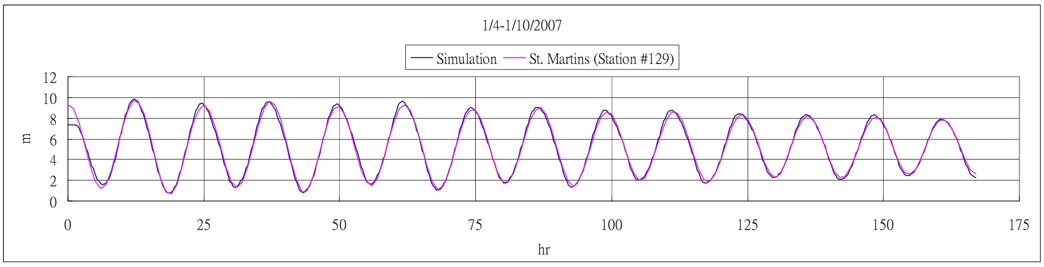

Figure 26- e3: Simulation Result at St. Martins between 1/4 and 1/10/2007

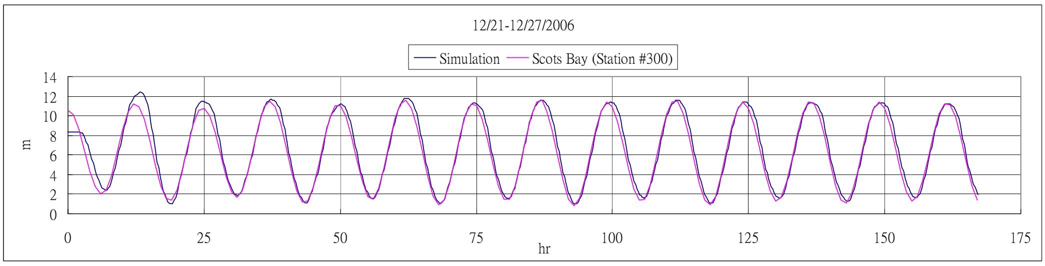

Figure 26- f1: Simulation Result at Scots Bay between 12/21 and 12/27/2006

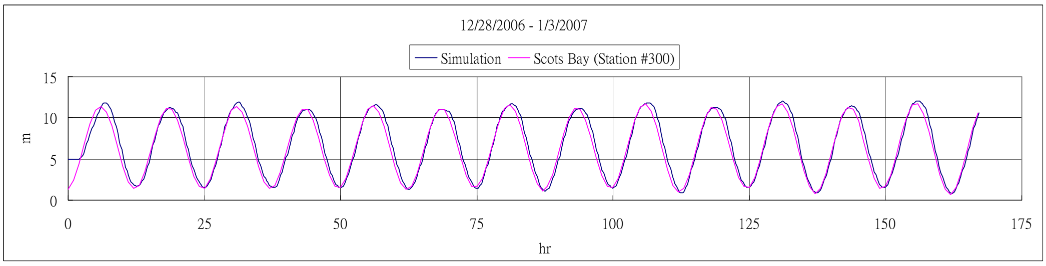

Figure 26- f2: Simulation Result at Scots Bay between 12/28/2006 and 1/3/2007

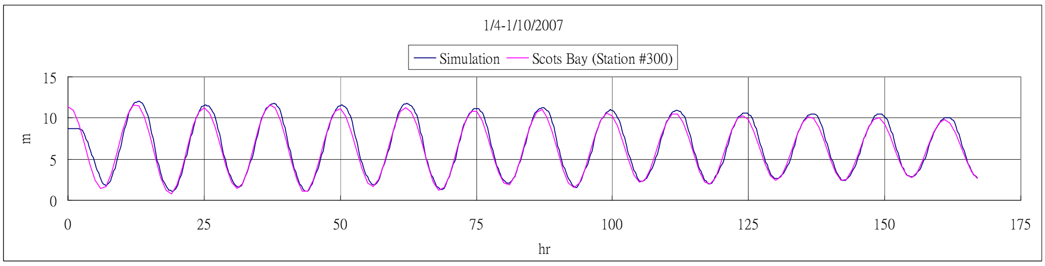

Figure 26- f3: Simulation Result at Scots Bay between 1/4 and 1/10/2007

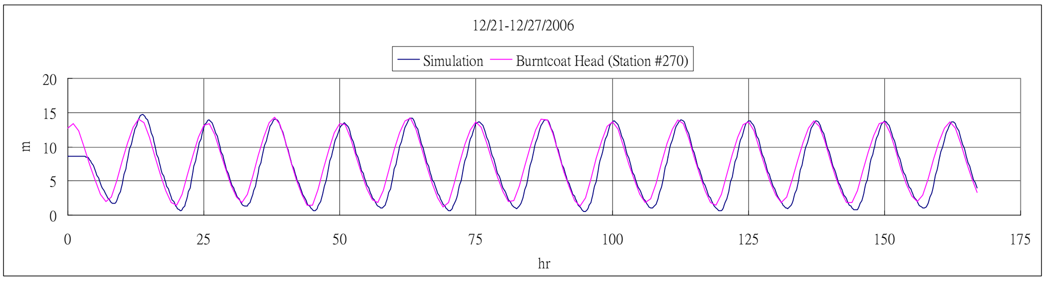

Figure 26- g1: Simulation Result at Burntcoat Head between 12/21 and 12/27/2006

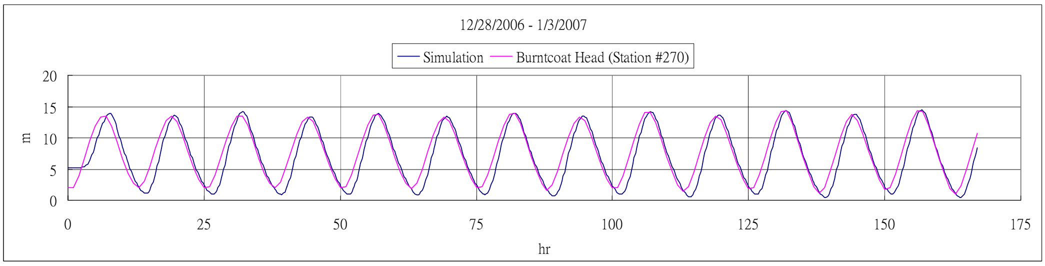

Figure 26- g2: Simulation Result at Burntcoat Head between 12/28/2006 and 1/3/2007

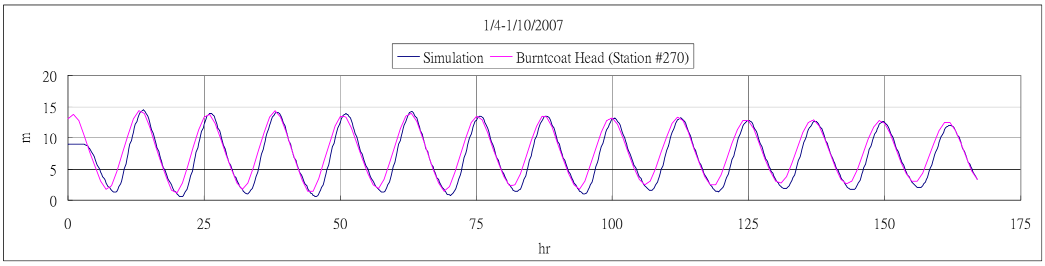

Figure 26- g3: Simulation Result at Burntcoat Head between 1/4 and 1/10/2007

The simulated results of the hourly tidal level are shown in Figure 27. These represent the water level response at one hour interval between 1 am to 8 pm for December 22, 2006. Since the major tidal period is around 12.5 hours, the twenty hours response showing in Figure 27 covers the entire repeated cycle. The unit for X and Y coordinate is kilometer. The water level at each point is represented by "h" in meters and referred to mean sea level. It is seen from Figures 27 that the tide gradually flows into and out of the bay, and the higher water levels are found in both the north basins.

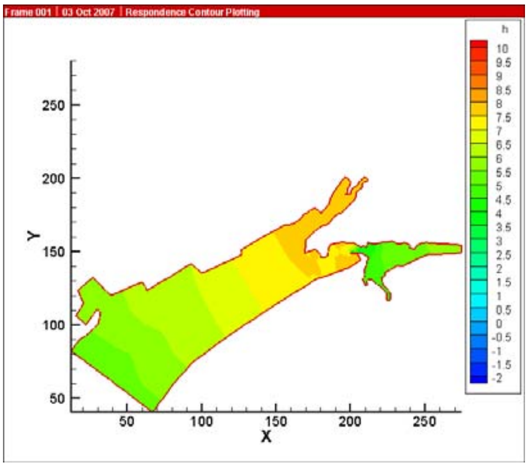

Figure 27-a: Water elevation, t=1 hour

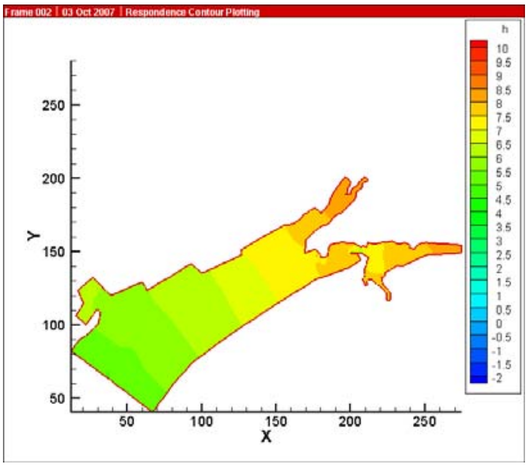

Figure 27-b: Water elevation, t= 2 hour

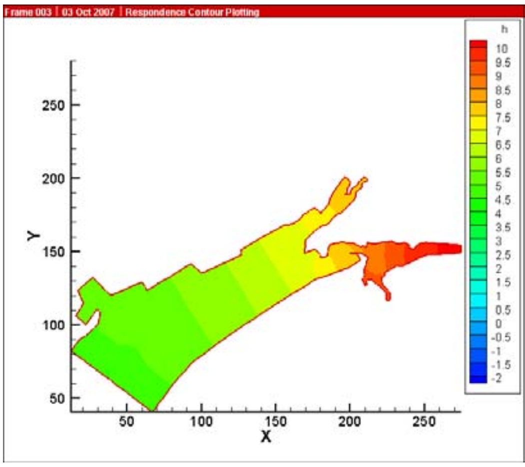

Figure 27-c: Water elevation, t = 3 hour

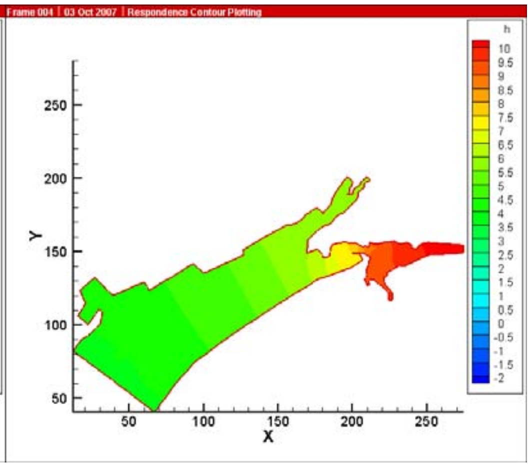

Figure 27-d: Water elevation, t = 4 hour

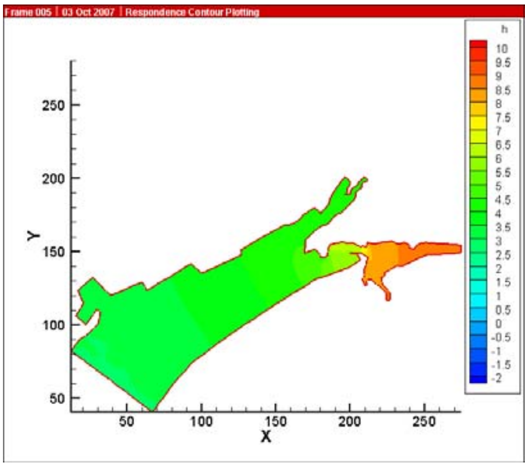

Figure 27-e: Water elevation, t = 5 hour

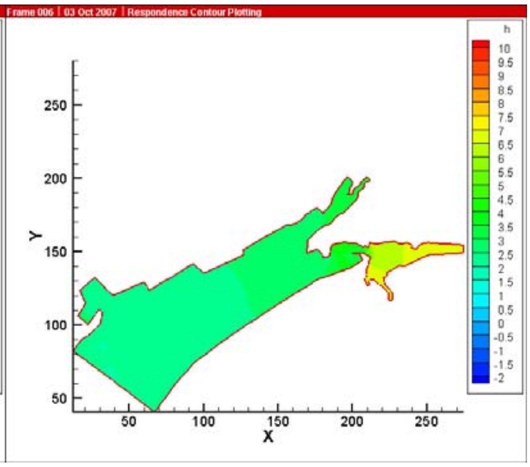

Figure 27-f: Water elevation, t = 6 hour

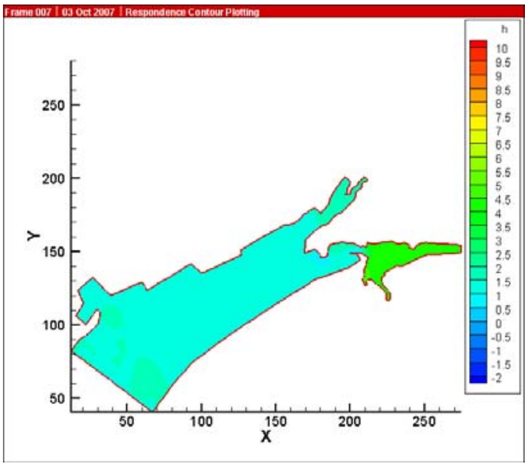

Figure 27-g: Water elevation t = 7 hour

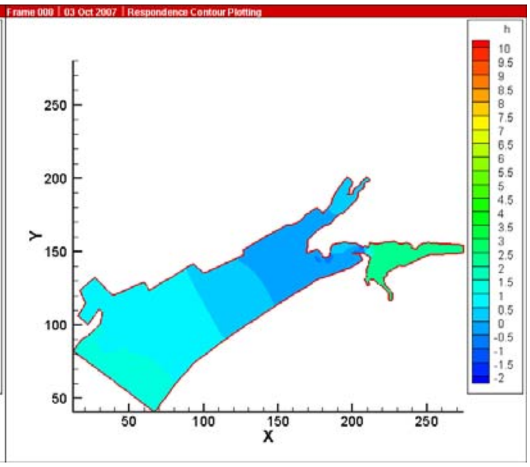

Figure 27-h: Water elevation t = 8 hour

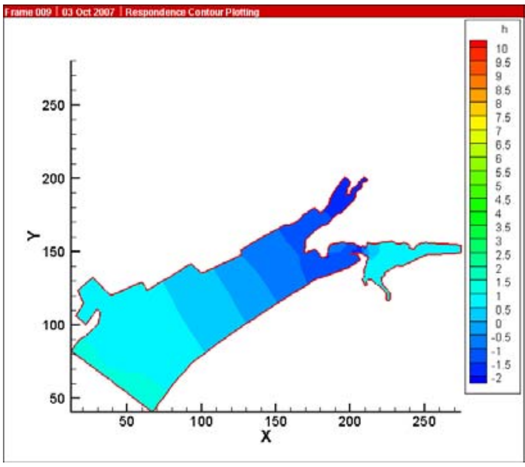

Figure 27-i: Water elevation, t = 9 hour

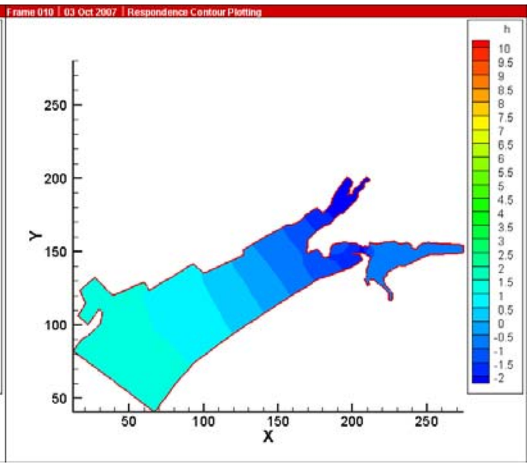

Figure 27-j: Water elevation, t = 10 hour

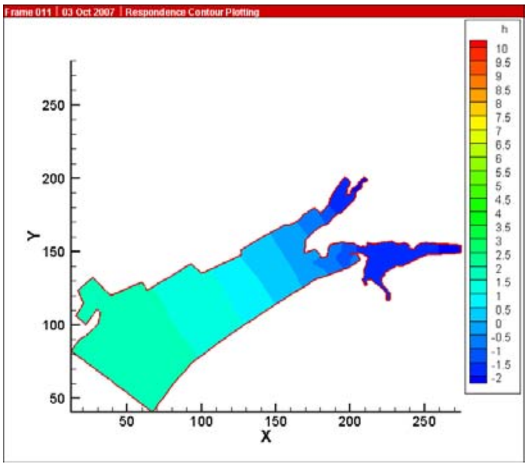

Figure 27-k: Water elevation, t = 11 hour

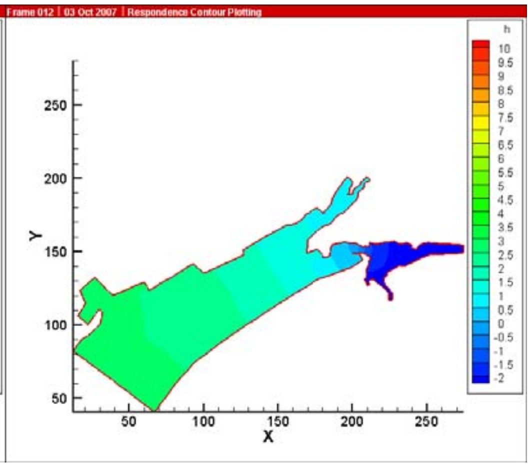

Figure 27-l: Water elevation, t = 12 hour

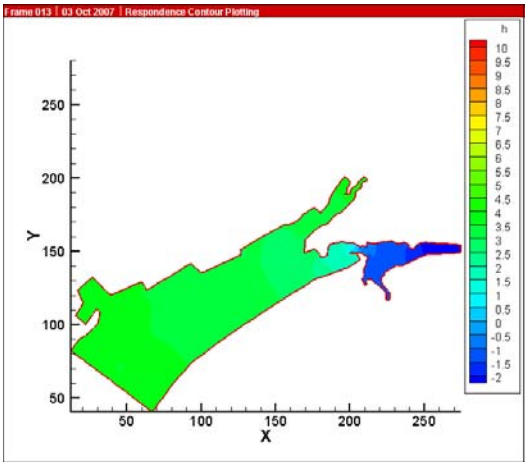

Figure 27-m: Water elevation, t = 13 hour

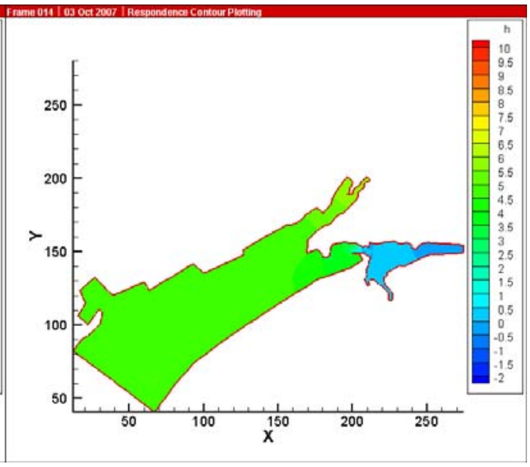

Figure 27-n: Water elevation, t = 14 hour

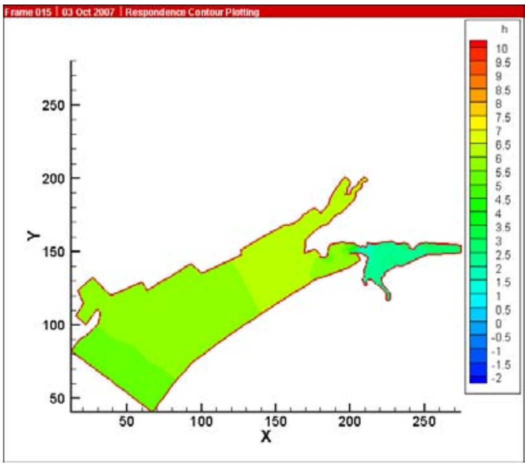

Figure 27-o: Water elevation, t = 15 hour

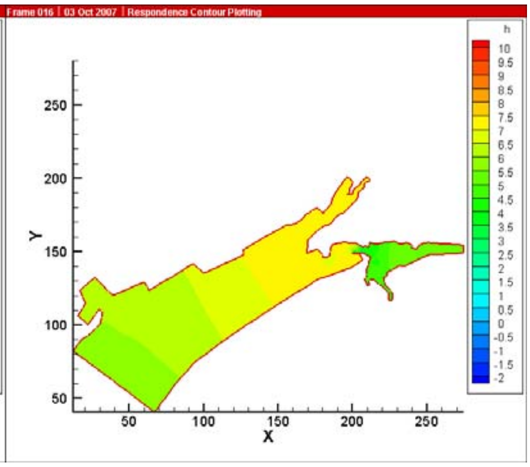

Figure 27-p: Water elevation, t = 16 hour

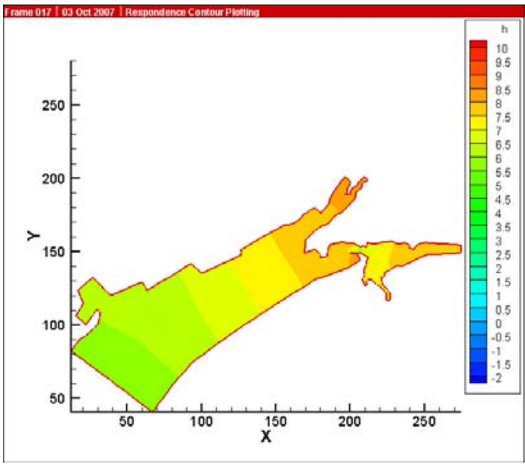

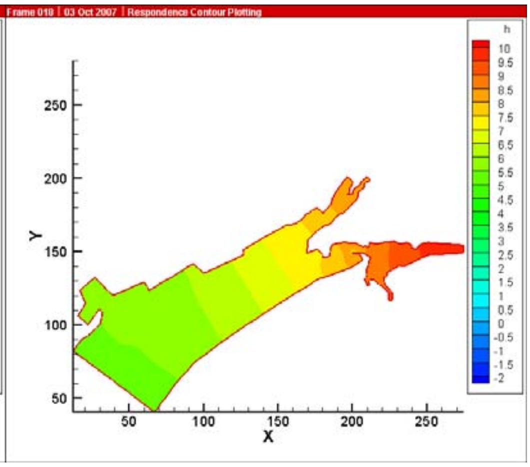

Figure 27-q: Water elevation, t = 17 hour Figure 27-r: Water elevation, t = 18 hour

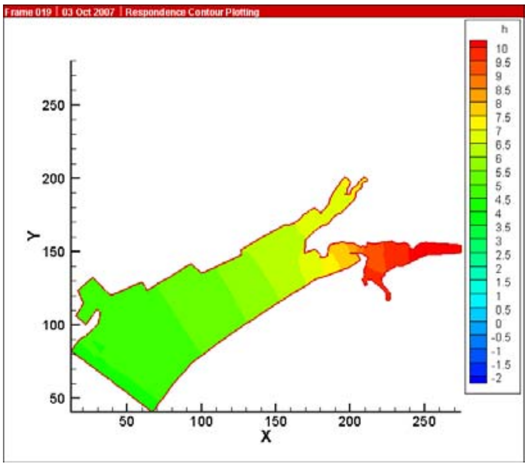

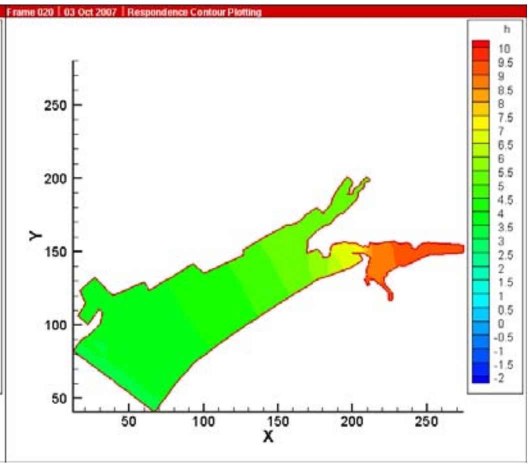

Figure 27-s: Water elevation, t = 19 hour Figure 27-t: Water elevation, t = 20 hour

The tidal current velocity for the model region is presented in Figure 28. The time period covered is between 1 am to 8 pm for December 22nd, 2006. The scale of one meter per second is shown as the legend at the upper right corner. It is seen from the vector plots that the largest velocity vector is found at the mouth of the Bay of Fundy, and at both the entrance of north basins, especially around the Minas Channel -- the entrance to the Minas Basin and the Cobequid Bay. It is because that the water body inside the basin needs to flow in and out of the basin to generate the spring or ebb tide. The larger of the basin and the tidal range, and the narrower of the flow channel, the larger tidal current will be generated.

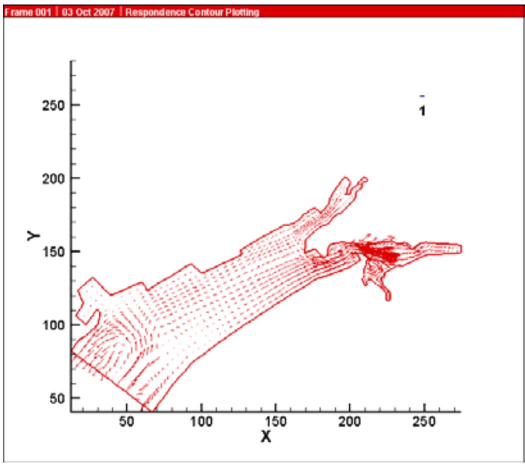

Figure 28-a: Current velocity, t=1 hour

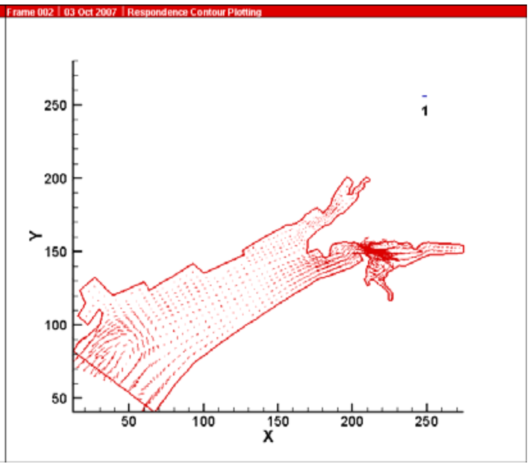

Figure 28-b: Current velocity, t= 2 hour

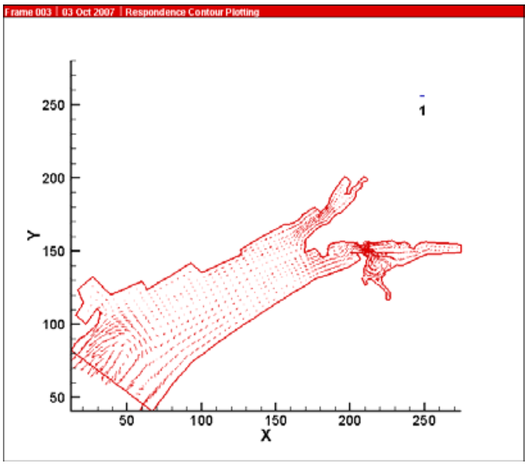

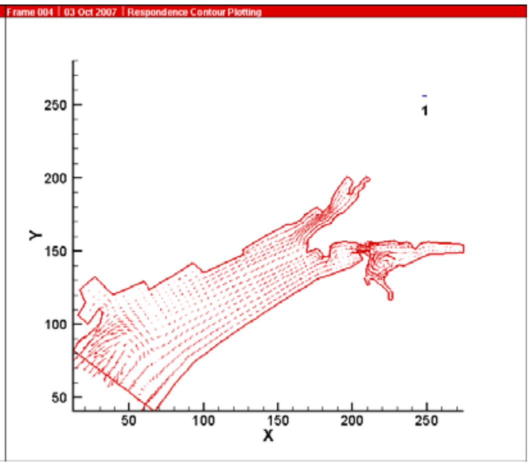

Figure 28-c: Current velocity, t = 3 hour

Figure 28-d: Current velocity, t = 4 hour

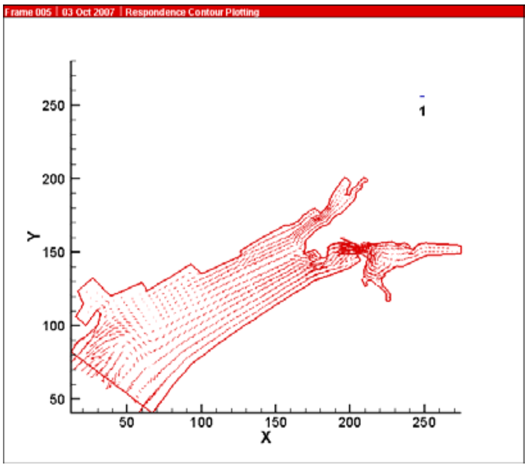

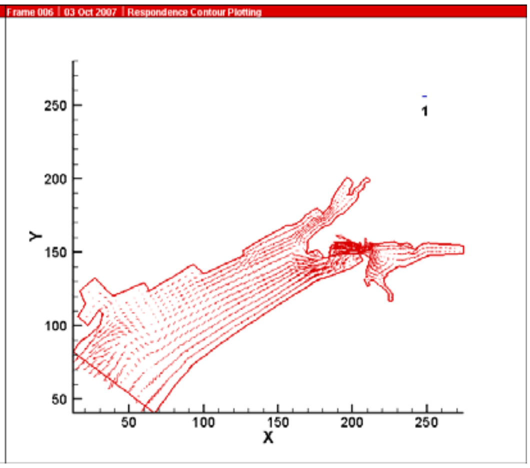

Figure 28-e: Current velocity, t = 5 hour

Figure 28-f: Current velocity, t = 6 hour

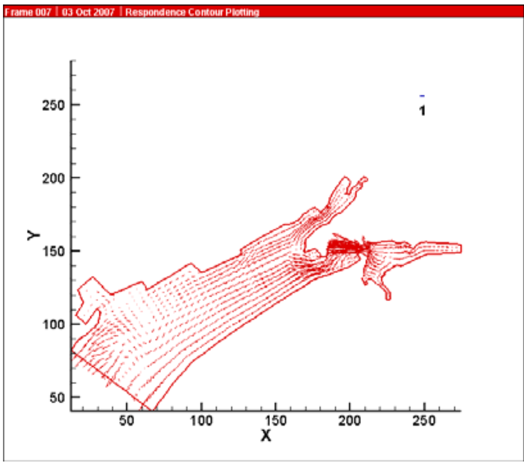

Figure 28-g: Current velocity, t = 7 hour

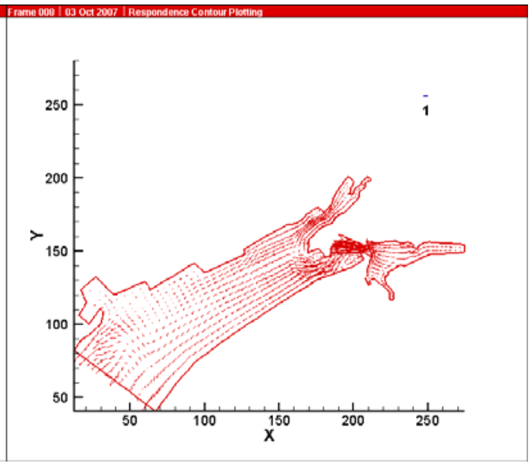

Figure 28-h: Current velocity, t = 8 hour

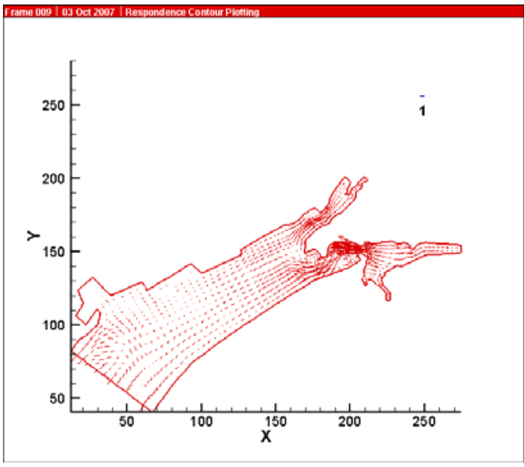

Figure 28-i: Current velocity, t = 9 hour

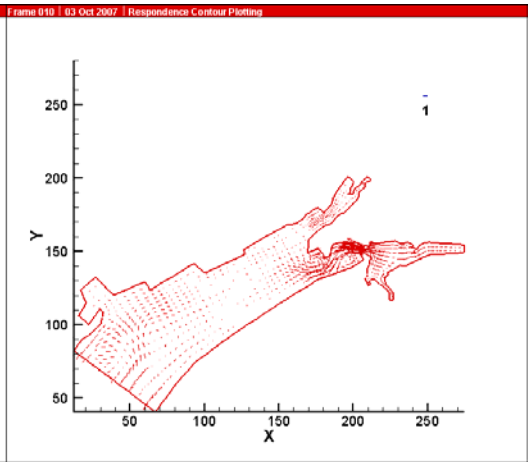

Figure 28-j: Current velocity, t = 10 hour

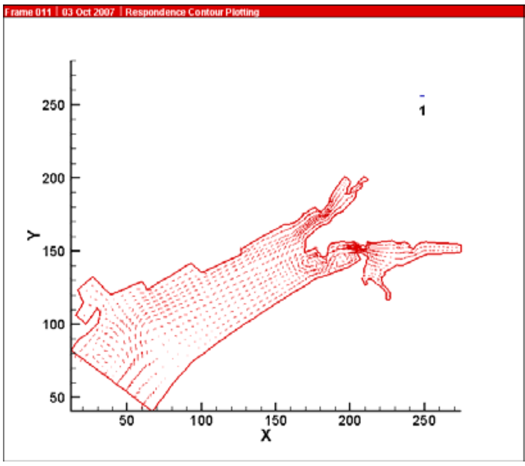

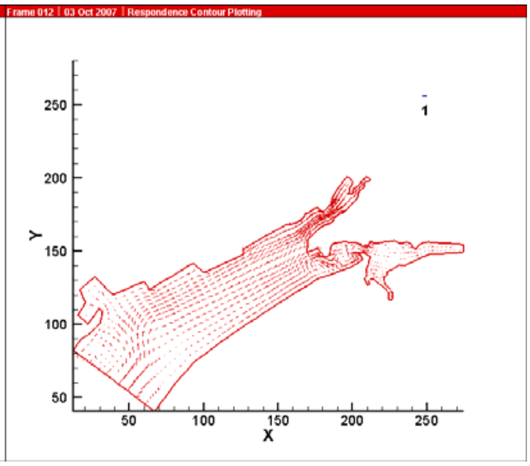

Figure 28-k: Current velocity, t = 11 hour   Figure 28-l: Current velocity, t = 12 hour

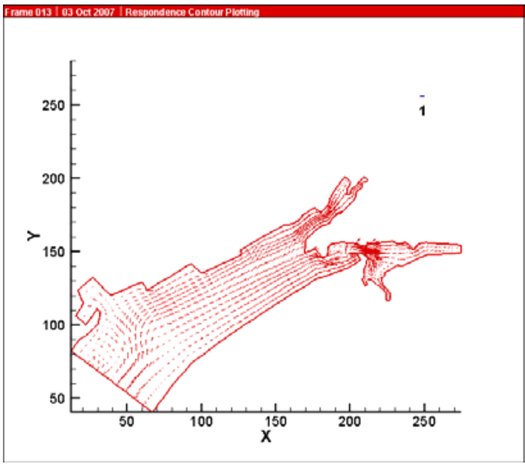

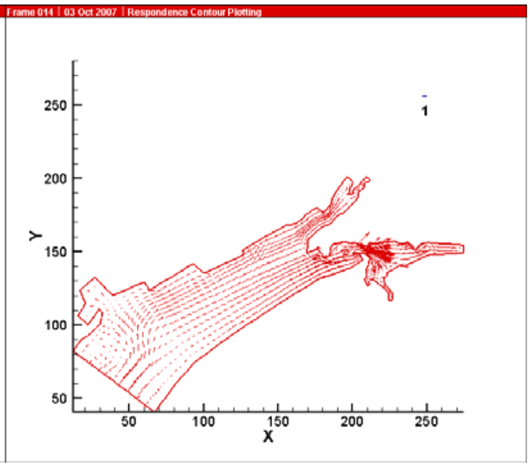

Figure 28-m: Current velocity, t = 13hour   Figure 28-n: Current velocity, t = 14hour

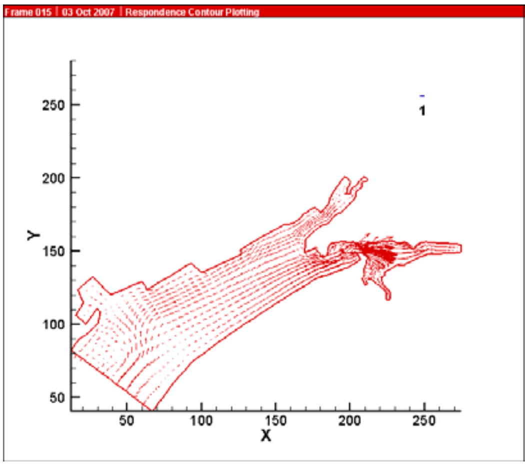

Figure 28-o: Current velocity, t = 15hour

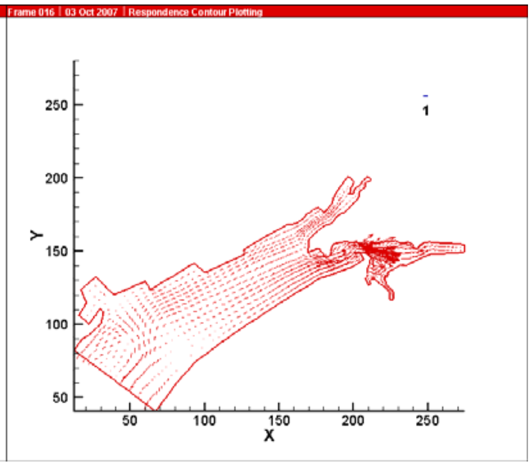

Figure 28-p: Current velocity, t = 16hour

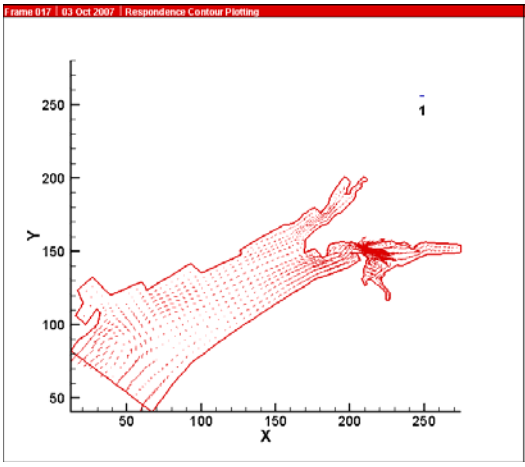

Figure 28-q: Current velocity, t = 17hour

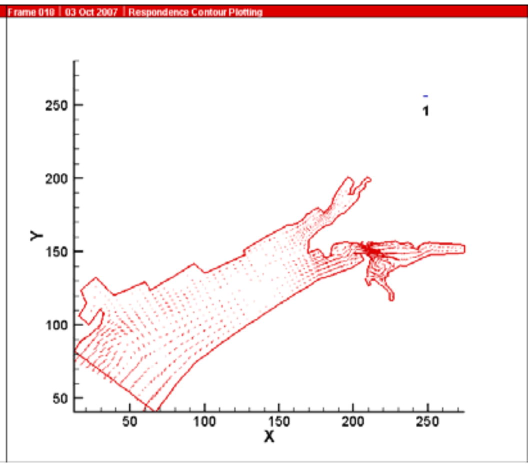

Figure 28-r: Current velocity, t = 18hour

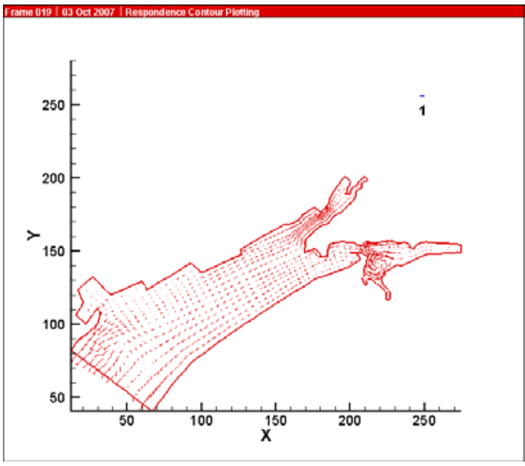

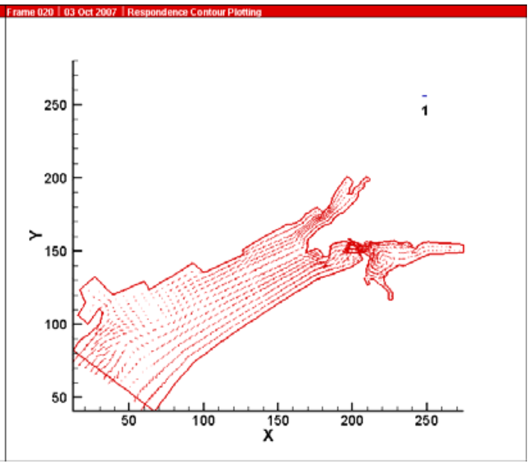

Figure 28-s: Current velocity, t = 19hour   Figure 28-t: Current velocity, t = 20hour

The maximum and minimum tidal ranges as well as the average tidal ranges for the period of December 12, 2006 to January 10, 2007 are shown in Figures 29 and 30 can be made. In these figures, “Z” represents tidal range, and the unit is in meters. Figure 29-a shows the maximum tidal range can be found at each location within this period of time. It is about 6 meters at the entrance of the Bay of Fundy and gradually increased to more than 14 meters to the north into the Cobequid Bay. Figure 29-b shows the minimum tidal range in the simulation period. Cobequid Bay maintains the highest minimum tidal range in the entire region at 12 meters. Since Cobequid Bay has the highest tidal range in this region, it also maintains a larger minimum tidal range. Thus, it is a favorable location for the generation of tidal power.

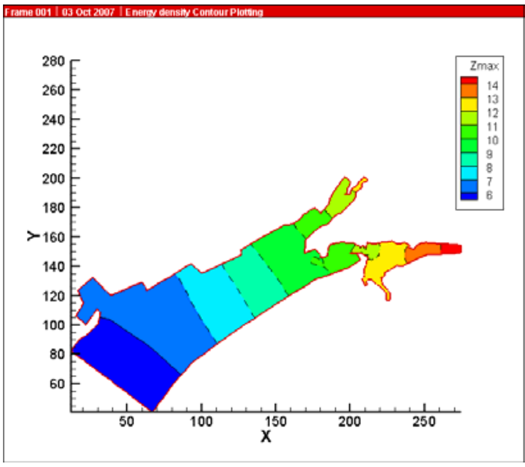

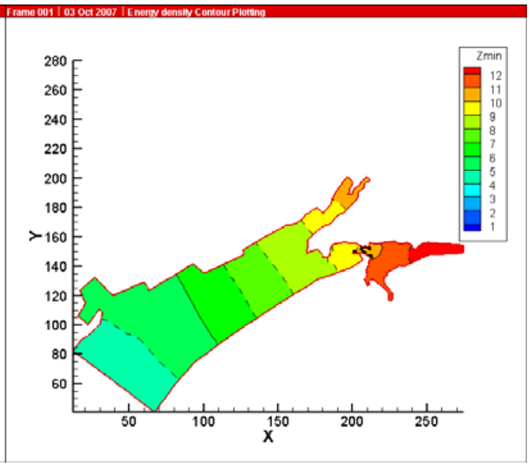

Figure 29-a: Maximum tidal range

Figure 29-b: Minimum tidal range

The average tidal ranges in an hour can be found in Figure 30. For example, within twelve hours, if there is a tidal pattern starting from spring tide, ebb tide and end at spring tide, there will be two tidal range found. In this case, the average tidal range in an hour can be calculated by add the tidal ranges and divided by twelve hours. This value provides an indication of the average energy it can generate since the energy output from a barrage type generation plant is proportional to the tidal range. Another factor for the energy output is the size of the basin (or head pond in a barrage type generation plant). For example, in going deep into Cobequid Bay, the average hourly tidal range increase which is prefer to tidal power generation, but the decreasing surface area of the basin offset the potential benefits.

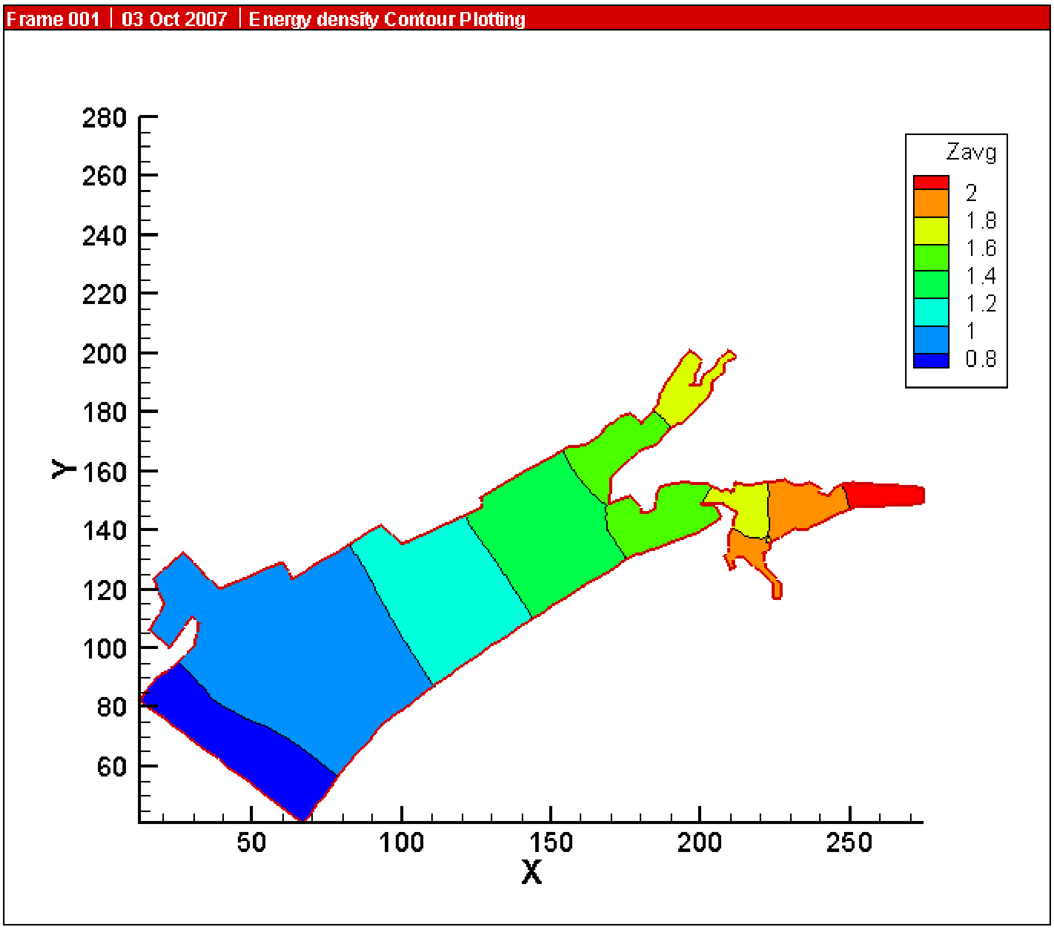

Figure 30: Average tidal ranges in an hour

For the tidal current turbine type of tidal power plant, current velocity is the key parameter for the choice of favorable location of installation. In this type of power plant, the energy output is transferred from kinetic energy which is proportional to the cubic power of the current velocity. Figure 31-a shows the average kinetic energy density, which is calculated from the average of the cubic power of current velocity in time (in hour), with a unit of m^3 /sec^3 /hour. A location with higher average kinetic energy density is more suitable for the tidal current turbine type of tidal power plant. In Figure 31-a, the suitable sites are concentrated in the entrance of Minas Basin, that is, the Minas Channel. A more detail plot is seen in Figure 31-b.

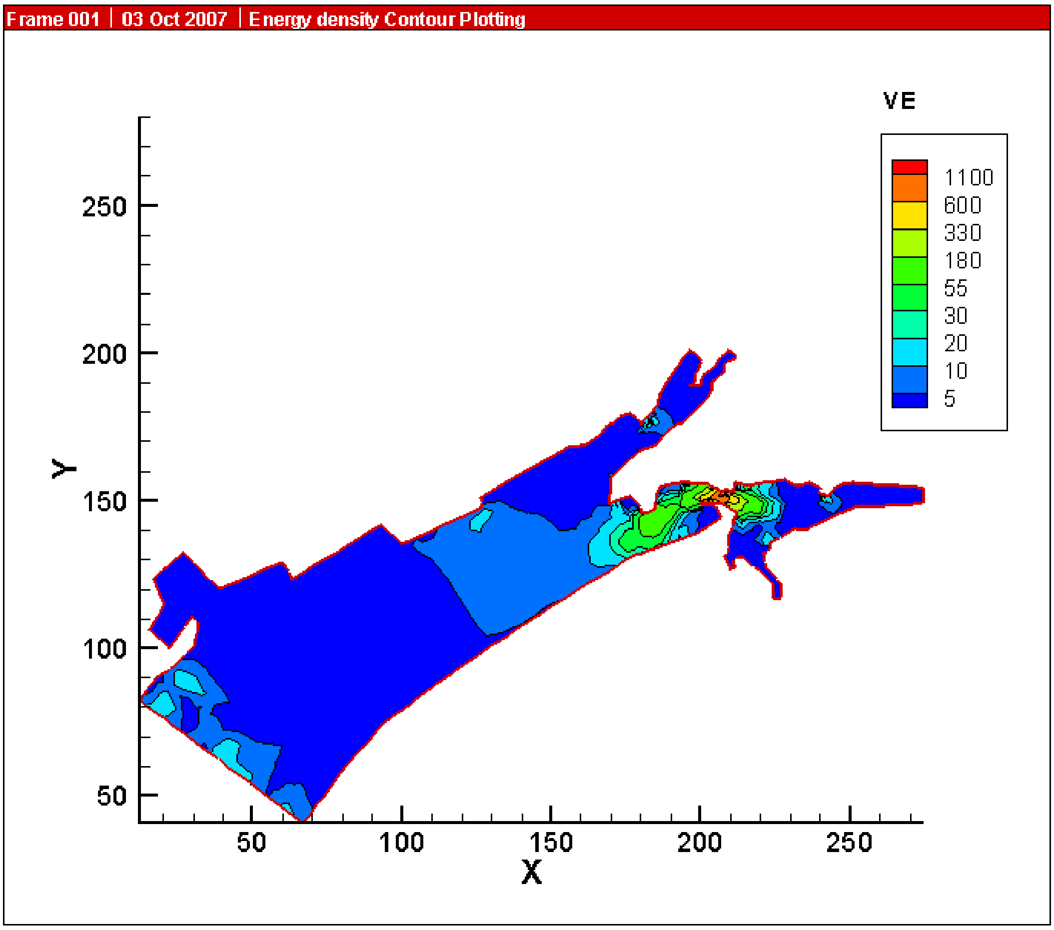

Figure 31-a: Average kinetic energy density (V^3)

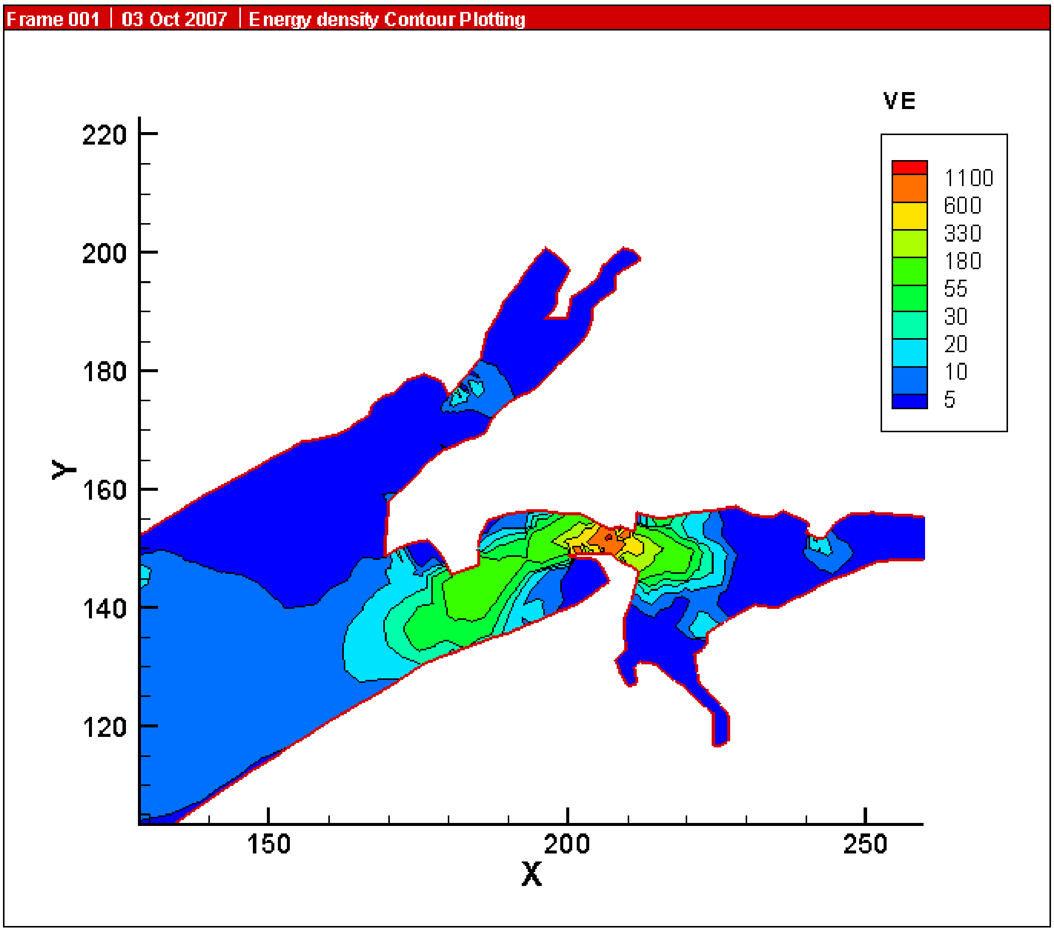

Figure 31-b: **Average kinetic energy density (V^3)**

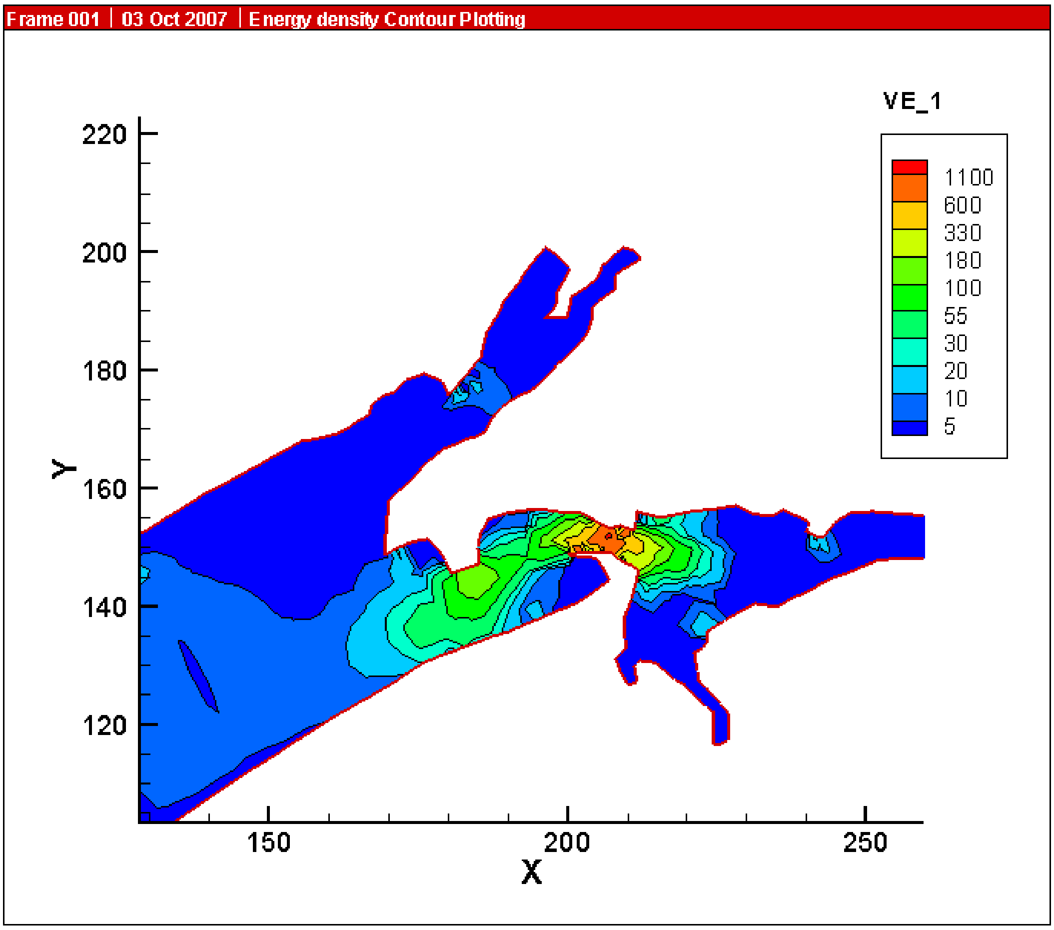

Figure 32-a: Average kinetic energy density (V^3)

– when current velocity is higher than 1 m/sec

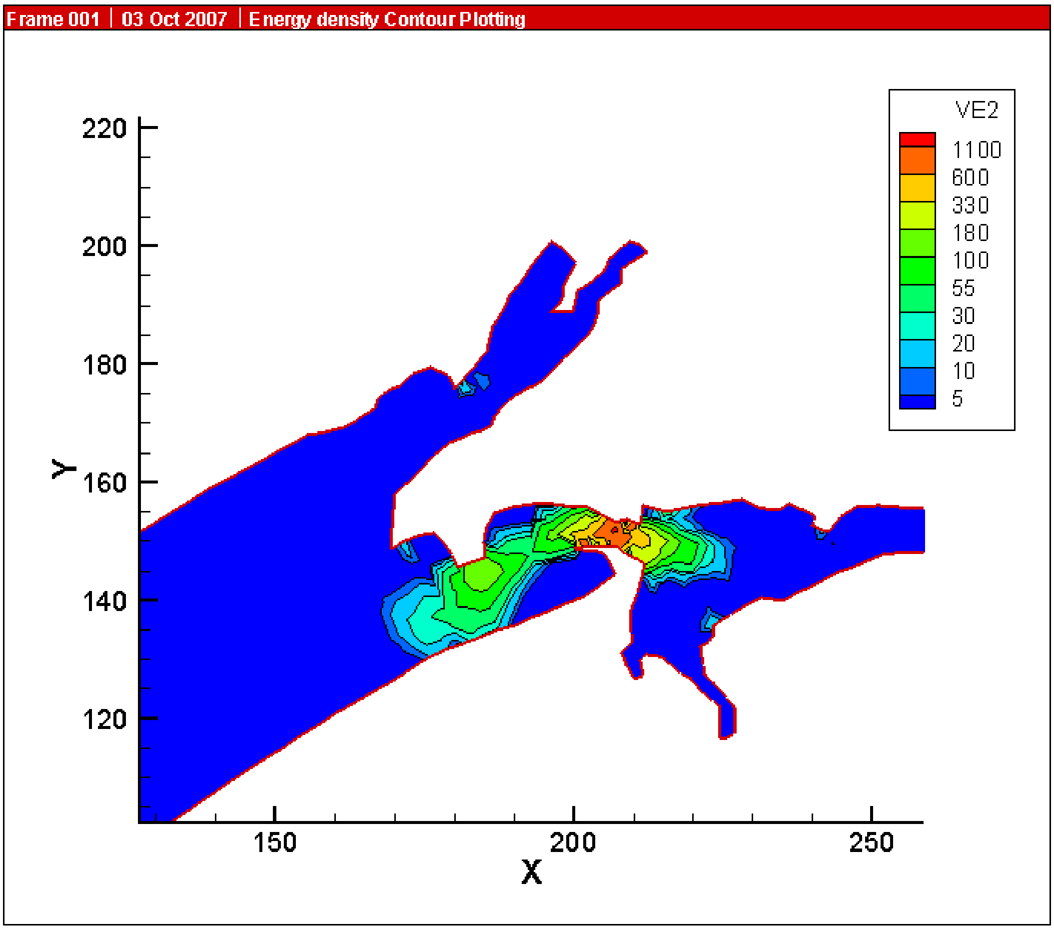

Figure 32-b: Average kinetic energy density (V^3)

– when current velocity is higher than 2 m/sec

A current turbine does not running all the time. Depend on the developing technology and design, different turbines have their own characteristic curve for performance which limit their operation pattern and operational current velocity. Usually, the turbine will stop operating when the current velocity is too high or too low. Since there is no prior reference for economically operated current turbine type tidal power plant, this study assumes the turbine will start running when the current velocity is higher than 1 m/sec (Figure 32-a) or higher than 2 m/sec (Figure 32-b). However, there is not too much difference between these two figures. In the region of Minas Channel, the velocity is higher than 1 or 2 meter per second most of the time.

Chapter 5: Tidal Power Calculation

The energy output from both barrage type of tidal power plant and tidal current turbine will be estimated according to the simulation result of tidal response and the tidal current velocity. The possible energy output will be calculated for some proposed sites and designs for the barrage type of tidal power plant; and the energy derived from tidal current turbine will use the current turbine specified by Marine Current Turbine, Ltd (shown in section 3.4.2).

5.1 Barrage Type of Tidal Power Plant

The potential energy output equation for the barrage type of tidal power plant is similar to that used for regular hydro power plant, but the tidal range is used instead of the hydraulic head. The energy output can be calculated by the following equation:

$$E = \gamma * Q * H * E_t * E_g * E_{tr} * L_t * L_{su} * T \tag{5.1}$$

Where:

E : energy generation in kilowatt-hours

γ : 10.1 kN/m^3 for sea water.

Q : turbine flow rate in cubic meter per second

H : net head on the turbine in meters

E_t, E_g, E_{tr} : turbine, generator, and transformer efficiency

L_t ,L_{su} : transmission and station loss factor

T : duration of operation in hours.

Since the tidal range is much less than the head of a regular hydropower plant, the low concentration of energy and the need for a low head hydraulic turbine present an economic draw back. Recent technology has improved the efficiency of low head hydraulic turbine, but to compensate for the low energy concentration a bigger pond is required. In equation (5.1), we noticed the multiple of Q*T represents the amount of water that can be used during the power generation, and the amount of water is proportional to the size of the headpond and the local tidal range. If the variation of the headpond area due to the changing of water elevation is small, the energy generated is proportional to the square of tidal range. Generally, Q is controlled by the sluice gates of the power plant and is designed as large as possible to make use of the tidal range but not too big to produce surge wave with impact to the downstream area.

All the efficiency terms in equation (5.1) depend on the design of a plant, including the choice of turbines, generators and design of transmission. Usually, the total efficiency for hydro-electric generation will be between 40% ~ 80%. Recent tidal power project in Sihwa Lake, South Korea plans to use ten "bulb-type" turbines for 26 MW each. According to VA Tech Hydro, the sub-contractor and technology provider (2005), the area of the headpond of the tidal power plant is 5.7 square kilometers, with the tidal head difference of 5.82 meters and annual circulation of 60 billion tones of sea water. We can find the efficiency of this plant to be around 35%. For the present study, it is assumed that 35%, 50% and 75% of the total efficiency is reached and presented.

An example of single effect operation for a M2 tide is illustrated in Figure 33.

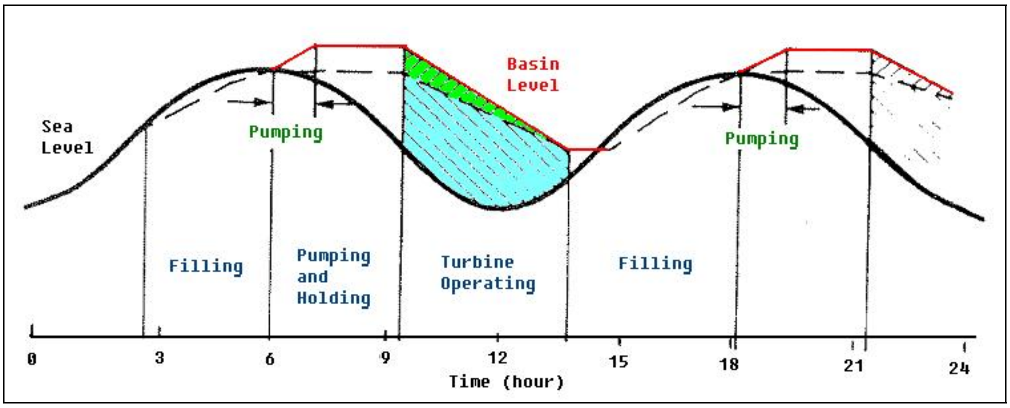

Figure 33: Single Effect Operation for a M2 Tide

This figure shows how to generate energy for a M2 tide in a single effect operation, when generating power during an ebb tide. Sea level outside the barrage moves normally up and down, and the water level inside the basin was controlled by the sluices and power house. We can see that the head difference (between the water level of headpond and sea level outside the barrage) is maintained within a range, which will be corresponded to the design rate of the turbines to make the maximum capacity rate of generation facility. The shaded area represents the energy-generating stage and is dependent on the design rate for sluices and turbines. Extra energy represented by the upper part of the shape area can be gotten by a pumping storage system.

In 1977, three sites were recommended by The Bay of Fundy Tidal Power Review Board for further study. They are shown in Figure 34:

Site A6 – Shepody Bay, at northwest part of Chignecto Bay.

Site A8 – Cumberland Basin, at northeast of Chignecto Bay.

Site B9 – Minas Basin.

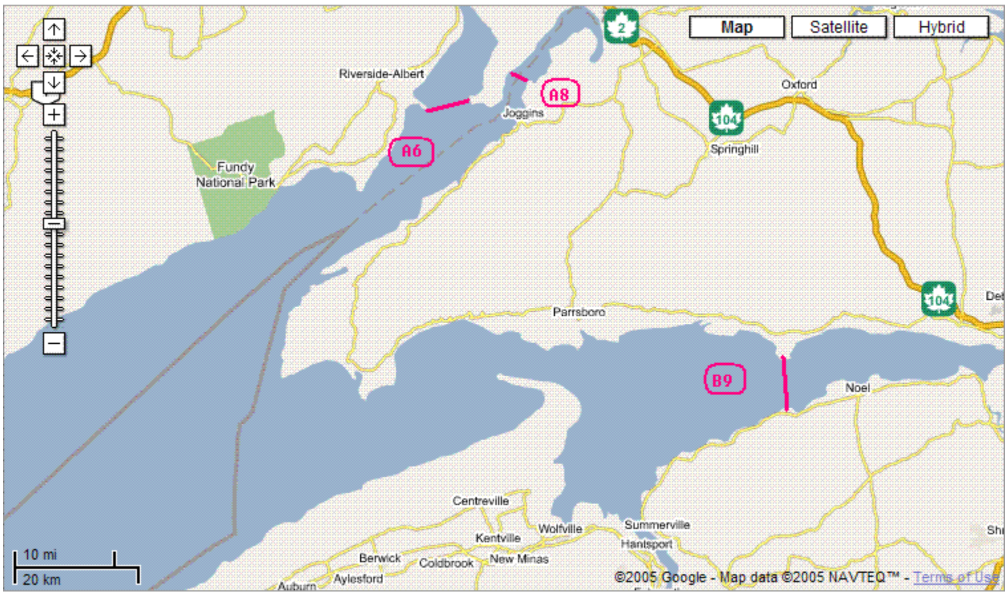

Figure 34: Sites for Barrage Type of Tidal Power Plant

Resource: http://map.google.com

From the numerical simulation at the recommended sites, we found the water elevation shown in Figure 35 for the period of December 12th, 2006 to January 10th, 2007. In Figure 35, the water elevation is for the mean sea water level, and the unit is meter.

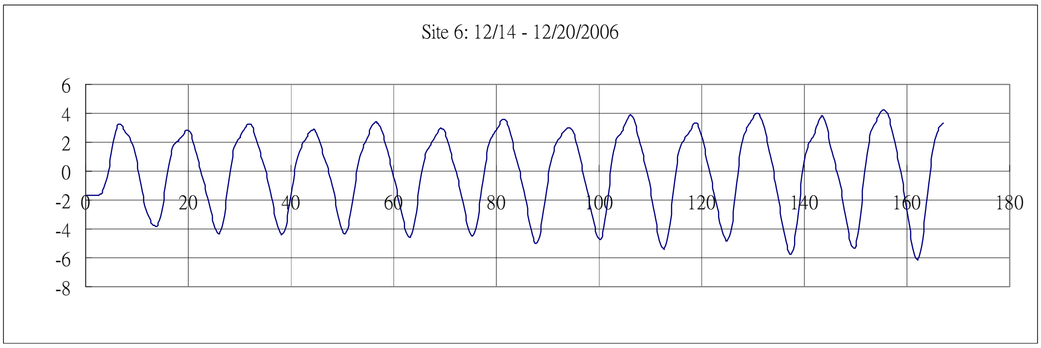

Figure 35- a1: Tidal response at site A6: 12/14 - 12/20/2006

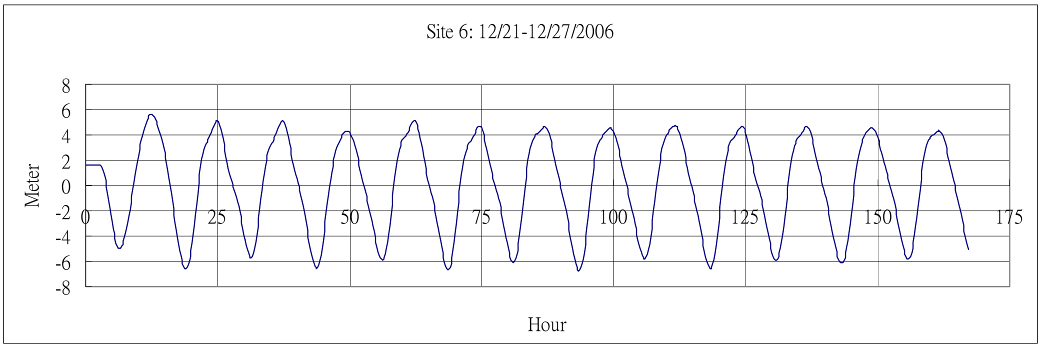

Figure 35- a2: Tidal response at site A6: 12/21-12/27/2006

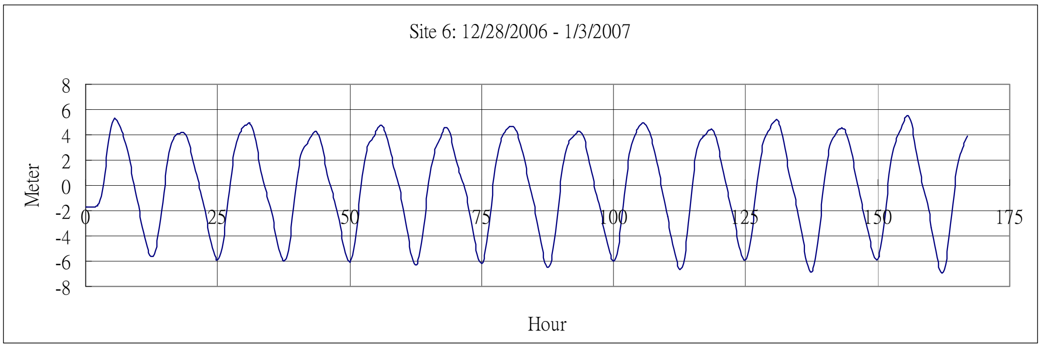

Figure 35- a3: Tidal response at site A6: 12/28/2006 - 1/3/2007

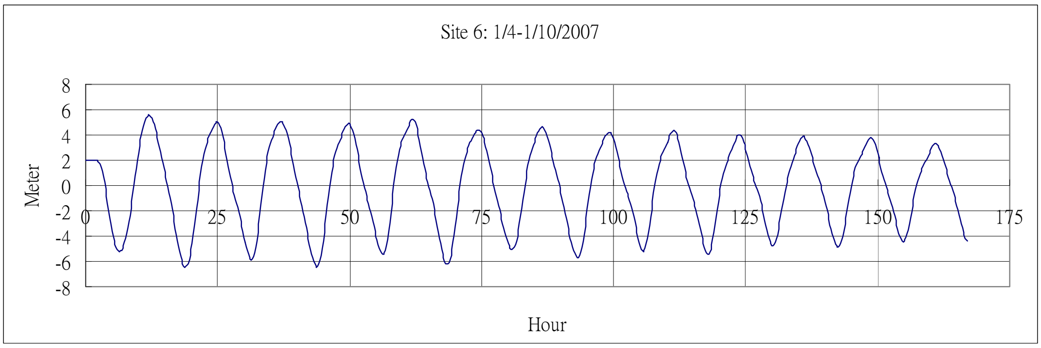

Figure 35- a4: Tidal response at site A6: 1/4 - 1/10/2007

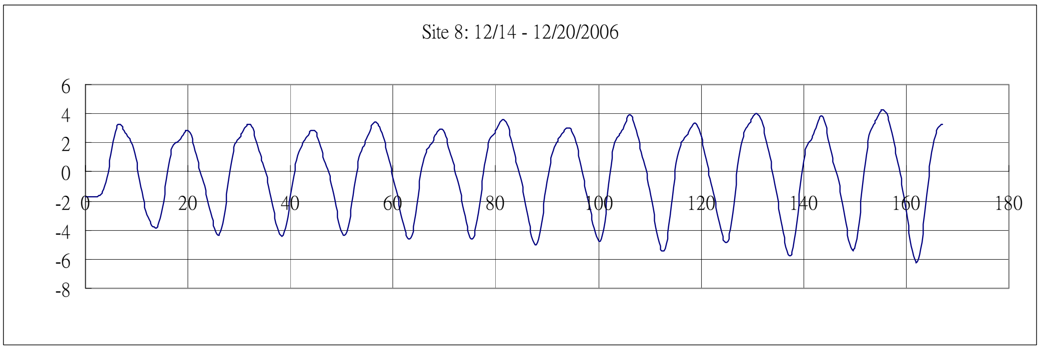

Figure 35- b1: Tidal response at site A8: 12/14 - 12/20/2006

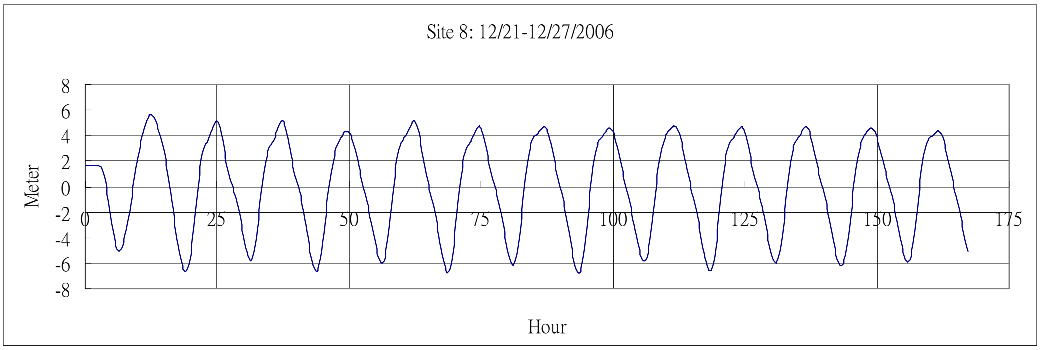

Figure 35- b2: Tidal response at site A8: 12/21-12/27/2006

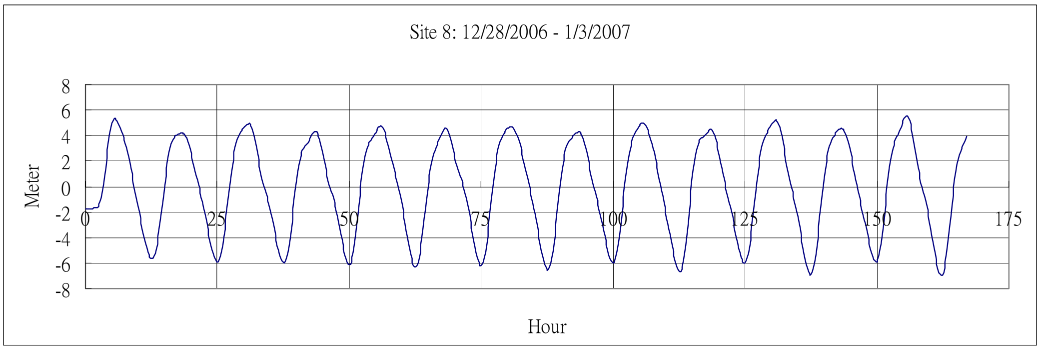

Figure 35- b3: Tidal response at site A8: 12/28/2006 - 1/3/2007

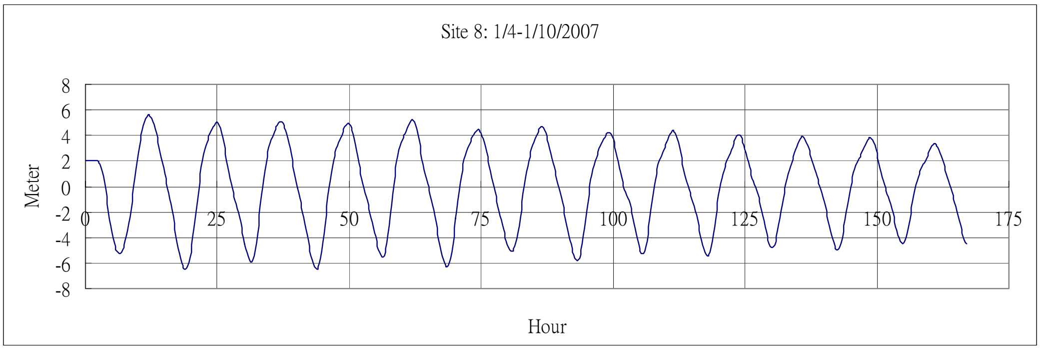

Figure 35- b4: Tidal response at site A8: 1/4 - 1/10/2007

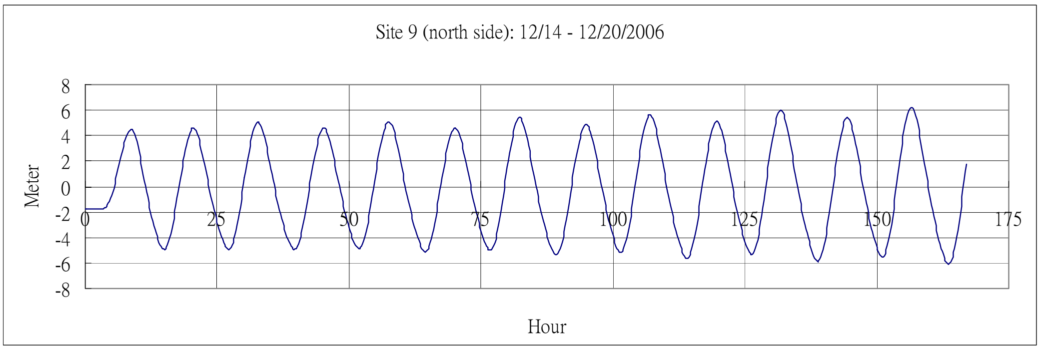

Figure 35- c1: Tidal response at site B9 (north): 12/14 - 12/20/2006

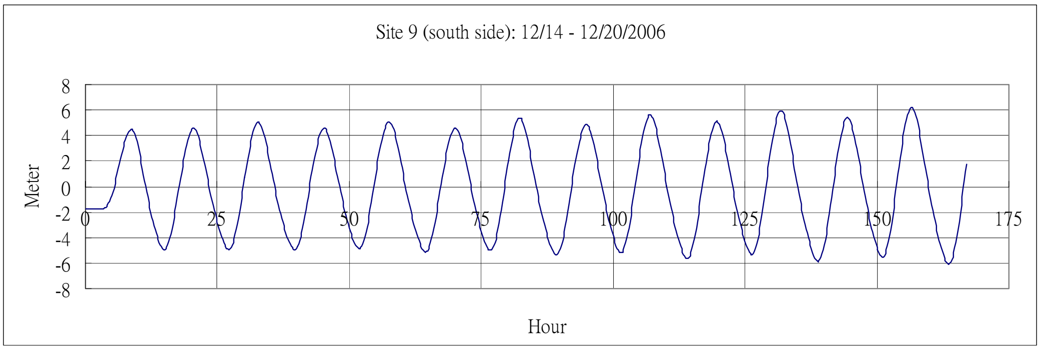

Figure 35- d1: Tidal response at site B9 (south): 12/14 - 12/20/2006

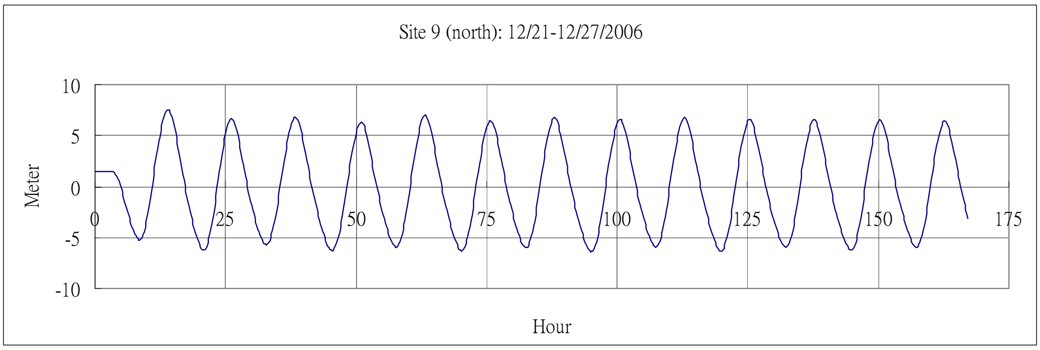

Figure 35- c2: Tidal response at site B9 (north): 12/21-12/27/2006

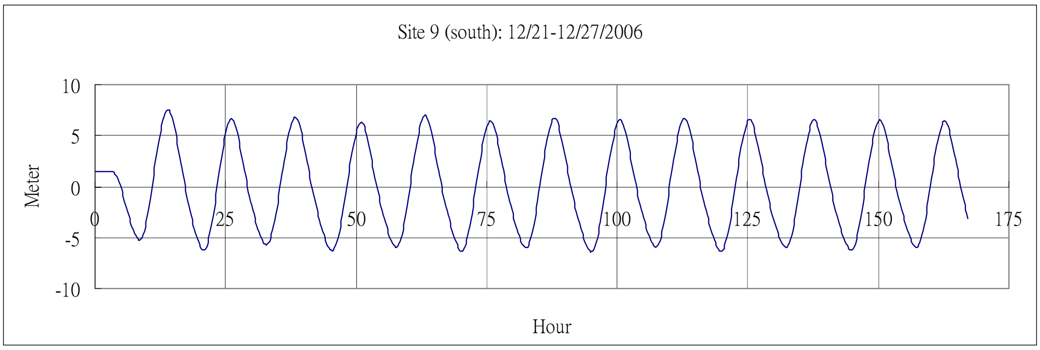

Figure 35- d2: Tidal response at site B9 (south): 12/21-12/27/2006

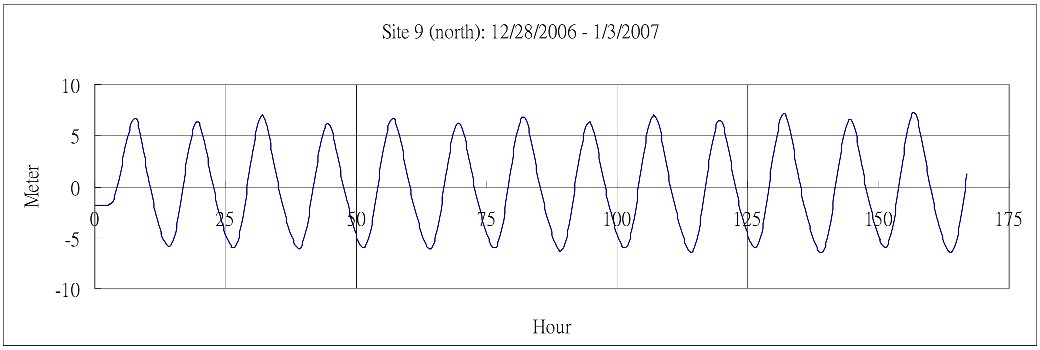

Figure 35- c3: Tidal response at site B9 (north): 12/28/2006 - 1/3/2007

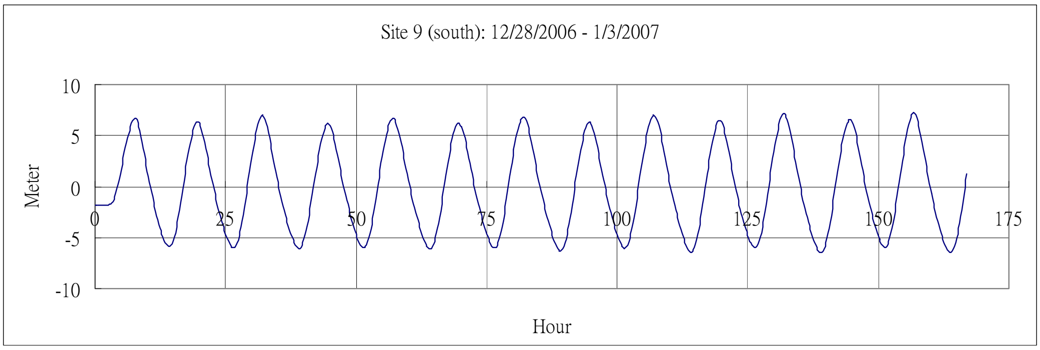

Figure 35- d3: Tidal response at site B9 (south): 12/28/2006 - 1/3/2007

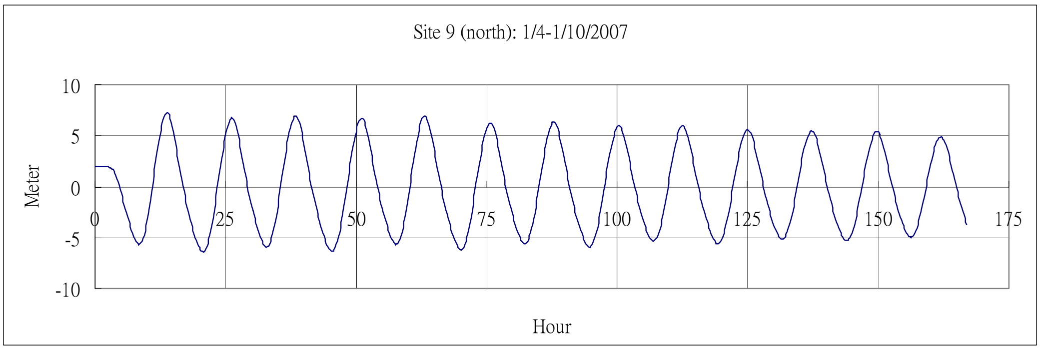

Figure 35- c4: Tidal response at site B9 (north): 1/4 - 1/10/2007

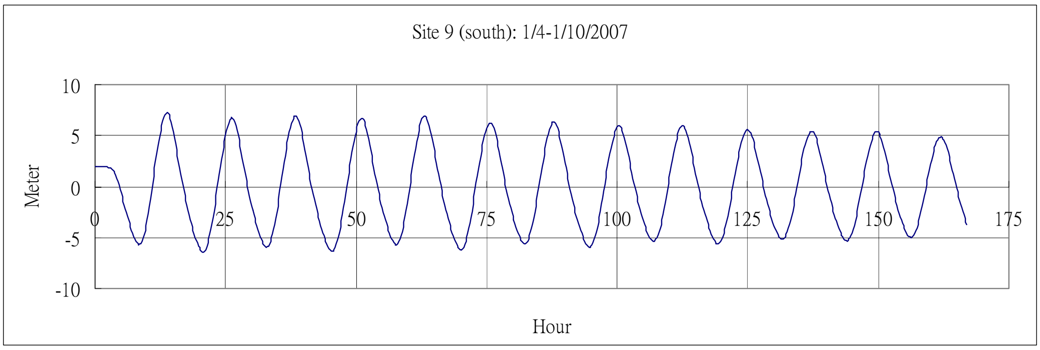

Figure 35- d4: Tidal response at site B9 (south): 1/4 - 1/10/2007

From the results presented in Figures 35, compared with Figure 25, the response in site A6, A8 is about 2 times the tide range at the entrance of the bay, and about 2.5 times the tide level at site B9. The average tidal range, hourly average square tidal range and the size of the basin for site A6, A8, and B9 are represented in Table 5.

Location		A6	A8	B9
Simulation Average Tidal Range (m)		10.98	11.08	12.78
Hourly-Average Square Tidal Range(m^2)		0.81	0.83	1.11
Basin Area (km^2)		130	100	300
Annual Energy Output (GWh)	35% efficiency	3261	2570	10312
	50% efficiency	4658	3672	14731
	75% efficiency	6987	5508	22097

Table 5: Potential Energy output from site A6, A8, and B9

In this table, the design characteristics used in Swales (1977) are reworked using the data generated from the present model. Three different efficiency of the power plant are assumed: 35%, 50% and 75% with 50% economic operation running time for a single basin- single effect operation. The average tidal range is the average for each cycle of tidal variation. The hourly average square tidal range is the summation of the square of tidal ranges during a year, and then divided by the total hours. Since we assume the area of the basin is not changing with the water elevation, the energy output will be proportional to the square of the tidal range. The basin area is the area at the high tide, which represents the maximal amount of water available for operation when multiplied by hourly average square tidal range. From Table 5 it is seen that the estimated annual energy output is around 3,300 to 7,000 GWh for site A6, 2,600 to 5,500 GWh for site A8, and 10,000 to 22,000 GWh for site B9.

5.2 Tidal Current Turbine

A tidal current turbine operates like a windmill running underwater. The energy generated from current can be calculated by the equation:

$$E = Co \cdot \rho A V^3 T / 2 \qquad (5.2)$$

where

E : energy generation in kilowatt-hours

Co : efficiency coefficient

ρ : the density of sea water, 1026 kg per cubic meter.

A : area of the cross section, blade sweep area.

V : current velocity, m/s.

T : operation duration, hours.

Several studies have been conducted to harvest energy from ocean current. However, most of them are still in the developing or experimental stages. Among various equipment providers, Marine Current Turbines Ltd (MCT) is a leader in this field. As indicated previously, according to their pilot project, MCT believes their turbine technology can be economically running if the current reaches a mean spring peak velocity about 2.25 to 2.5m/s (4.5 to 5 knots) in the water depth of 20 to 30m. As such, from Figures 28, 31, and 32, it seems that the Minas Channel can be a possible site for harnessing the current energy, where the current velocity can reach more than 8 m/s based on the present hydrodynamic model results.

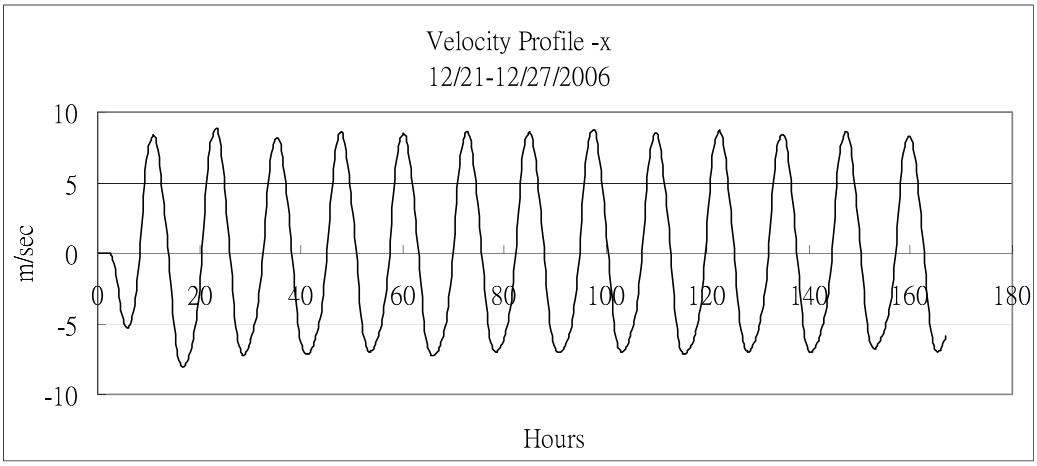

Figure 36 – a: Current velocity profile in X direction at Minas Channel

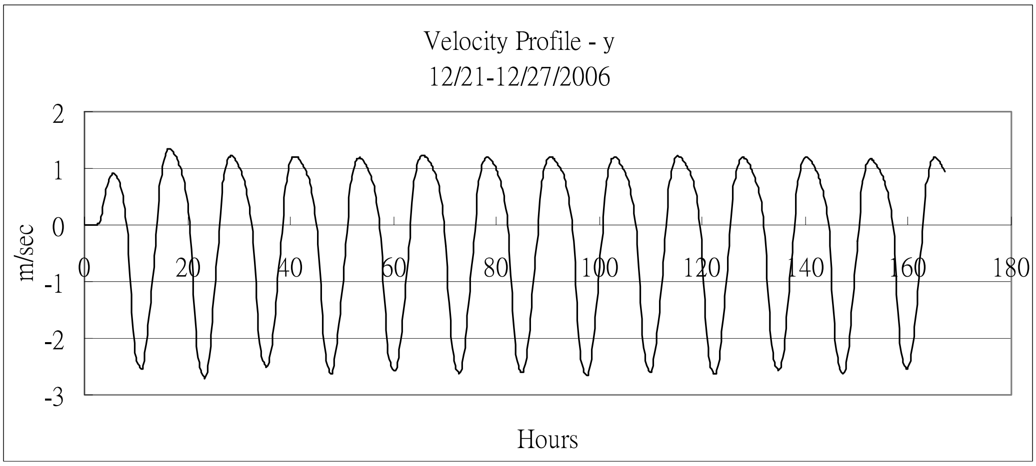

Figure 36 – b: Current velocity profile in Y direction at Minas Channel

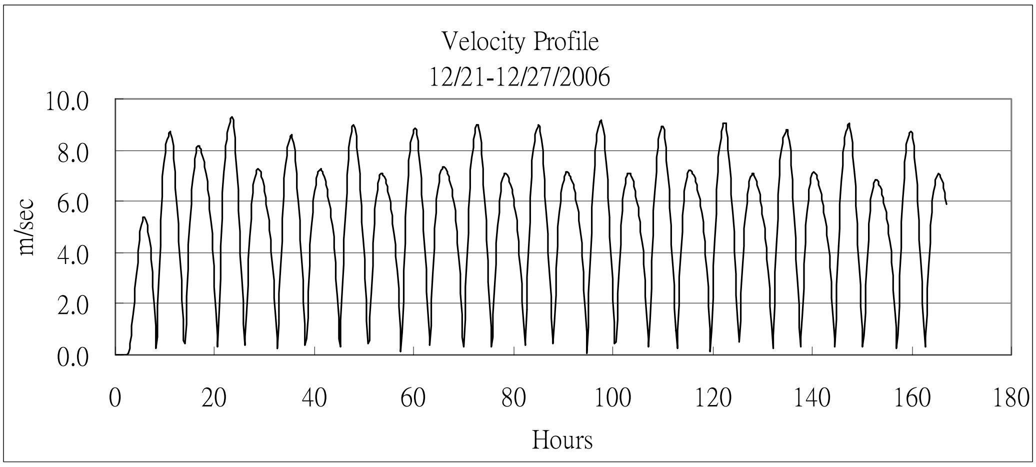

Figure 36 – c: Absolute current velocity profile at Minas Channel

The pilot turbine model (SeaFlow) of Marine Current Turbines Ltd. has 11 m diameter blade system which makes the swift area equal to 95 square meters. The efficiency coefficient of this turbine is not released to public, but we can get a reasonable estimation of 16% by the relationship between the power rate (300kW) and operational current speed (2.7 m/sec). The efficiency coefficient is also very close to 15% which was suggested by OEER (Offshore Energy Environmental Research Association, 2005). From Figure 31, the energy density in Minas channel is as high as 1196 (m^3 / sec^3 per hour). From equation (5.2), using 16% as the efficiency coefficient, the annual energy output will be 163.4GWh.

Chapter 6: Economic Feasibility

The purpose of economic feasibility study is to identify the power generation projects which can operate at an acceptable benefit – cost ratio. It should provide a measure of benefits to cost attributed by the projects as well as the impact to society and environment. This study focuses on the cost of power generation by evaluating the total power generated and the cost to build and to operate the power generating facilities. From the computed at-site cost of energy, the economic feasibility of tidal power generation will be analyzed. The issue of environmental impact as well as impacts to the society due to these power generation ideas will not be addressed in this study.

To estimate the engineering cost of a power generation project, three direct costs must be considered:

- Equipment (turbine, generator, control system, and powerhouse)
- Construction Materials (loose rock, sand and gravel)
- Soft Costs (design, construction financing, permitting, etc.)

Other than direct costs, some indirect costs include:

- Indirect construction items
- Project management
- Owners expense
- Interest during the construction

A contingency allowance is also part of the engineering cost in case of unforeseen events which could impact the overall costs such as accidents, unexpected rise of material cost, etc.

It should be noted that the parameters and assumptions made is only for economic analysis. The tidal power project similar to other type of engineering projects is sensitive to interest rate and the cost of fuels, and cost of manufacturing of the turbine/ generator may also modify the cost figures significantly.

6.1 Barrage Type of Tidal Power Plant

This study examines the schemes and designs of tidal power plants at the mouth of Cumberland Basin (A8), Cobequid Bay (Site B9), and Shepody Bay (Site A6) originally proposed by the Bay of Fundy Tidal Power Review Board in 1977. They were the most promising and economic sites in the Bay of Fundy, according to the studies at that time. The proposed design included the barrage design, the number of sluices and generating units with rate capacity, provided by optimization analysis. The design characteristics are shown in table 6. Even though the construction of the tidal plant at any one of the sites was considered technically feasible, they were never built.

Item	Units	Site B9	Site A6	Site A8
Total number of generating units		106	53	37
Total number of sluices		60	30	24
Number of spare generating units		6	3	2
Turbine diameter	m	7.5	7.5	7.5
Generator rated capacity	MW	38	31	31
Turbine rated head	m	7.5	6.5	6.5
Total installed capacity	MW	4028	1643	1147
Operating capacity	MW	3800	1550	1085
Annual output	million kWh	12653	4533	3423

Table 6: Summary of Characteristics of Single-effect Tidal Power Schemes

For the purpose of economic feasibility study, several assumptions are made. They are adopted from the proposal (the Bay of Fundy Tidal Power Review Board, 1977) and modified to accompany the recent economic condition.

- Project operation life is 75 years. This is common to hydroelectric power plants. The oldest commercial operational tidal power plant, La Rance of France, has been operated since 1966 and it is still running.
- Interest rate is set as 5.5%. It is based on the average Contract Mortgage Rate for the past 15 years.
- The cost of turbine (electrical equipment) is current price which referred to VA Hydro, the sub-contractor and technical provider of Sihwa Lake tidal power plant. It includes the equipments and installation cost on the facility. It is approximated three quarter to one million dollars per one mega-watts design rate.

- Maintenance & operation cost is 0.621% of capital cost.
- Annual cost is computed as amortization of capital cost (direct, indirect and contingency cost) plus operation & maintenance cost.

The at-site cost of energy is computed as follows:

$$C_E = \frac{C_0(CRF + M)}{E} \tag{6.1}$$

The Capital Recovery Factor (CRF) is obtained as:

$$CRF = \frac{i(1+i)^n}{(1+i)^n - 1} \tag{6.2}$$

where

C_E : At-site cost of energy. ($/kWh).

Co: Total capital investment. ($)

M : Annual operation & maintenance cost (%)

E : Annual energy produced. (kWh)

i : Interest rate

n : Operating period. (year)

The indirect and contingency costs are assumed as follows (adopt from the Bay of Fundy Tidal Power Review Board, 1977, with its methodology):

- Indirect construction items: ten percent of total direct cost;

- Project management: ten percent of total direct cost;
- Owners expense: three percent of total direct cost;
- Interest during the construction: accumulated at interest rate according to disbursement schedules;
- Contingency allowance: 12.5% of total direct and indirect cost.

Item	Units	Site B9	Site A6	Site A8
Direct Cost				
Civil work	million $	3527	2382	1330
Mechanical and electrical	million $	3800	1550	1085
Total direct costs	million $	7327	3932	2415
Indirect and contingency	million $	5862	3145	1611
Total capital costs	million $	13189	7077	4027
Amortization	million $	739	396	226
Operation & maintenance cost	million $	82	44	25
Annual cost	million $	821	440	251
At-site cost of Energy	$/kWh	0.0649	0.0971	0.0732

Table 7: Summary of At-site Costs of Single-effect Tidal Power Schemes

Table 7 represents the financial analysis for a single basin, single effect operation tidal plants at three recommended sites. In this table, direct cost includes the cost of civil work and the cost for mechanical and electrical equipments with installation. For the cost of electrical equipments with installation, the higher end of estimation is chosen (one million dollars per one mega-watts rate equipment). The total cost can be paid through total of 75 years and the annual payment is shown in the item of amortization. Since we assume that the operation and maintenance cost is 0.621% of the total capital cost each year, the annual cost of operation and maintenance can be added to the amortization of the total capital cost. The sum of these two costs is the annual cost to build and operate a barrage type tidal power plant for 75 years of its life. Compared with Table 6 for the annual energy output, the at-site cost of energy can be found. This "at-site" cost does not consider any cost to connect to the power grid of transportation or storage for the power being produced.

Energy Charge /kWh	CA$	US$	Note
Private residence	0.1067	0.1087	
Commercial			adjustable by load factor
Small Commercial	0.1181	0.1204	< 24 MWh. Charge CA$0.1039 after 200kWh
Commercial	0.0878	0.0895	CA$0.062 after 200kWh
Large Commercial	0.0598	0.0609	> 18 kW
Industrial			adjustable by load factor
Small Industrial	0.0767	0.0782	CA$0.0585 after 200kWh
Medium Industrial	0.0546	0.0556	
Large Industrial	0.0547	0.0557	> 1.8 MW
Extra Large Industrial	0.05655	0.0576	commit no less than 20 MW

Table 8: Electric billing from NOVA SCOTIA POWER INC.
Source: www.nspower.ca
CA$/US$ Exchange rate=1.01916

Table 8 shows the recent local electric company bill. The data is obtained from Nova Scotia Power Inc., and the cost of energy estimation is the highest possible (with the highest electrical equipments with installation charge) and it is compatible to the recent energy market. We can see that the at-site energy cost is very competitive for Site B9 which is less than seven cents per kWh, and is acceptable for the other sites.

6.2 Tidal Current Turbine

As mentioned earlier, Marine Current Turbines Ltd (MCT) installed and tested their first commercial-scale rotor system off Lynmouth, Devon, UK. This experimental unit was installed in May 2003 and uses 300kW single 11m diameter rotor and will only generally operate with the tide in one direction. This project costs around 6 million US dollars. Assume a similar unit is installed at Minas Channel, Bay of Fundy, we need to select a possible size of the turbine since the current velocity is higher than the location of the recent pilot study of Marine Current Turbines, Inc. Since the only change to be made is the rate of the current turbine, the cost will be increased but not by much, and the increase of the cost will be compensated by the decreasing of cost when a pilot model has been modified to a commercial model.

A 300kW unit with 11m diameter rotor requires a minimum flow velocity of 2.3 m/s, if the efficiency is assumed 16%. For a M2 tide, there will 705 cycle of tide annually and each cycle has two periods of the same magnitude of tidal current but different direction. According to the present numerical model results, the average tidal current at the best area for tidal current turbine is around 5.38 m/sec, and the duration for the velocity higher than 5.38 m/sec is around seven hours each tidal cycle. It is also noted that the duration for the current velocity which is less than minimum requirement for turbine (0.75 m/sec) is around 10.4 hours. According to equation 5.2, for the current velocity 5.8 m/sec with efficiency around 16%, the rate of power output is around 1.2 MW. The similar assumption and calculation can be made and the result is shown in Table 9.

Rate (MW)	1.2	2.1	2.7
Sweep area (m^2)	95	95	95
Efficiency	16%	16%	16%
Energy per cycle (MWh)	9.53	15.10	17.85
Annual Energy (MWh)	6720.28	10647.19	12583.19

Table 9: Power output for different rates of turbines

In this table, rate 1.2 MW is good for the maximum current velocity around 5.5 m/sec, 2.1 MW for the velocity 6.5 m/sec, and 2.7 MW for 7 m/sec current. The energy output for each type of turbine rate is generated from the minimum operation velocity (0.75 m/sec) to the maximum working velocity with a uniform efficiency. In reality, the efficiency will reach maximum when it is getting close to rate velocity and decreases when the velocity decreases. The annual energy output is calculated from 705 tidal cycles per year (since there is 705 tidal cycles each year for M2 tide).

From the design of the turbine/generator installed by MTC, the construction cost is reported to be seven million US dollars. Assume the unit's operating period is 20 years, and the operation & maintenance cost is another 1 million US dollars per year.

Compared with the annual total energy generated between 6.7 million kWh to 12.6 million kWh, we can calculate the at-site energy cost by equation 6.1 and the capital recovery factor (CRF) by equation 6.2, and we assume that the interest rate is 5.5% as indicated in previous analysis.

Rate (MW)	1.2	2.1	2.7
Capital Cost (million $)	7	7	7
Amortization (million $)	0.59	0.59	0.59
Maintenance & operation(million $)	1	1	1
Annual cost (million $)	1.59	1.59	1.59
At-site Cost of Energy ($/kWh)	0.235966	0.148937	0.126022

where

CRF=	0.083679	i=	0.055
		n=	20

Table 10: Financial analysis for current turbine

Table 10 indicates the at-site cost of the energy from current turbine type of power plant. The at-site energy cost varies from $0.13 /kWh to $0.24/kWh. Such estimate results are not very encouraging at this point even though it was based on several conservative assumptions, when compared with the current electric billing in Table 8. Further investigation is required to ascertain its efficiency, such as a more accurate installation and operation & maintenance cost, the characteristic curve for the turbine, the design operating period, and the development of more advanced turbine/ generator.

Compared with the analysis for barrage-type of tidal power generation, current turbine are more expensive. One of the possible reasons is the conservative assumptions made in this study. The current turbine's efficiency for the generation is assumed 16%, which is much lower than wind turbines' efficiencies, relatives to the efficiency of 35% to 75% for barrage-type tidal power generation. Another possible reason is the high cost estimation which is based on the pilot project of MCT. The cost of construction of a current turbine should be reduced when it is in mass production. Since it prevents the disadvantage of channel blocking by a barrage, with a possible reducing cost and increasing efficiency, the current turbine may be the future of tidal power generation.

Chapter 7: Conclusion and Future Work

Because of the rising cost of energy, environmental concern, and government support, people are interested in alternative or green energy sources. In order to research the potential of tidal energy, one source of alternative energy, this study examines the area of the Bay of Fundy as an example. The Bay of Fundy has the largest tidal range in the world (approximately 16 meters) with suitable surrounding oceanographic and economic conditions to become a prime location for harnessing tidal power using the daily rising and ebbing tide. It is a good location to examine if the tidal power is feasible for additional energy sources.

In this study, a 2-D finite element model has been developed and applied to simulate the tidal responses in the Bay of Fundy, including water level and water particle velocities. The simulation result is used to choose the location for energy development and to predict possible energy which can be developed using different types of generation methods.

Fluid motion is assumed to be governed by the shallow water equation since the wave length associated with tide is much longer than the water depth in the Bay of Fundy. A three-node triangular element is used in this 2-D model. The simulated area covers the entire Bay of Fundy from the mouth of the bay (the straight line between Tiverton, Nova Scotia and Wood Island) to the north region including Cobequid Bay and Chignecto Bay. By using a real time series of water elevation at the entrance of the bay, the computer model finds tidal response at each node in the study area, which is then verified by the observation record from several tidal gauge stations inside the Bay.

A barrage type of tidal power plant uses the potential energy produced by the tidal range, and real-time series of computer simulated water elevation at specific locations are taken to calculate the potential energy generated; on the other hand, the computer-simulated current velocity is used to compute the kinetic energy generated by tidal current using a turbine type of power generation. The energy output compared with the recent development cost defines the cost for unit energy. This study shows that the at-site cost of energy for barrage type tidal power plants is around $0.065 to $0.097 per kWh at the recommended Shepody Bay (project A6), Cumberland Basin (project A8), and Cobequid Bay (project B9). The cost of energy for the current turbine type tidal power plants is $0.13 /kWh to $0.24/kWh at the Minas Channel, the area with the highest current velocity. Compared with a recent bill from the local power company, the unit cost for the barrage type of power plant is feasible but the cost for the current turbine is higher than the recent market price.

Based on the results generated in the present study, the barrage type of tidal power plant is economically feasible but the environmental concern of channel blocking by barrage will be a formidable constraint. The current turbine type of tidal power plant, even at the most suitable sites, is not economically feasible under current technology. It may become feasible as oil prices continue to increase and more efficient turbines become available. Further studies are needed to improve the characteristic curve for the turbine/generator efficiency to reduce the energy lost during power generation for both the barrage type and tidal current turbine type power plant.

References

"International Energy Outlook", Energy Information Administration, DOE, USA, 2007

"Norway's Special Report to Earth Summit+5", United Nations. *http://www.un.org/esa/earthsummit/norway/english2.htm*)

"Our Common Future", World Commission on Environment and Development, New York: Oxford University, 1987.

"Preliminary Reassessment of Feasibility of Tidal Power Development in the Bay of Fundy", 1974, Bay of Fundy Tidal Power Review Board, Sep.

"Reassessment of Fundy Tidal Power", 1977, Bay of Fundy Tidal Power Review Board, Nov.

"Workshop on Tidal Power and the Environment in the 21st Century Summary Report", 2005, Offshore Energy Environmental Research Association, Acadia University, Canada.

Abosedra, Salah, and Baghestani, Hamid, 2004. On the predictive accuracy of crude oil futures prices, *Energy Policy,* 32, pg 1389-1293.

Bardi, Ugo, 2005. Mineral economy: a model for the shape of oil production curves, *Energy Policy*, 33, pg 53-61.

Bentley, R.W., 2002. Oil Forecasts, Past and Present, *International Workshop on Oil Depletion*, Uppsala, Sweden, May 23-24.

Bishop, Roy, Highest Tides in the World. *http://www.town.wolfville.ns.ca/visitors/sites/highesttides/highesttides.html*

Brater, E.F., King, H.W., Lindell, J.E., Wei, C.Y., 1996, Handbook of Hydraulics 7th edition, McGraw Hill, pp 7.60.

Brown, E. et al., 1999. Waves, Tide and Shallow-water Processes, Butterworth-Heinemann.

Burdette, Mike, 2005. "Petroleum Supply and Market Outlook", Briefing for the 7th Annual International Airport Operations/Jet Fuel Conference, Orlando, Florida, Feb.

Bureau of Energy, MOEA, Taiwan (1999). General Report for New and Green Energy Research and Development. May.

Canadian Hydrographic Service (CHS). *http://www.waterlevels.gc.ca/english/Canada.shtml*

Crowe, C.T., Elger, D.F., and Roberson, J.A., 2001. Engineering Fluid Mechanics, John Wiley & Sons, Inc.

Connor, J. and Wang, JD., 1974. Finite element modeling of hydrodynamic circulations, *Numerical Methods in Fluid Dynamics*. Pentech Press, London, pg 355-367.

Department of Economic and Social Development, United Nations. http://www.un.org/esa/

Division for Sustainable Development, ESA, United Nations. http://www.un.org/esa/sustdev/sdissues/energy/enr.htm

Dronkers, J.J., 1964. Tidal Computations in Rivers and Coastal Waters, North-Holland Publishing Company, Amsterdam.

Energy Information Administration, Department of Energy, USA, http*://tonto.eia.doe.gov/*

Gordon, D.C. Jr. and Dadswell, M.J., 1984. Update on the marine environmental consequences of tidal power development in the upper reaches of the Bay of Fundy, Can. Tech. Rep. Fish. Aquat. Sci. No. 1256: vii + 686p.

Greenberg, D., 1969. Modification of the M2 Tide due to Barriers in the Bay of Fundy. *Journal of the Fisheries Research Board of Canada*, Vol. 26, No. 11, pp.2775-2783.

Greenberg, D., Shore, J., Shen, Y., 1997. Modelling tidal flows in Passamaquoddy Bay. Proc. Of Maritime Atlantic Ecozone Science Workshop, pg.58-64, Nov.

Grotkop, G., 1973. Finite Element Analysis of Long-period Water Waves. Computer Methods in Applied Mechanics and Engineering, Vol. 2, pg 147-159.

Haas, R, et al. , 2004. How to promote renewable energy systems successfully and effectively, *Energy Policy,* 32, pg 833-839.

Horn, Manfred, 2004. OPEC's optimal crude oil price, *Energy Policy,* 32, pg 269-280.

Hubbert, M.K., 1962. National Research Council publication 1000-D, Washington, DC, p54.

Industrial Technology Research Institute of Taiwan, *http://www.itri.org.tw*

Karbuz, Sohbet, 2004. Conversion factors and oil statistics. Energy Policy, 32, pg 41-45.

Kaufmann, RK, and Laskowski, C., 2005. Causes for an asymmetric relation between the price of crude oil and refined petroleum products. *Energy Policy*, 33, pg 1587-1596.

Khilyuk, L.F. and Chilingar, G.V., 2004, Global warming and long-term climatic changes: a progress report. International Journal of Geosciences, Environmental Geology, 46, no. 6-7.

Laherrere, Jean, 2000. The Hubbert curve: its strengths and weakness. Version proposed to Oil and Gas Journal. Feb. *http://dieoff.org/page191.htm*

Laherrere, Jean, 2003. How to estimate future oil supply and oil demand? *International conference on Oil Demand, Production and Costs - Prospects for the Future*, The Danish Technology Council and the Danish Society of Engineers, Copenhagen, December 10.

Laherrere, Jean, 2003. Comments by Jean Laherrere on the article by Paul Holberg & Richard Hirsch: “Can we identify limits to worldwide energy resources". Oil and Gas Journal, pp.20-26, June.

Lawton, F. L., 1970. Economics of Tidal Power. *Proceedings of an international Conference on the Utilization of Tidal Power*, pp.105-129, May.

Lee, K.K., Chen, C.L., Leonard, K.M., Morris, R.D., Day, H.J., 1985. A Hydrodynamic and Water Quality Model for the Fox River and Green Bay. Sea Grant Institute, University of Wisconsin.

Leendertse, J.J., 1967. Aspects of a computational Model for Long-period Water-wave Propagation. *Rand Coportation Memorandum*, RM-5294-PR.

Leendertse, J.J., 1970. A Water-quality Simulation Model for Well-Mixed Estuaries and Coastal Seas: Vol. I, Principles of Computation. *Rand Coportation Memorandum*, RM-6230-RC.

Longwell, H.J., 2002. The future of the oil and gas industry: past approaches, new challenges. World Energy vol5 no3, http://www.worldenergysource.com/articles/pdf/longwell_WE_v5n3.pdf

Lynch, DR and Gray, WG, 1979. A wave equation model for finite element tidal computations. *Comput. Fluids*, 7, pg 201-228.

MacAvoy, Paul, 1982. Crude Oil Price. Ballinger Publish Company.

Museum of Natural History, Nova Scotia. *http://museum.gov.ns.ca*

New York State Energy Research and Development Authority, *http://www.nyserda.org/ContactInformation/Default.asp*

Noreng, Oystein, and Tauris, IB, 2002. Crude power: politics and the oil market, London.

Norton, W.R. and King, I.P., 1978. A Two-Dimensional Finite Program for Problems in Horizontal Free Surface Hydrodynamics. Operating Instructions for the computer Program RMA-2, Resource Management Associates.

Pao, RHF, 1966. Fluid Dynamics, C. E. Merill Books.

Rao, Desiraju B., 1968. Natural Oscillations of the Bay of Fundy. *Journal of the Fisheries Research Board of Canada*, Vol. 25, No. 6, pp.1097-1114.

Sankaranarayanan, S. and McCay, Deborah F., 2003. Three-Dimensional Modeling of Tidal Circulation in Bay of Fundy. *Journal of Waterway, Port, Coastal and Ocean Engineering.*, Vol. 129, No. 3, pp.114-123, May.

Shepherd, P., Partridge, V.A., and Hicklin, P.W., 1995. Changes in sediment types and invertebrate fauna in the intertidal mudflats of the Bay of Fundy between 1977 and 1994. CWS Technical Report series No. 237. Canadian Wildlife Service, Sackville, N.B.

Swales, M.C., 1977, Tidal Power Plant Design and Operation. *Fundy Tidal Power and The Environment,* Proceeding of a workshop on the Environmental Implications of Fundy Tidal Power held at Wolfville, Nova Scotia, Nov. pp.35-44.

Taylor, C. and Davis, J.M., 1975. Tidal Propagation and Dispersion in Estuaries. Finite Element in Fluids, Vol 1, London.

Walters, RA and Cheng, RT, 1979. A two-dimensional hydrodynamic model of a tidal estuary. *Advanced Water Resource*, 2, pg 177-184.

Walters, RA and Cheng, RT, 1980. Accuracy of an Estuarine Hydrodynamic Model Using Smooth Elements. *Water Resource Research,* Vol 16, No 1, pg 187-195.

Wang, JD. and Connor, J., 1975. Mathematical Modeling of the Near Coastal Circulation, *Report No. 200*, Ralph M Parson Laboratory, Massachusetts Institute of Technology, Cambridge, Mass..

World Energy Council. http://www.worldenergy.org/

Zarnikau, J., 2003. "Consumer Demand for 'Green Power' and Energy Efficiency." Energy Policy, 31, pg. 1661-1672.

Zero Waste New Zealand Trust, *http://www.zerowaste.co.nz*